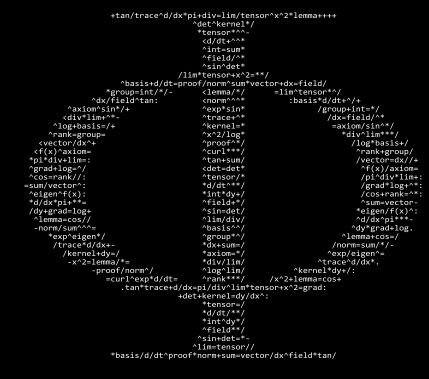
PHI TECHNICAL MONOGRAPHS

Volume VIII

Prime Ends and Conformal Boundary Geometry

Boundary topology, analysis and applications



PHI research collective

Preface

A conformal map identifies the interiors of two domains exactly, but its behavior at their boundaries can be much less simple. A single physical boundary point may admit several approaches that the map must distinguish. Conversely, one direction on the circle can accumulate on a whole continuum in the target. Prime ends preserve the missing information. They give a boundary on which a conformal map is a homeomorphism even when the ordinary boundary is neither a curve nor locally connected.

This volume continues the geometric sequence of the PHI Technical Monographs. Volume VI developed extremal length and variational geometry; Volume VII developed the hyperbolic metric, Schwarz's lemma and planar conformal mapping. Here the principal source is Section 8, "Carathéodory boundary," of Mikhail Lyubich's *Conformal Geometry and Dynamics of Quadratic Polynomials*. In the supplied 702-page manuscript, this section occupies pages 146–152. We develop its boundary theory into a connected account of topology, analysis, energy and information, with detailed proofs and worked investigations.

The first part distinguishes ordinary crosscuts, landing crosscuts and proper arcs. Spherical area and extremal length then control short cuts and small continua. These estimates lead to the prime-end compactification, impressions, conformal boundary extension and the role of local connectivity. Slits and combs show why the definitions need their stated hypotheses. Naturality is treated with explicit map directions: fixing physical boundary points is not automatically the same as fixing all the approaches to them.

The next part studies accesses and landing rays. The normalization at infinity retains logarithmic capacity, and the Joukowski map provides an exactly computable slit model. Harmonic analysis supplies a complementary view of the boundary. Starting with measure and Fourier tools, we prove radial convergence, boundary uniqueness and almost-everywhere landing, keeping exceptional sets distinct from statements at every boundary point.

The final part treats energy, recovery and computation. Continuous boundary data need not have finite Dirichlet energy. Unique recovery from exact interior data need not be stable under noise. Finitely many function values cannot control every bounded holomorphic function at the boundary. Each positive estimate is therefore accompanied by its function class, observation model and norm. Electrostatic slit and wedge models, and analytic quadrature estimates, use these same distinctions in concrete calculations.

This is an expository mathematical work. Classical results and elementary model calculations are not presented as new discoveries. The bibliography and source guide identify the principal source, imported prerequisites and corrections to statements whose normalization or interpretation matters. The literal fixed-parameter formulation of source Exercise 8.2 is tested by an explicit spiral counterexample. A geometric repair allowing independent cut parameters or reparametrization remains a separate source obligation. The boundary theorems use an independent landing-crosscut construction; the proposed repair is not a hidden premise of their proofs. Source coverage does not mean that every literal source formulation holds unchanged.

The public and internal editions share the same mathematical chapters. The internal edition adds teaching routes and assessment material. Light and dark readings have identical mathemat-

ical text and numbering. Figures are original monochrome vector illustrations with monospace labels. Their sampled curves illustrate stated analytic formulas; they are not numerical certificates of the theorems. No physical measurements or hardware experiments are reported. Lean, Rocq and computer-algebra developments remain a subsequent programme; this volume makes no claim of new kernel-checked or CAS-certified results.

Reading routes

For a first reading, follow the coordinate and cluster-set chapters before the topological development. The distinction between a physical point and an ideal boundary point is essential before discussing accesses. The local connectivity chapter explains when a continuous physical boundary map exists; the slit model explains why it need not be one-to-one. The harmonic analysis chapters can then be read as a second route to boundary values, concerned with almost every direction rather than all directions at once.

Readers interested in partial differential equations should continue from Poisson extension to the energy and normal-flux chapters, then to the slit and wedge models. Readers interested in inverse problems should study the spectral action of the Poisson kernel before the recovery bounds and finite sampling obstruction. The computational chapter gives exact truncation and aliasing identities before discussing stopping rules. No application requires treating an illustration as evidence for an unstated physical hypothesis.

Conventions and prerequisites

Write $\mathbb{D} = \{z \in \mathbb{C} : |z| < 1\}$, $\mathbb{H} = \{z : \operatorname{Im} z > 0\}$ and $\widehat{\mathbb{C}} = \mathbb{C} \cup \{\infty\}$. A domain is nonempty, open and connected. A conformal disk is a domain conformally equivalent to $\mathbb{D}$; equivalently, in the planar setting used here, it is simply connected with complement containing at least two points. The planar Riemann mapping theorem is a named classical input, developed in the preceding volume. The one-point-complement case is excluded rather than forced into disk notation.

We use elementary complex integration, the identity and maximum principles, power and Laurent series, holomorphic inverse functions, and primitives of holomorphic functions on simply connected domains. Standard real-analysis inputs include completeness of the real numbers, compactness, Lebesgue measure and integration, monotone and dominated convergence, Tonelli–Fubini, and change of variables. The Fourier and differentiation tools needed for boundary limits are developed explicitly in the text. The classical topological inputs are the Jordan curve theorem, topological Schönflies, the existence of an arc in a path between distinct endpoints, and the connected-complement criterion for planar simple connectivity. These inputs are distinguished from the conformal boundary theorems proved here.

Spherical length uses the round unit-sphere density $2/(1 + |z|^2)$ and total spherical area 4π. Chordal distance is separately normalized in Chapter 1. Circle measure is $dm(t) = dt/(2\pi)$, while planar Dirichlet energy uses ordinary Euclidean area. This difference accounts for the factor 2π in the spectral energy formula. Limits at infinity use a spherical coordinate unless an explicit Euclidean asymptotic is given. Every exterior map has its leading coefficient specified; the normalization $B(z) \sim z$ is reserved for capacity one.

An access concerns a particular way of approaching a physical boundary point; an impression may contain more than one point. A radial limit is not a full unrestricted boundary limit. A statement holding almost everywhere does not exclude a nonempty exceptional set. These distinctions will remain explicit throughout the proofs.

Contents

Preface **i**

1 Conformal coordinates and the boundary problem **1**
1.1 Prerequisites and the uniformization input 1
1.2 Spherical and Euclidean geometry 2
1.3 Disk, half-plane and exterior coordinates 4

2 Cluster sets and tests for boundary continuity **6**
2.1 Full cluster sets 6
2.2 Properness and where cluster values can lie 7
2.3 A bounded analytic counterexample to full continuity 8
2.4 Topological and analytic routes to injectivity 8

3 Crosscuts, separation and the meaning of an end **11**
3.1 The topological inputs and their scope 11
3.2 Regular nesting and why it must be stated 12
3.3 Landing approximations and what they preserve 14

4 Area, modulus and continuity on small continua **17**
4.1 The precise curve-family modulus 17
4.2 Short crosscuts from finite spherical area 19

5 Prime-end compactification and impressions **22**
5.1 Construction without a hidden boundary-continuity assumption 22
5.2 Impressions, cluster sets and physical projection 24

6 Local connectivity and conformal boundary extension **27**
6.1 From local connectedness to small connecting arcs 27
6.2 The boundary extension equivalence 29
6.3 A quantitative form and its input requirements 30
6.4 Boundary-arc uniqueness and Jordan injectivity 30

7 Naturality, tame ends and boundary-fixing maps **33**
7.1 A noncuspidal tame end 34

8 Accesses, landing curves, and the Lindelöf principle **37**
8.1 A local definition of an access 37
8.2 A finite-area estimate for bounded conformal maps 38
8.3 The landing theorem, including unbounded domains 40
8.4 Uniform approach inside a Stolz region 41
8.5 Accessible points and angles 41
8.6 Cross-cuts made from rays and an equipotential 42

9 Exterior uniformization and its normalization **44**
9.1 Full compact sets and the coefficient at infinity 44
9.2 Rays and equipotentials as actual curves 45
9.3 The circular conductor as a normalization control 46

10 A slit resolved into its two sides **48**
10.1 The Joukowski map and its inverse branch . . . 48
10.2 Ellipses, hyperbolas, and exact landing . . . 49
10.3 Landing-angle measure and the arcsine law . . . 50
10.4 Boundary data on a slit: physical values and side values . . . 51

11 Length, exceptional sets, and differentiation **53**
11.1 The measure and integration boundary . . . 53
11.2 Completeness without a functional-analysis black box . . . 56
11.3 A covering estimate and the maximal function . . . 56
11.4 Lebesgue points . . . 57
11.5 Solved investigations: measure and limits . . . 58

12 Poisson averages and boundary reconstruction **60**
12.1 Derivation and elementary properties of the kernel . . . 60
12.2 Kernel bounds and nontangential approach . . . 61
12.3 Fourier reconstruction and an elementary completeness proof . . . 63
12.4 Solved investigations: kernels and traces . . . 64

13 Hardy traces and Fatou's boundary theorem **67**
13.1 The square-integrable analytic class . . . 67
13.2 Bounded holomorphic functions . . . 69
13.3 A second construction of the boundary datum . . . 69
13.4 Solved investigations: analytic boundary phenomena . . . 71

14 Logarithmic rigidity and boundary uniqueness **73**
14.1 The logarithmic mean and its zero correction . . . 73
14.2 A second proof through regularized subharmonicity . . . 75
14.3 Quantitative smallness and equality examples . . . 76
14.4 Zeros and the necessity of the measure threshold . . . 77

15 Almost-everywhere landing and harmonic measure **79**
15.1 The exterior normalization and its bounded analytic reduction . . . 79
15.2 An independent geometric route through area . . . 80
15.3 Defining the landing measure . . . 82
15.4 Accessible mass and the absence of atoms . . . 83
15.5 Boundary data and the Dirichlet interpretation . . . 85
15.6 Solved investigations: landing and transported measure . . . 85
15.7 The source appendix's exact conclusion . . . 87

16 Boundary traces, Dirichlet energy and normal flux **88**
16.1 An exact spectral energy formula . . . 88
16.2 The variational meaning of the extension . . . 89
16.3 Normal derivatives and the Dirichlet-to-Neumann operator . . . 91
16.4 Conformal transfer of energy . . . 91

17 Recovering boundary information from interior data **94**
17.1 Forward stability and inverse discontinuity . . . 94
17.2 A regularized reconstruction with an explicit prior . . . 95
17.3 Analytic priors change the rate . . . 97

18 Finite observations and honest boundary guarantees **99**
18.1 An indistinguishable holomorphic alternative . . . 99
18.2 Boundary samples and finite Fourier models . . . 100
18.3 What a complete boundary claim must specify . . . 101

19 Potential, flux, and the geometry of a sharp boundary **103**
19.1 The model and the quantities it predicts . . . 103
19.2 An equipotential annulus with an exact flux . . . 104
19.3 The charge on the two sides of a slit . . . 105

19.4 A wedge and the exponent selected by its opening . . . 106
19.5 An incompatible boundary condition and divergent energy . . . 107
19.6 Which corner mode is actually present? . . . 108

20 Sampling a boundary with a quantitative contract **111**
20.1 Data, normalization, and aliasing . . . 111
20.2 From samples to an interior polynomial . . . 112
20.3 The apparent Cauchy quadrature and its kernel bias . . . 113
20.4 A finite stopping rule with a noise floor . . . 114
20.5 A geometric bound for a sampled curve . . . 115
20.6 A full geometry contract for the slit model . . . 115
20.7 What a finite grid cannot decide . . . 116

21 Source correspondence and proof dependencies **119**
21.1 The six named results . . . 120
21.2 Corrections, conventions and remaining source work . . . 121
21.3 Dependencies and evidence level . . . 121

References **122**

Chapter 1

Conformal coordinates and the boundary problem

A conformal map describes an open region exactly. It need not describe its boundary by an ordinary one-to-one correspondence. A slit can have two sides which approach the same physical point; a narrow channel can separate routes whose endpoints are close in the plane; and an increasingly complicated boundary can prevent a continuous boundary extension altogether. These are different phenomena. The purpose of a prime end is to retain a manner of approach rather than merely to append a point of the ambient plane.

Throughout the book, Ω denotes a domain, meaning a nonempty connected open subset of the Riemann sphere $\widehat{\mathbb{C}} = \mathbb{C} \cup \{\infty\}$. A *conformal disk* is a domain conformally equivalent to $\mathbb{D} = \{z : |z| < 1\}$. Its physical boundary is $\partial\Omega$, taken in $\widehat{\mathbb{C}}$. Its ideal boundary will be written $\partial_P\Omega$. The letter f normally denotes a conformal map $\mathbb{D} \to \Omega$, and $g = f^{-1}$ its inverse. This convention removes the source's typographical ambiguity between the unit disk and an arbitrary conformal disk.

1.1 Prerequisites and the uniformization input

The elementary analytic inputs are the integral theorem and formula of Cauchy, Taylor and Laurent expansions, the maximum principle, the identity theorem and the inverse function theorem for a nonzero complex derivative. These are the standard undergraduate complex-analysis boundary of the present book. Elementary real analysis includes compactness, uniform continuity, the fundamental theorem of calculus, and the change-of-variables theorem for smooth planar maps. The later measure-theoretic chapters state their measure construction inputs and develop the differentiation and boundary-limit arguments they use. No theorem about prime ends is assumed in these opening chapters.

We use the following precise form of planar uniformization. A proper simply connected plane domain $\Omega \subsetneq \mathbb{C}$ admits a conformal bijection $f : \mathbb{D} \to \Omega$. If $a \in \Omega$ and a positive real direction in the tangent coordinate at a are fixed, f is uniquely determined by $f(0) = a$ and $f'(0) > 0$ in that coordinate. On the sphere, the same statement applies to a simply connected domain whose complement has at least two points, after a Möbius change of chart. The entire plane and the sphere are excluded. This is the Riemann mapping theorem, developed in the preceding PHI monograph's planar-uniformization chapter. Its use here is a declared classical input, not a new solution of an open uniformization problem.

Existence supplies an interior coordinate; it supplies no continuity at an arbitrary physical boundary point. In particular, none of the boundary extension results below is included in this input. Conversely, once existence is granted, uniqueness follows from the elementary disk

argument proved next. Readers may therefore separate the analytic existence theorem from the new boundary work rather than using a boundary theorem to justify an interior map whose boundary behavior is still at issue.

For the normalized maps just described, the uniqueness calculation is

$$A = f_2^{-1} \circ f_1, \quad A(0) = 0, \quad |z| = |A^{-1}(A(z))| \le |A(z)| \le |z|, \quad A'(0) = \frac{f_1'(0)}{f_2'(0)} > 0.$$

The two inequalities force a rotation, and its positive real derivative forces its multiplier to equal one.

Lemma 1.1 (The disk Schwarz lemma)**.** *If $h : \mathbb{D} \to \mathbb{D}$ is holomorphic and $h(0) = 0$, then $|h(z)| \le |z|$ and $|h'(0)| \le 1$. Equality at a nonzero point, or $|h'(0)| = 1$, implies $h(z) = \lambda z$ for a constant $|\lambda| = 1$.*

Proof. The function $H(z) = h(z)/z$, with $H(0) = h'(0)$, is holomorphic by the Taylor expansion at zero. For $0 < r < 1$, the maximum principle gives $|H(z)| \le 1/r$ on $|z| \le r$. Fix z and let $r \uparrow 1$ to obtain $|H(z)| \le 1$. If equality holds at any point of the disk, the maximum principle makes H constant. The same argument includes equality at zero. Otherwise its modulus is strictly less than one everywhere, proving all claims. The case $h \equiv 0$ satisfies the inequalities without an equality case of modulus one. □

Proposition 1.2 (Automorphisms and normalization)**.** *Every holomorphic automorphism of $\mathbb{D}$ has the form*

$$A(z) = \lambda \frac{z - a}{1 - \bar{a}z}, \qquad a \in \mathbb{D}, \quad |\lambda| = 1.$$

It extends to a homeomorphism of $\overline{\mathbb{D}}$. Two conformal maps of $\mathbb{D}$ onto the same domain differ by such an automorphism. In particular, the normalized Riemann map is unique.

Proof. For $M_a(z) = (z - a)/(1 - \bar{a}z)$ a direct subtraction gives

$$1 - |M_a(z)|^2 = \frac{(1 - |a|^2)(1 - |z|^2)}{|1 - \bar{a}z|^2}.$$

Its denominator never vanishes on $\overline{\mathbb{D}}$, so M_a maps the disk into itself and the circle into itself. Solving $w = M_a(z)$ gives $z = (w + a)/(1 + \bar{a}w)$, an inverse with the same properties. If $A(a) = 0$, then $A \circ M_a^{-1}$ fixes zero. Applying Lemma 1.1 to it and its inverse shows equality in the modulus inequality and hence that it is a rotation. The formula follows. If f_1, f_2 have the same image, $f_2^{-1} \circ f_1$ is an automorphism. If both maps take zero to a, that automorphism is a rotation; positive derivatives force its rotation factor to be one. □

This argument has a boundary consequence without presupposing a physical boundary extension: changing the Riemann coordinate changes the ideal circle by a circle homeomorphism. Thus a construction made in a disk coordinate can be intrinsic even when the map from that circle to the physical boundary is not defined everywhere. The coordinate must still be tracked in statements about angle, Lebesgue measure, or external-ray normalization.

1.2 Spherical and Euclidean geometry

For finite z, w define the chordal distance

$$q(z, w) = \frac{|z - w|}{\sqrt{1 + |z|^2}\sqrt{1 + |w|^2}}, \qquad q(z, \infty) = \frac{1}{\sqrt{1 + |z|^2}}.$$

This is half the Euclidean distance between the corresponding points of the unit sphere under stereographic projection. It is therefore a metric, and $\widehat{\mathbb{C}}$ is compact in this metric. We use the spherical line and area elements

$$ds_s = \frac{2|dz|}{1+|z|^2}, \qquad dA_s = \frac{4\,dx\,dy}{(1+|z|^2)^2}.$$

The sphere has area 4π. Some formulas become shorter with the line element divided by two, but then the area must be divided by four as well. The geometric conclusions do not depend on that convention.

Proposition 1.3 (Metric comparisons)**.** *For $|z|, |w| \le R$,*

$$\frac{|z-w|}{1+R^2} \le q(z,w) \le |z-w|.$$

If γ is a rectifiable curve, the chordal distance between any two of its points is at most half its spherical length. A Möbius map and its inverse are uniformly continuous on the sphere.

Proof. The first estimates follow immediately from the two denominator factors. Stereographic projection takes the spherical line element to ordinary arc length on the unit sphere. The straight chord is no longer than an arc joining its endpoints; dividing the chord length by two proves the second claim. A Möbius map is a continuous bijection of the sphere, including at its pole and at infinity. A continuous map on a compact metric space is uniformly continuous, and its inverse is another Möbius map. □

Small Euclidean diameter and small spherical diameter are equivalent on a fixed bounded set, with constants depending on that set. They are not uniformly interchangeable over the whole plane. For example, the real segment $[R, 2R]$ has Euclidean diameter R but chordal diameter at most $1/R$. A null-chain definition intended to cover domains containing infinity must use spherical size or explicitly localize to a bounded chart.

The example can be evaluated without an asymptotic convention:

$$\operatorname{diam}_{\mathrm{E}}[R, 2R] = R, \qquad \operatorname{diam}_q[R, 2R] = \frac{R}{\sqrt{1+R^2}\sqrt{1+4R^2}} \le \frac{1}{2R} \quad (R > 0).$$

Here the chordal diameter is attained by the endpoints, since stereographic angle is monotone on the positive real axis.

Proposition 1.4 (Conformal spherical area)**.** *For a conformal injection $f : U \to \widehat{\mathbb{C}}$,*

$$\int_U \left(\frac{2|f'(z)|}{1+|f(z)|^2}\right)^2 dA(z) = \operatorname{area}_s(f(U)) \le 4\pi.$$

The expression at a pole is interpreted in the reciprocal coordinate and has a removable coordinate singularity. For a decreasing family of measurable subsets $E_n \subset U$ with empty intersection, the integral over E_n tends to zero.

Proof. At a finite regular point, the real derivative of a holomorphic map is a rotation and dilation by $|f'|$, with Jacobian $|f'|^2$. The usual area change of variables gives the equality on compact subsets avoiding poles. An injective meromorphic map has at most one pole; in the coordinate $v = 1/f$ the displayed density equals $2|v'|/(1+|v|^2)$. Exhaustion and monotone convergence yield the equality on U. Injectivity is essential: otherwise multiplicity would appear in the area formula. The final claim is continuity from above for the finite measure with this integrable density, or follows directly by dominated convergence.

Writing $\rho_f = 2|f'|/(1+|f|^2)$ makes the two limiting steps explicit:

$$\frac{2|(1/f)'|}{1+|1/f|^2} = \frac{2|f'|}{1+|f|^2}, \qquad 0 \le \mathbf{1}_{E_n}\rho_f^2 \le \rho_f^2 \in L^1(U), \quad \mathbf{1}_{E_n}\rho_f^2 \longrightarrow 0.$$

The first identity holds off zeros and poles and extends in the appropriate coordinate; the second gives the asserted integral limit.

□

The last assertion is qualitative unless a bound for the area of $f(E_n)$ is available. It must not be replaced by an invented rate. The shrinking crosscut arguments will select short curves by integrating their squared lengths against this finite area; the selection is an analytic existence argument, not a grid-based numerical certificate.

1.3 Disk, half-plane and exterior coordinates

The Cayley map $C(z) = (1+z)/(1-z)$ sends $\mathbb{D}$ to the right half-plane. Its inverse is $(w-1)/(w+1)$, and

$$\operatorname{Re} C(z) = \frac{1-|z|^2}{|1-z|^2}.$$

Multiplication by i then gives an upper-half-plane coordinate. At the distinguished boundary point 1, large $|w|$ corresponds to small $|1-z|$. At a different marked point, first rotate the disk. This operation does not assert that the physical image of a half-plane semicircle is a Euclidean semicircle; only its source geometry has been simplified.

In particular, writing $w = C(z)$ gives the exact coordinate relations

$$1 - z = \frac{2}{w+1}, \qquad 1-|z|^2 = \frac{4\operatorname{Re} w}{|w+1|^2}, \qquad C'(z) = \frac{2}{(1-z)^2}.$$

Thus the target half-plane condition and the scale of approach are separately visible in the same change of variables.

A non-tangential approach to $\zeta \in \partial\mathbb{D}$ remains in a region

$$S_A(\zeta) = \{z \in \mathbb{D} : |z-\zeta| \le A(1-|z|)\}, \qquad A > 1.$$

A limit on every such region is an angular or non-tangential limit. A radial approach $r\zeta$ lies in every $S_A(\zeta)$, so an angular limit implies a radial limit. Neither conclusion automatically gives the limit under every approach through the disk.

For a proposed limit b in a metric target, the angular assertion has the quantifier order

$$\forall A > 1\ \forall \varepsilon > 0\ \exists \delta > 0 : \quad z \in S_A(\zeta),\ |z-\zeta| < \delta \implies d(F(z), b) < \varepsilon.$$

The choice of δ may depend on A; deleting the restriction $z \in S_A(\zeta)$ would assert a stronger, unrestricted limit.

For an exterior domain associated with a compact full nondegenerate hull K, the coordinate is usually a map from $\{|w| > 1\} \cup \{\infty\}$ to $\widehat{\mathbb{C}} \setminus K$. Its Laurent expansion at infinity has a positive leading coefficient after normalization. That coefficient carries geometric scale and cannot generally be replaced by one. The exterior chapters will develop the coefficient and its interpretation directly. The substitution $z = 1/w$ changes approach from $|w| > 1$ to approach from $|z| < 1$ but reverses angular orientation; every use of that substitution keeps the angle change.

Investigation 1.5 (Changing the marked point)**.** Let $f : \mathbb{D} \to \Omega$ be normalized at $f(0) = a$. For $b = f(\alpha)$, construct a disk parametrization taking zero to b, and determine how its boundary circle coordinate differs from that of f.

Solution. The map $T_\alpha(z) = (z + \alpha)/(1 + \bar{\alpha}z)$ sends zero to α. Thus $f \circ T_\alpha$ takes zero to b. Its derivative at zero is $f'(\alpha)(1 - |\alpha|^2)$. Precomposition with a rotation makes that derivative positive in a selected target coordinate. The corresponding boundary coordinates differ by T_α and that rotation, both circle homeomorphisms. Uniform angular spacing is not preserved unless $\alpha = 0$; differentiation along the circle gives the density factor $(1 - |\alpha|^2)/|1 + \bar{\alpha}e^{it}|^2$. The ideal boundary is unchanged, but the marked interior point changes the angular measure associated with it.

Investigation 1.6 (A metric endpoint at infinity)**.** Let $\gamma(t) = t^{-1} + i \sin(t^{-2})$ for $0 < t \leq 1$. Does γ land on the sphere as $t \downarrow 0$? Must its Euclidean length be finite?

Solution. Since $|\gamma(t)| \geq t^{-1}$, $q(\gamma(t), \infty) \leq t$, so the curve lands at infinity. Its real part has unbounded variation, already implying infinite Euclidean length. Spherical landing is a statement about convergence, not rectifiability. Even finite endpoint distance gives no bound on the length of a curve that oscillates before arriving. This is why shrinking-crosscut lemmas establish length estimates separately instead of inferring them from endpoint positions.

Investigation 1.7 (Normalization and a shrinking derivative)**.** For real $0 < a < 1$, compute the derivatives on the circle of $M_a(z) = (z - a)/(1 - az)$ at 1 and -1. Explain why a bound uniform in all disk automorphisms cannot follow merely from the fact that both boundaries are unit circles.

Solution. Since $M_a'(z) = (1 - a^2)/(1 - az)^2$, the derivative magnitudes are $(1 + a)/(1 - a)$ at 1 and $(1 - a)/(1 + a)$ at -1. One diverges and the other tends to zero as $a \uparrow 1$. Domain regularity alone therefore does not control boundary distortion if the marked point is allowed to approach the boundary. Fixing the center of the disk removes this family: an automorphism fixing zero is a rotation, whose boundary derivative has constant magnitude one.

Chapter 2

Cluster sets and tests for boundary continuity

Before constructing prime ends, it is useful to isolate what compactness alone can say. The results in this chapter apply to continuous maps from a disk to a compact metric space. They do not require a conformal map, and their limitations are correspondingly important. In the conformal setting the compact target is the sphere, so an unbounded Euclidean image causes no loss of compactness.

2.1 Full cluster sets

Let X be a compact metric space with metric d, and let $F : \mathbb{D} \to X$ be continuous. For $\zeta \in \partial\mathbb{D}$ define

$$C(F, \zeta) = \bigcap_{r>0} \overline{F(\mathbb{D} \cap B(\zeta, r))}^{X}.$$

It is enough to intersect over $r = 1/n$. This is the full cluster set: it uses every approach in the disk, rather than only a radius or a selected curve. A sequence tending to ζ may approach tangentially, oscillate between channels, or alternate between different subsets.

Lemma 2.1 (Compact connected cluster sets)**.** *$C(F, \zeta)$ is nonempty, compact and connected. It consists exactly of the limits of sequences $F(z_n)$ with $z_n \to \zeta$ in $\mathbb{D}$.*

Proof. The sets $\mathbb{D} \cap B(\zeta, 1/n)$ are nonempty and convex, hence connected. Their images are connected, and their closures are compact connected nonempty subsets of X. These closures form a decreasing sequence. Compactness gives a nonempty intersection. To see connectedness, suppose the intersection were separated into two nonempty compact pieces. Choose disjoint open neighborhoods of those pieces with disjoint closures. Every sufficiently late member of the decreasing sequence lies in the union of these neighborhoods: otherwise points outside the union have a convergent subsequence lying in the intersection. That late connected set meets both neighborhoods, a contradiction.

A sequential limit belongs to every closure in the definition. Conversely, for x in the intersection choose $z_n \in \mathbb{D} \cap B(\zeta, 1/n)$ with $d(F(z_n), x) < 1/n$. Then $z_n \to \zeta$ and $F(z_n) \to x$.

Equivalently, the sequential characterization just proved is

$$x \in C(F, \zeta) \quad \Longleftrightarrow \quad \exists (z_n) \subset \mathbb{D} : \quad |z_n - \zeta| + d(F(z_n), x) \longrightarrow 0.$$

Both terms are controlled in the constructed sequence, rather than merely the distance of x from an image closure.

□

Proposition 2.2 (The singleton criterion)**.** *F extends continuously to $\mathbb{D} \cup \{\zeta\}$ if and only if $C(F, \zeta)$ is a singleton. If that singleton is $\{x\}$, the only possible extension value is x.*

Proof. A continuous extension forces every approaching sequence to converge to the extension value. For the converse, if continuity at ζ failed, there would be an $\varepsilon > 0$ and a sequence $z_n \to \zeta$ with $d(F(z_n), x) \geq \varepsilon$. Compactness gives a convergent subsequence of the image. Its limit belongs to $C(F, \zeta)$ by Lemma 2.1 but differs from x, a contradiction. This also proves uniqueness.

The contradiction also yields the uniform-in-a-cap formulation

$$C(F, \zeta) = \{x\} \quad \Longleftrightarrow \quad \lim_{r \downarrow 0} \sup_{z \in \mathbb{D} \cap B(\zeta, r)} d(F(z), x) = 0.$$

The supremum is finite because X is compact. If it stayed above a positive number along shrinking caps, the same subsequence argument would apply.

□

Theorem 2.3 (From pointwise cluster data to a global extension)**.** *If $C(F, \zeta)$ is a singleton for every $\zeta \in \partial\mathbb{D}$, the pointwise extension $\overline{F} : \overline{\mathbb{D}} \to X$ is continuous and therefore uniformly continuous. If F is a conformal bijection onto $\Omega \subset \widehat{\mathbb{C}}$, its boundary extension, when it exists, maps the circle onto $\partial\Omega$.*

Proof. Only continuity at a boundary point ζ remains to be checked. Consider any sequence $w_n \in \overline{\mathbb{D}}$ tending to ζ. For an interior w_n, put $z_n = w_n$. For a boundary w_n, continuity at that one point, already proved by Proposition 2.2, permits a choice $z_n \in \mathbb{D}$ with $|z_n - w_n| < 1/n$ and $d(F(z_n), \overline{F}(w_n)) < 1/n$. Thus $z_n \to \zeta$, and the singleton criterion forces $F(z_n) \to \overline{F}(\zeta)$. The same limit holds for $\overline{F}(w_n)$. Sequential continuity on a metric space is continuity. Uniform continuity follows from compactness of the closed disk.

For the approximating points in this argument the relevant estimate is

$$d(\overline{F}(w_n), \overline{F}(\zeta)) \leq \frac{1}{n} + d(F(z_n), \overline{F}(\zeta)) \longrightarrow 0, \qquad |z_n - \zeta| \leq \frac{1}{n} + |w_n - \zeta| \longrightarrow 0.$$

It handles boundary and interior terms of the sequence together.

For the final assertion, take a physical boundary point b and a sequence $x_n \in \Omega$ tending to b. A subsequence of $f^{-1}(x_n)$ converges in $\overline{\mathbb{D}}$. Its limit cannot lie in the interior, since interior continuity would put b in Ω. It is a circle point whose extension value is b. Conversely, a circle value cannot lie in Ω: continuity of f^{-1} there would turn an interior sequence approaching the circle into a sequence converging to an interior point. This proves equality of the image with the physical boundary. □

The proof contains a useful distinction. Pointwise singleton information at every boundary point produces uniform continuity by a compactness argument, but it does not supply a computable modulus of continuity. An explicit rate requires additional quantitative input. The later stability chapter makes that distinction concrete for boundary recovery from interior measurements.

2.2 Properness and where cluster values can lie

Proposition 2.4 (Interior compact sets stay away from the ideal boundary)**.** *Let $f : \mathbb{D} \to \Omega$ be a homeomorphism. For every compact $K \subset \Omega$, the set $f^{-1}(K)$ is compact in $\mathbb{D}$ and is contained in $\{|z| \leq r_K\}$ for some $r_K < 1$. If z_n leaves every compact subset of $\mathbb{D}$, no subsequential limit of $f(z_n)$ on the sphere lies in Ω.*

Proof. The inverse map is continuous, so the image $f^{-1}(K)$ of the compact set K is compact. Its continuous modulus attains a maximum strictly below one. If $f(z_{n_j}) \to b \in \Omega$, choose a closed coordinate disk about b compactly contained in Ω. Eventually all these images belong to that compact disk, forcing the preimages into one fixed compact subset of $\mathbb{D}$, a contradiction.

For nonempty K, compactness gives the explicit positive separation

$$r_K = \max_{w \in K} |f^{-1}(w)| < 1, \qquad \operatorname{dist}(f^{-1}(K), \partial\mathbb{D}) = 1 - r_K > 0.$$

No uniform lower bound in K is asserted as K approaches the boundary.

□

In particular, a radial curve under a conformal map can only accumulate on the physical boundary. Its cluster set is connected by the same nested-tail argument as Lemma 2.1, but its connected cluster set can be smaller than the full cluster set of the corresponding circle point. The impression of a prime end will agree with the full cluster set. A landing ray can therefore identify an accessible point without proving that the entire impression is a singleton.

2.3 A bounded analytic counterexample to full continuity

Example 2.5 (One radius and an entire disk of cluster values)**.** The bounded holomorphic function

$$F(z) = \exp\left(-\frac{1+z}{1-z}\right), \qquad z \in \mathbb{D},$$

has radial limit zero at 1, while its full cluster set at 1 is the closed unit disk. In particular, a radial limit need not be a full boundary limit even for a bounded holomorphic function.

Proof. The real part of $(1+z)/(1-z)$ is positive, so $0 < |F(z)| < 1$. Along real $r \uparrow 1$ this real part tends to infinity, and $F(r) \to 0$. For a with $0 < |a| < 1$, write $a = e^{-x}e^{-iy_0}$ with $x > 0$. Set $w_n = x + i(y_0 + 2\pi n)$ and $z_n = (w_n - 1)/(w_n + 1)$. Then $z_n \in \mathbb{D}$, $z_n \to 1$, and $F(z_n) = a$. For $|a| = 1$, replace x by $1/n$ in this construction to obtain $F(z_n) \to a$. The value zero is already obtained radially. No cluster value can have modulus greater than one. These observations give the full cluster set exactly.

The constructed sequence satisfies the exact identities

$$1 - z_n = \frac{2}{w_n + 1} \longrightarrow 0, \qquad 1 - |z_n|^2 = \frac{4\operatorname{Re} w_n}{|w_n + 1|^2} > 0, \qquad F(z_n) = e^{-w_n}.$$

For fixed $x > 0$, the last expression equals a for every n; with $x = 1/n$, its modulus tends to one while its argument remains fixed.

□

This function is not injective: adding $2\pi i$ in the half-plane coordinate does not change its value. It is therefore an analytic control for limit distinctions, not a counterexample to a theorem whose hypotheses include univalence. Keeping that hypothesis visible prevents a common misapplication of illustrative examples.

2.4 Topological and analytic routes to injectivity

A continuous surjection from a circle onto a boundary need not be injective. The elementary continuous image theorem preserves connectedness and compactness, not the number of preimages

of a point. For a slit, the two boundary sides give different ideal points with the same physical endpoint. For a Jordan domain, the stronger geometric hypothesis will rule out this identification. The relevant inference is a theorem about separation and accesses, not an immediate consequence of the interior map being injective.

There is, however, a general compact-space criterion that will be used repeatedly. A continuous bijection from a compact space to a Hausdorff space is a homeomorphism. Indeed, the image of a closed subset is compact and therefore closed, so the inverse is continuous. To use this criterion one must prove boundary injectivity separately. It cannot be substituted for that proof.

The book uses the Jordan curve theorem and its elementary crosscut-separation consequences as stated topological inputs where indicated. The conformal Schönflies result is then a boundary correspondence theorem developed from those inputs. No proof of the Jordan curve theorem is silently hidden in a drawing, and no statement about arbitrary higher-dimensional spheres is inferred from the planar theorem.

Investigation 2.6 (A cluster set from nested tails)**.** Let $\gamma(t) = \sin(1/t)$ for $0 < t \le 1$. Find the intersection of the closures of $\gamma((0, 1/n))$. Explain what changes if the target is $\mathbb{R}$ and the curve is $\gamma(t) = 1/t$.

Solution. Every sufficiently short interval of positive t contains full oscillations, so each closed image is $[-1, 1]$ and the intersection is $[-1, 1]$. For $1/t$ in $\mathbb{R}$, the closures are $[n, \infty)$ up to an immaterial endpoint, and their intersection is empty. The compact-target hypothesis in the cluster lemma is therefore necessary. On the sphere the latter curve has the singleton cluster set $\{\infty\}$, restoring the compact setting.

Investigation 2.7 (Boundary surjectivity without injectivity)**.** Suppose a conformal map onto a slit domain extends continuously to the closed disk. Can interior injectivity alone prove that the extension is a homeomorphism? Identify the exact missing step in the compact-space argument.

Solution. Interior injectivity rules out equal images for two points of $\mathbb{D}$, but does not rule out equal images for two distinct points of $\partial\mathbb{D}$. The compact-space theorem requires a bijection on the entire closed disk. Surjectivity of the boundary follows from Theorem 2.3; the missing assertion is boundary injectivity. In the Joukowski model developed later, two angles map to every interior point of the slit. That explicit model resolves the logical question by showing that the missing step is false, rather than merely unproved, for a slit.

Investigation 2.8 (A quantitative version of the singleton criterion)**.** Suppose for every $\zeta \in \partial\mathbb{D}$ and $0 < r < r_0$ one has

$$\operatorname{diam} F(\mathbb{D} \cap B(\zeta, r)) \le \omega(r), \qquad \omega(r) \longrightarrow 0.$$

Prove that the boundary extension exists and that $d(\overline{F}(\zeta), \overline{F}(\eta)) \le \omega(2|\zeta - \eta|)$ when $0 < 2|\zeta - \eta| < r_0$, assuming ω is nondecreasing.

Solution. Every cluster set has diameter zero, so the singleton criterion and global extension theorem apply. Put $s = |\zeta - \eta| > 0$. Points of $\mathbb{D}$ sufficiently close to either ζ or η lie in $B(\zeta, 2s)$. The distance of their images is at most $\omega(2s)$; take separate limits to the two boundary points. The same argument bounds the distance between an interior point z close to ζ and the extension value using $\omega(2|z - \zeta|)$. Thus an explicit oscillation bound supplies a boundary modulus, whereas bare existence of singleton cluster sets supplies no numerical function ω.

Investigation 2.9 (The meaning of an almost-everywhere statement)**.** Explain why a theorem giving radial limits for Lebesgue-almost every angle does not imply that every physical boundary point is accessible, and does not imply a full boundary extension.

Solution. The exceptional set is measured in the circle parameter, not in physical arclength. Different angles can represent different accesses to the same physical point, and some physical points need not be radial values at all. Moreover, radial convergence controls only one approach per angle. The full cluster set can contain values obtained by tangential or oscillating approaches that are invisible on that radius. The preceding exponential example proves the second logical distinction even without an exceptional set at the chosen angle. A prime-end theorem identifies the correct circle of approaches; a local-connectivity theorem supplies the stronger global continuity conclusion under additional topological hypotheses.

Chapter 3

Crosscuts, separation and the meaning of an end

Source correspondence. Lyubich, §8.1.1 and Exercises 8.1–8.2.

Throughout these chapters, Ω is a simply connected proper domain in $\widehat{\mathbb{C}}$ whose complement contains at least two points. A Riemann map $f : \mathbb{D} \to \Omega$ is fixed temporarily, with $f(0) = a$, and $g = f^{-1}$. Lengths and diameters on the sphere use the spherical metric. On compact coordinate neighborhoods the Euclidean and spherical metrics are comparable; we specify a coordinate before using a Euclidean annulus estimate.

There are three different objects at a rough boundary: a physical point of $\partial\Omega$, an approach to that point, and a whole boundary direction of the conformal disk. They agree for a Jordan domain. They need not agree for a slit domain, and an arbitrary boundary direction need not have a single physical limit. Keeping these objects separate is the central task of prime-end theory. In particular, attaching the set $\partial\Omega$ to Ω does not always produce a closed disk.

3.1 The topological inputs and their scope

We use the Jordan curve theorem in its topological form: an embedded circle in the sphere has precisely two complementary domains, each with that circle as boundary. We also use its planar Schoenflies form: either closed side of a Jordan curve is homeomorphic to a closed disk. This is a theorem about homeomorphisms, not the conformal boundary-extension theorem proved below. We also use the planar simply-connectedness criterion: a domain in the sphere is simply connected if and only if its complement is connected. This is understood for a domain, and simple connectivity includes path connectedness. It does not apply to an arbitrary disconnected open set. An additional elementary continuum-topology input is the arc theorem: the image of a path joining two different points in a Hausdorff space contains an embedded arc joining those points. Neither statement is inferred from a picture or from a numerical drawing. They are classical topological prerequisites, recorded here so that subsequent analytic arguments have a visible dependency boundary.

The Riemann mapping theorem is the analytic existence input. Volume VII gives its planar proof through a normal-family extremizer. The present arguments also apply to a conformal disk in the sphere by changing coordinates. They do not assert that an arbitrary simply connected topological space admits a complex structure or a conformal parametrization.

Definition 3.1 (Proper crosscuts)**.** A proper crosscut is an embedding $\sigma : (0, 1) \to \Omega$ which is proper as a map into Ω: the inverse image of every compact subset is compact. We require $a \notin \sigma((0, 1))$. A landing crosscut is a proper crosscut which has limits at both parameter ends in $\partial\Omega$ and whose continuous extension is injective except that its two end values may agree. An

ordinary crosscut has different end values and is an embedded closed arc. The two ends of a landing crosscut are retained as two ends even when their physical points coincide.

For a continuous map on $(0,1)$, the compact-set formulation is equivalently the following uniform exclusion of both parameter tails:

$$\forall K \Subset \Omega \ \exists \delta_K \in (0,1/2): \qquad \sigma\big((0,\delta_K)\cup(1-\delta_K,1)\big)\cap K = \varnothing.$$

Indeed, a compact inverse image stays a positive distance from both ends; conversely the displayed inclusion confines the closed inverse image of K to the compact interval $[\delta_K, 1-\delta_K]$.

The last convention is useful and necessary. A conformal image of an ordinary disk crosscut can have the same physical limit at both ends. It remains an embedded open arc and still separates the domain. Calling it an ordinary crosscut would erase a distinction which becomes important at slit tips. Whenever a proof uses a Jordan arc obtained by adjoining a complementary arc, the ordinary case is treated separately from the coincident-end case.

Proposition 3.2 (Separation by a proper crosscut)**.** *The complement $\Omega \setminus \sigma$ of a proper crosscut has exactly two components. Both meet each sufficiently small neighborhood in Ω of an interior point of the crosscut. One component contains a; the other is called its fjord.*

Proof. Choose a homeomorphism $T : \Omega \to \mathbb{R}^2$, using the Riemann map followed by a disk-to-plane homeomorphism. Parametrize $(0,1)$ by $\mathbb{R}$. Properness means that the image of either infinite end eventually leaves every compact set of the plane. Consequently $T\sigma$ extends continuously to an injective map from the one-point compactification of $\mathbb{R}$ to the one-point compactification of $\mathbb{R}^2$. These compactifications are a circle and a sphere, respectively. The extended map is an embedding, since a continuous injection from a compact space to a Hausdorff space is a homeomorphism onto its image. Its image is therefore a Jordan curve passing through the point at infinity.

The Jordan curve theorem gives two complementary components. Removing the point at infinity does not remove a point of either component, because that point lies on the curve. Pulling the components back by T proves the first assertion. The local two-sided assertion follows by applying a local Schoenflies chart along the Jordan curve. Finally a lies in exactly one component because it is not on the crosscut. No assertion about landing at the physical boundary has been used. □

Remark 3.3. An embedded arc which is not proper need not separate. A finite line segment strictly inside a disk has a connected complement: a path can go around either endpoint. Properness prevents these two passages. It is not a decorative condition to be added after the separation argument.

For an ordinary crosscut in $\mathbb{D}$, the closure of its fjord has a boundary arc on $\partial\mathbb{D}$. The relevant arc is the one lying on the side away from 0. If the crosscut is contained in a sufficiently small disk centered on $\partial\mathbb{D}$, its fjord is contained in that same small disk. Here and below "sufficiently small" includes exclusion of the basepoint. Indeed, $\mathbb{D} \setminus \overline{B(\zeta, r)}$ is connected for $\zeta \in \partial\mathbb{D}$ and $0 < r < 1$. It lies on the basepoint side of any crosscut contained in $B(\zeta, r)$; the other side has nowhere to meet its complement. This simple observation converts small crosscuts into small fjords in the disk, although it is false for general physical domains without further hypotheses.

3.2 Regular nesting and why it must be stated

A sequence of crosscuts is intended to describe an entire approach region, not merely a thin family of paths which happen to have the same limit. We therefore make the regularity requirement in

the chain description explicit. First describe a regular disk chain: its crosscuts have pairwise disjoint closures in $\overline{\mathbb{D}}$; their fjords V_n satisfy $V_{n+1} \subset V_n$; and their Euclidean diameters tend to zero. The closures of their boundary arcs are nested strictly inside the preceding boundary arcs. The last condition is the endpoint formulation of regular nesting; it can also be required directly when selecting a subsequence of crosscuts.

For the moment a regular landing chain in Ω means the image of such a chain under f, with each crosscut landing in the physical sphere. This coordinate-first definition specifies the objects without presupposing the boundary theorem. We shall prove independence of the conformal coordinate, produce representatives of arbitrarily small spherical length, and establish an intrinsic null-chain criterion whenever the crosscut closures are disjoint in the physical sphere. The distinction is useful at a boundary point with more than one access, where physical closure can forget which side of a slit is meant.

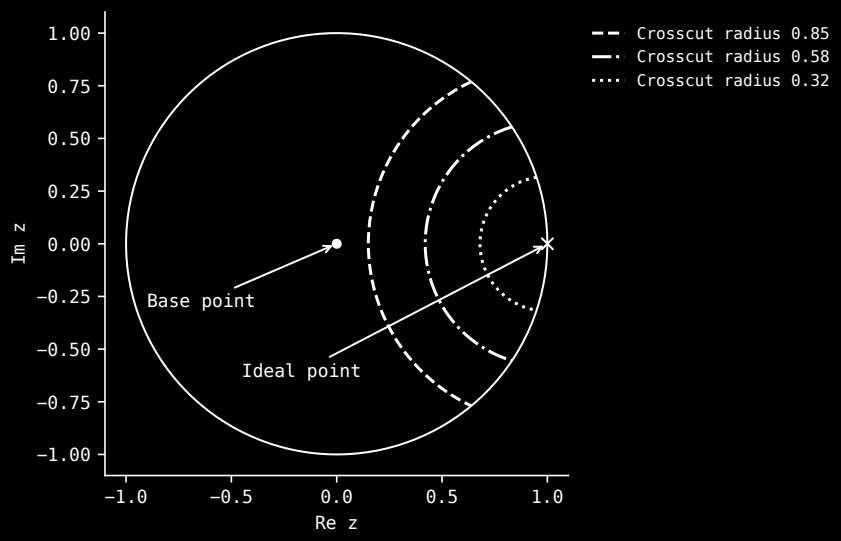


Figure 3.1: A regular chain of disk crosscuts and its fjords. The root stays on the opposite side, the closures of successive crosscuts are disjoint, and the whole fjord neighborhoods shrink to one circle point. The drawing illustrates the geometric definition; no pixel measurement is used as evidence.

Two chains (F_n) and (F'_m) are cofinal if each fjord of either chain contains some fjord of the other. Cofinality is an equivalence relation. Reflexivity and symmetry are immediate. For transitivity, if F_n is given, choose $F'_m \subset F_n$ and then $F''_k \subset F'_m$; the reverse inclusion condition is proved in the same order. A particular parametrization or a particular list of crosscut lengths is not part of an end.

Writing the two requirements together makes their quantifiers explicit:

$$(F_n) \sim (F'_m) \quad \Longleftrightarrow \quad \begin{aligned} &(\forall n\ \exists m:\ F'_m \subset F_n),\\ &(\forall m\ \exists n:\ F_n \subset F'_m). \end{aligned}$$

The index chosen for one inclusion may depend on the requested neighborhood; there is no requirement that the two lists have matching indices or matching rates of shrinkage.

Example 3.4 (An irregular shrinking nest)**.** In the disk take the straight chords joining 1 to $e^{i/n}$, and let V_n be their small fjords. After passing to a subsequence these fjords are nested and their diameters tend to zero. Every closure contains 1. Nevertheless, no V_n contains a full disk cap $\mathbb{D} \cap B(1, r)$. A standard cap chain at 1 is therefore not cofinal with this nest. The chord endpoints remain fixed at 1, violating regular nesting. Diameter shrinkage by itself cannot be substituted for the complete chain definition.

This example explains a convention which is sometimes implicit in compressed accounts. If all shrinking nests are admitted while equivalence is defined by cofinal inclusion, one obtains more classes than the boundary circle. One must either impose the separation and regularity conditions on chains, or define boundary directions directly by the conformal compactification. The present treatment does both and states the relationship precisely.

3.3 Landing approximations and what they preserve

Proper arcs can have complicated cluster sets at their ends. Source Exercise 8.2 asks for a Hausdorff approximation by an ordinary crosscut which retains a middle subarc and has two short new terminal pieces. Its literal parameter requirement needs care: preserving the supplied map on $[\delta, 1-\delta]$ imposes a relation between the two truncation depths which is not invariant under reparametrization. The following explicit example disproves that fixed-parameter assertion. It does not settle the geometric approximation problem with independently chosen cuts.

Example 3.5 (Why a fixed common truncation parameter is too restrictive)**.** The literal formulation of source Exercise 8.2 asks that the supplied parametrization $\sigma : (0,1) \to \Omega$ be retained on one symmetric interval $[\delta, 1-\delta]$, while both replacement ends have arbitrarily small length. With that fixed-parameter interpretation the assertion is false, already for $\Omega = \mathbb{D}$. The following example does not refute a geometric formulation allowing two independently chosen cut parameters, or allowing the original arc to be reparametrized first.

For $s, u \geq 0$ define two spirals

$$L(s) = \left(1 - \frac{1}{s+2}\right) e^{is}, \qquad R(u) = \left(1 - \frac{1}{u+3}\right) e^{iu}.$$

Each is simple because its radius is strictly increasing. They are disjoint: equality of radii would force $s - u = 1$, whereas equality of arguments would force $s - u \in 2\pi\mathbb{Z}$. The segment $J = [1/2, 2/3]$ joins $L(0)$ to $R(0)$ without meeting either spiral elsewhere. Indeed, the next positive-real intersection of either spiral has parameter at least 2π and radius greater than $2/3$. Put

$$\sigma(t) = \begin{cases} L(1/t - 3), & 0 < t \leq 1/3, \\ t/2 + 1/3, & 1/3 \leq t \leq 2/3, \\ R((1/(1-t) - 3)^2), & 2/3 \leq t < 1. \end{cases}$$

The pieces agree at their endpoints. The resulting map is continuous, injective, and proper in $\mathbb{D}$, since both end radii tend to 1. To check the inverse, a convergent image sequence with an interior limit lies in a compact subset of the disk. Properness keeps its parameters in a compact subinterval; injectivity makes every convergent parameter subsequence have the same limit. Thus the inverse is continuous and the map is a proper embedded arc. It avoids the basepoint 0. Its image $A = \sigma((0,1))$ has the entire unit circle in its closure: for each angle θ, the values $L(\theta + 2\pi n)$ tend to $e^{i\theta}$ as $n \to \infty$ through nonnegative parameters.

We show that no ordinary crosscut σ' can satisfy the literal requirements with Euclidean Hausdorff tolerance and terminal lengths less than $\eta = 1/100$. Write $B = \sigma'([0,1])$ and first suppose $0 < \delta \leq 1/2$.

If $\delta < 1/3$, set $S = 1/\delta - 3$. The retained core is exactly

$$L([0, S]) \cup J \cup R([0, S^2]).$$

If $S < 2$, this core lies in $|z| \leq 6/7$. The right-arm radius is at most $1 - 1/(4+3) = 6/7$; the left arm and joining segment have smaller radii. If $1/3 \leq \delta \leq 1/2$, the core is a subsegment of J

and the same bound holds. Every point of either new terminal arc is within distance η of its endpoint on the core. Hence B lies in $|z| \le 6/7 + \eta$, and

$$\sup_{a \in A} \operatorname{dist}(a, B) \ge 1/7 - \eta > \eta,$$

contrary to Hausdorff approximation.

It remains to consider $\delta < 1/3$ and $S \ge 2$. The first terminal arc, traversed in reverse, would connect $a = L(S)$ to $\partial\mathbb{D}$, have length less than η, and avoid the retained core except at a. Denote this terminal arc by Γ. It is contained in $B(a, \eta)$, and $|a| \ge 3/4$. On this ball the continuous angle branch

$$\vartheta(z) = S + \operatorname{Arg}(e^{-iS} z)$$

is well defined with the displayed argument in $(-\pi/2, \pi/2)$, because

$$\operatorname{Re}(e^{-iS} z) > 74/100, \qquad |\operatorname{Im}(e^{-iS} z)| < 1/100.$$

In particular, $|\vartheta(z) - S| < \arctan(1/74) < 1$. For $S \ge 2$ the interval $[S-1, S+1]$ lies in $[0, S^2]$, so the retained right spiral contains its polar graph at every angle occurring on Γ. The continuous function

$$H(z) = |z| - \left(1 - \frac{1}{\vartheta(z) + 3}\right)$$

satisfies

$$H(a) = -\frac{1}{(S+2)(S+3)} < 0, \qquad H(b) = \frac{1}{\vartheta(b) + 3} > 0 \quad (b \in \Gamma \cap \partial\mathbb{D}).$$

The intermediate value theorem gives a point of Γ where $H = 0$. At this point $z = R(\vartheta(z))$ with $0 < \vartheta(z) < S^2$. Thus the terminal arc intersects the retained right arm, contradicting the injectivity of σ'. The intersection is neither a, where $H < 0$, nor its boundary endpoint, where $H > 0$.

Allowing $\delta > 1/2$ would not help. The two terminal parameter intervals then overlap and cover $[0, 1]$, so their length bounds imply $\operatorname{diam} B < 2\eta$. But $\operatorname{diam} A = 2$, and a Hausdorff approximation within η would imply $\operatorname{diam} A \le \operatorname{diam} B + 2\eta < 4\eta$.

Finally this is also a spherical counterexample. On $\overline{\mathbb{D}}$ the normalized chordal distance

$$q(z, w) = \frac{|z - w|}{\sqrt{1 + |z|^2}\sqrt{1 + |w|^2}}$$

is at least $|z - w|/2$, and its induced length element is at least $|\,\mathrm{d}z|/2$. The usual round spherical distance and length are no smaller. Thus spherical tolerance and terminal lengths less than $1/200$ would give the impossible Euclidean bounds above. A different constant normalization only changes this numerical tolerance.

The obstruction is the demand that the two cuts have the same parameter distance from the ends: the left cut is at angle S, while the retained right arm already reaches angle S^2. No conclusion about independently chosen cuts, or about a reparametrized geometric version of the exercise, has been proved by this example.

The corrected geometric question is still separate. Compactness of the sphere gives a finite ε-net for the image closure with centers on a sufficiently long middle subarc. A point close to the complement can also be joined to a nearest complementary point by a short spherical segment whose open portion stays in the domain. Those observations do not show that two independently selected attachments can simultaneously avoid the retained arc, remain mutually disjoint and have different physical endpoints. A complete proof with those requirements remains

an explicitly recorded obligation; the counterexample above must not be relabeled as a disproof of that different assertion.

The compactification and boundary-extension arguments below do not require either approximation assertion. They construct landing crosscuts directly from finite area, retaining the two landing ends when they coincide physically, and prove a separate intrinsic criterion for ordinary null chains whose closed crosscuts are already disjoint.

Investigation 3.6 (Properness under change of coordinates)**.** Let $h : \Omega \to \Omega'$ be a homeomorphism. Prove that σ is a proper crosscut if and only if $h\sigma$ is proper. Explain why ordinary landing is not preserved by an arbitrary homeomorphism of the open domains.

Solution. For a compact set $K \subset \Omega'$, the set $h^{-1}(K)$ is compact, so $(h\sigma)^{-1}(K) = \sigma^{-1}(h^{-1}K)$ is compact. Apply the same argument to h^{-1} for the converse. To see the limitation, let $\Omega = \mathbb{D}$ and write $h(re^{it}) = re^{i(t+q(r))}$, where q is continuous on $[0, 1)$, $q(0) = 0$, and $q(r) \to +\infty$ as $r \uparrow 1$. This is a disk homeomorphism with the obvious inverse. A radius has no limiting image angle. Thus properness is a property of the open-domain topology, whereas physical landing needs information about the map near the boundary.

Investigation 3.7 (A slit has two sides)**.** For $\Omega = \widehat{\mathbb{C}}\backslash[-1, 1]$, examine the two curves approaching 0 from the upper and lower half-planes. Show that they cannot be joined near 0 inside Ω without leaving a fixed small neighborhood.

Solution. Choose $0 < r < 1$. The intersection $B(0, r) \cap \Omega$ is the disjoint union of its upper and lower half-disks. A connecting path inside this intersection would have a point on the real axis by the intermediate value theorem for its imaginary part. Such a point lies in the deleted interval. The two curves therefore determine different local approaches even though their physical limit is the same. The exterior Joukowski parametrization developed later identifies their two different boundary angles explicitly.

Investigation 3.8 (Changing the basepoint)**.** Suppose a sequence of fjords shrinks in disk coordinates to $\zeta \in \partial\mathbb{D}$. Show that two fixed interior basepoints choose the same fjord side for all sufficiently late crosscuts.

Solution. Both basepoints have positive Euclidean distance from ζ. Eventually the closure of the small fjord is contained in a neighborhood of ζ which excludes them both. They then lie in the other component. Removing finitely many initial crosscuts does not change a cofinal class, so the end does not depend on the chosen root. A root is useful for assigning a side, not an additional datum of the boundary point.

Chapter 4

Area, modulus and continuity on small continua

Source correspondence. Lyubich, §8.1.2, Lemmas 8.4 and 8.6, Remark 8.5 and Corollary 8.8.

The crucial estimates in this chapter are inequalities over complete curve families. They do not follow from sampling a few radial lines. The upper bound comes from a logarithmic annulus surrounding a small target continuum; the lower bound comes from a whole angular interval in the disk. Their incompatibility proves the uniform statement needed for prime ends.

4.1 The precise curve-family modulus

For a family Γ of locally rectifiable curves in a plane domain, define

$$\mathcal{M}(\Gamma) = \inf_{\rho} \int \rho^2 \, \mathrm{d}A, \qquad \int_\gamma \rho \, \mathrm{d}s \geq 1 \quad (\gamma \in \Gamma),$$

where ρ ranges over nonnegative Borel functions. An integral may be infinite. Curves of infinite length are interpreted by integrals over compact subarcs; a density may still have a finite or infinite integral along them. For the estimates used here, all radial segments in the lower-bound family are rectifiable, and the upper-bound density works for every joining curve. There is consequently no exceptional-curve convention hidden in the proof.

Lemma 4.1 (Conformal invariance)**.** *If $F : U \to V$ is a conformal bijection, then $\mathcal{M}(F\Gamma) = \mathcal{M}(\Gamma)$.*

Proof. For an admissible density ρ on V, put $\widetilde{\rho}(z) = \rho(F(z))|F'(z)|$. Change of variables along a compact rectifiable curve gives equal weighted lengths. Applying the formula on successive compact subarcs and taking increasing limits gives the same conclusion for every locally rectifiable curve. Area change of variables gives

$$\int_U \widetilde{\rho}^2 \, \mathrm{d}A = \int_U \rho(F(z))^2 |F'(z)|^2 \, \mathrm{d}A(z) = \int_V \rho(w)^2 \, \mathrm{d}A(w).$$

Thus $\mathcal{M}(\Gamma) \leq \mathcal{M}(F\Gamma)$. The inverse conformal map gives the reverse inequality. The same calculation proves invariance under a change of conformal metric, including passage from a stereographic plane coordinate to the spherical metric. □

Lemma 4.2 (A small target has small connecting modulus)**.** *Suppose $E \subset \{|w - b| \leq \delta\}$ and $K \subset \{|w - b| \geq R\}$, where $0 < \delta < R$. Let $\Gamma(E, K)$ be all curves joining E to K in any intervening domain. Then*

$$\mathcal{M}(\Gamma(E, K)) \leq \frac{2\pi}{\log(R/\delta)}.$$

Proof. Use the density

$$\rho(w) = \frac{\mathbf{1}_{\{\delta<|w-b|<R\}}}{|w-b|\log(R/\delta)}.$$

Every joining curve crosses the annulus from its inner to its outer circle. Since the radial distance is a 1-Lipschitz function along an arclength parametrization, the integral of ρ on the crossing is at least $\log(R/\delta)/\log(R/\delta) = 1$. More formally apply the fundamental theorem of calculus to $\log|w-b|$ on successive compact crossings and then pass to the endpoints. Integration in polar coordinates gives

$$\int \rho^2 \,\mathrm{d}A = \frac{2\pi}{\log^2(R/\delta)} \int_\delta^R \frac{\mathrm{d}r}{r} = \frac{2\pi}{\log(R/\delta)}.$$

Restricting the density to the domain cannot increase its area integral. For an arclength-parametrized crossing γ_0 with $\delta < |w-b| < R$ except at its two endpoints, the admissibility calculation can also be written without suppressing its derivative:

$$1 = \frac{\left|\int_{\gamma_0} \mathrm{d}\log|w-b|\right|}{\log(R/\delta)} \le \frac{1}{\log(R/\delta)} \int_{\gamma_0} \frac{\mathrm{d}s}{|w-b|} \le \int_\gamma \rho \,\mathrm{d}s.$$

Here the absolute value is outside the signed logarithmic integral; a crossing which changes radial direction only increases the upper bound. □

Lemma 4.3 (An angularly wide continuum has positive modulus)**.** *Let $E \subset \mathbb{D} \setminus \overline{D(0,r_0)}$ be a compact connected set, where $0 < r_0 < 1$. Let $J = \{z/|z| : z \in E\}$, and write $|J|$ for its angular length in radians, with $|\partial\mathbb{D}| = 2\pi$. The family of all curves in $\mathbb{D}$ joining E to the circle $|z| = r_0$ satisfies*

$$\mathcal{M} \ge \frac{|J|}{\log(1/r_0)}.$$

Proof. For each angle t in J, choose any radius $s_t > r_0$ with $s_t e^{it} \in E$. The segment from $r_0 e^{it}$ to $s_t e^{it}$ belongs to the joining family. If ρ is admissible, then

$$1 \le \int_{r_0}^{s_t} \rho(re^{it})\,\mathrm{d}r \le \left(\int_{r_0}^1 \rho(re^{it})^2 r\,\mathrm{d}r\right)^{1/2} (\log(1/r_0))^{1/2}.$$

The rightmost bound no longer depends on the selection s_t, so no measurable-selection theorem is needed. Integrate its square over the compact set of angles J and use polar coordinates. Taking the infimum over admissible densities proves the result. Connectedness ensures that J is a connected subset of the circle, hence a closed arc or the entire circle; it will allow angular diameter to control $|J|$. □

Theorem 4.4 (Uniform inverse continuity on continua)**.** *For every $\varepsilon > 0$ there is $\delta > 0$ such that every compact connected set $E \subset \Omega$ with spherical diameter less than δ satisfies*

$$\operatorname{diam} g(E) < \varepsilon.$$

The same conclusion holds for a connected arc, not necessarily closed in Ω, when all of its compact subarcs have spherical diameter less than δ.

Proof. If the first statement fails, choose compact continua E_n whose spherical diameters tend to zero while $\operatorname{diam} g(E_n) \ge \varepsilon$. Choose $w_n \in E_n$. Compactness of the sphere gives a subsequence with $w_n \to b$; the diameter condition then implies that all of E_n converges uniformly to b. If $b \in \Omega$, continuity of g on a compact neighborhood gives a contradiction. Thus $b \in \partial\Omega$.

For every $r < 1$, the image $f(\overline{D(0,r)})$ is a compact subset of Ω disjoint from b. Hence $g(E_n) \subset \{r < |z| < 1\}$ for all large n. In particular the minimum radius of $g(E_n)$ tends to 1. For z, w with radii at least r, write $z = su$, $w = tv$, where $|u| = |v| = 1$. Then

$$|u - v| \geq |z - w| - |z - u| - |w - v| \geq |z - w| - 2(1 - r).$$

Thus, for large n, the radial projection J_n of $g(E_n)$ has chordal diameter at least $\varepsilon/2$. Since chordal distance is at most angular length, $|J_n| \geq \varepsilon/2$.

Fix $r_0 = 1/2$ and $K = f(\{|z| = r_0\})$. Choose a stereographic coordinate finite at b, and then $R > 0$ such that K avoids the closed coordinate disk of radius R about b. The sets E_n lie in disks of radii $\delta_n \downarrow 0$ about b. The modulus of curves joining E_n to K is at most $2\pi/\log(R/\delta_n)$ by Lemma 4.2. Conformal invariance and Lemma 4.3 give the lower bound $\varepsilon/(2\log 2)$ for the same modulus. The upper bound tends to zero, which is impossible.

More explicitly, the contradiction is already forced by the finite threshold

$$\delta_n < R\exp\left(-\frac{4\pi\log 2}{\varepsilon}\right) \quad \Longrightarrow \quad \mathcal{M} < \frac{\varepsilon}{2\log 2} \leq \mathcal{M}.$$

This threshold concerns the chosen coordinate and fixed root curve; the preceding compactness argument is what allows those choices to remain fixed along the subsequence.

For the arc statement, any two points belong to a compact subarc. Apply the first part to that subarc and take the supremum over pairs. The proof does not require a modulus of continuity for g on all pairs of nearby points: those points must belong to the specified small connected set. □

The last sentence is essential. Across a slit, two points can be close in the physical metric while belonging to different approach regions. There need not be a small continuum in the domain joining them. The theorem controls connected geometry, and this is exactly what a crosscut supplies.

The same calculation separates the angular and radial errors. For a compact connected E, suppose that in the chosen coordinate $E \subset B(b, \delta)$, the root curve lies outside $B(b, R)$, and $g(E) \subset \{r < |z| < 1\}$ with $0 < r_0 \leq r < 1$ and $0 < \delta < R$. Writing J for the radial projection of $g(E)$ gives

$$\operatorname{diam} g(E) \leq 2(1 - r) + |J| \leq 2(1 - r) + \frac{2\pi\log(1/r_0)}{\log(R/\delta)}.$$

For the first inequality write each point as its radial projection plus an error of size at most $1 - r$; the second is the comparison of the two modulus bounds. Both terms must be controlled to obtain a diameter bound.

Corollary 4.5 (Landing is preserved by the inverse map)**.** *If $\gamma : [0, 1) \to \Omega$ is continuous and $\gamma(t) \to b \in \partial\Omega$, then $g(\gamma(t))$ converges to one point of $\partial\mathbb{D}$.*

Proof. Every sufficiently late tail has arbitrarily small spherical diameter. Any two of its points are joined by a compact subarc of the same tail. Theorem 4.4 says that the corresponding disk tail has arbitrarily small diameter. It is therefore Cauchy and converges in $\overline{\mathbb{D}}$. The limit cannot lie in $\mathbb{D}$, because continuity of f would then put b in Ω. □

4.2 Short crosscuts from finite spherical area

For a conformal map $F : \mathbb{H} \to \Omega$, let $F^{\#}$ denote its spherical length derivative, so that $F^{\#}(z)|\,\mathrm{d}z|$ is the pullback spherical line element. Injectivity and change of variables imply

$$\int_{\mathbb{H}} (F^{\#})^2\,\mathrm{d}A = \operatorname{area}_{\mathrm{sph}}(\Omega) \leq 4\pi$$

when the sphere has radius one. The integral is finite even when Ω is unbounded in every useful Euclidean chart. This is why spherical length is the natural global convention.

Theorem 4.6 (Good semicircles)**.** *Let $S_t = \{te^{iu} : 0 < u < \pi\}$ and let $A_r = \{r/2 < |z| < r,\ \operatorname{Im} z > 0\}$. There is a radius $t \in (r/2, r)$ for which $F(S_t)$ has finite spherical length $L(t)$ and*

$$L(t)^2 \le \frac{\pi}{\log 2} \int_{A_r} (F^{\#})^2 \, \mathrm{d}A.$$

One can choose radii $t_n \downarrow 0$ with $1 < t_n/t_{n+1} < 4$ and $L(t_n) \to 0$. Each image has physical limits at both ends.

Proof. For almost every t, Cauchy–Schwarz on the semicircle gives

$$L(t)^2 = \left(\int_0^{\pi} F^{\#}(te^{iu}) t \, \mathrm{d}u \right)^2 \le \pi t^2 \int_0^{\pi} F^{\#}(te^{iu})^2 \, \mathrm{d}u.$$

Consequently

$$\int_{r/2}^{r} \frac{L(t)^2}{t} \, \mathrm{d}t \le \pi \int_{A_r} (F^{\#})^2 \, \mathrm{d}A.$$

The measure $\mathrm{d}t/t$ of the interval is $\log 2$, so at least one radius satisfies the displayed bound. Choose such a radius in every dyadic annulus $(2^{-n-1}, 2^{-n})$. Consecutive choices decrease and their ratio is less than 4. Absolute continuity of the area integral makes the right-hand side tend to zero. Finally a curve of finite length in the complete sphere has Cauchy tails at either parameter end, and therefore has limits there. Those limits are on $\partial\Omega$: an interior limit would contradict continuity of F^{-1} as the parameter approaches the real axis. □

The estimate is the elementary length–area calculation behind the source's extremal-length argument. These are compatible formulations: integrating the Cauchy–Schwarz inequality over the foliation calculates the same rectangle modulus. The dyadic choice proves a factor 4 between successive radii. A factor 2 does not follow just by choosing one radius independently in each dyadic interval. The later hyperbolic argument uses $\log 4$, for which this proof supplies exactly the required justification.

The good radii can also be chosen uniformly with respect to a boundary center in the disk. For $\zeta \in \partial\mathbb{D}$, apply the same polar length–area argument to arcs $\mathbb{D} \cap \partial B(\zeta, t)$, whose angular length is at most π. All shells with $t < r$ lie in $\{1 - r < |z| < 1\}$. The integral of $(f^{\#})^2$ over this outer strip tends to zero independently of ζ. Thus a single error bound works for the length of one chosen crosscut at each center and each sufficiently small scale. The selected radius may depend on the center; no continuous selection of radii is being asserted.

Lemma 4.7 (Two landing curves with one angle)**.** *If two curves in $\mathbb{D}$ land at the same boundary point and their images under f land physically at b and c, respectively, then $b = c$.*

Proof. Use the half-plane coordinate with the common boundary point at 0. Every sufficiently small semicircle centered at 0 meets a late portion of each curve: the modulus along either curve is continuous, tends to zero, and starts above that semicircle's radius. For the good radii in Theorem 4.6, choose one meeting point on each curve. Their images approach b and c. They lie on an image crosscut of length tending to zero, so their spherical distance tends to zero. Therefore $b = c$. □

Investigation 4.8 (The logarithmic obstruction)**.** Suppose a target continuum lies in $|w - b| \le \delta$, a fixed root curve lies outside $|w - b| = R$, and its disk preimage lies outside $|z| = 1/2$ with angular span α. Derive an explicit restriction on α.

Solution. The two modulus estimates give $\alpha/\log 2 \le 2\pi/\log(R/\delta)$, hence $\alpha \le 2\pi \log 2/\log(R/\delta)$. This is a quantitative version of the contradiction argument. It is slow: to force $\alpha < \eta$ it is enough that $\delta < R\exp(-2\pi\log 2/\eta)$. The statement is conditional on the preimage lying in the specified outer annulus. It is not a global Lipschitz estimate for a Riemann map.

Investigation 4.9 (Why the continuum hypothesis cannot be deleted)**.** Give a domain and pairs z_n, w_n with $|z_n - w_n| \to 0$ for which $|g(z_n) - g(w_n)|$ does not tend to zero.

Solution. Use the exterior of $[-1, 1]$ and points approaching an interior slit point from its two sides. The inverse exterior Joukowski coordinate has two boundary values there; at 0 they correspond to i and $-i$. Inverting the exterior circle to obtain a disk coordinate preserves their separation. The two-point sets have small physical diameter but are disconnected. Every continuum in the domain joining the points must pass around an endpoint of the slit, and its diameter stays bounded below. This is precisely the obstruction excluded by Theorem 4.4.

Investigation 4.10 (A fixed fraction of good radii)**.** Let $A = \int_{A_r} (F^{\#})^2 \,\mathrm{d}A$. Show that at least half the $\mathrm{d}t/t$-measure of $(r/2, r)$ consists of radii satisfying $L(t)^2 \le 2\pi A/\log 2$.

Solution. If the bad set had logarithmic measure greater than $\log 2/2$, its contribution to $\int L(t)^2 \,\mathrm{d}t/t$ would exceed πA, contrary to the integrated inequality. This gives a positive-measure set of acceptable radii rather than a single unspecified witness. It does not choose their locations effectively from an oracle for F; that would require an input representation and certified access to the area integral.

In fact, for $\mu(B) = \int_B \mathrm{d}t/t$ and any $\lambda > 1$, the same argument gives the full threshold tradeoff

$$\mu\left\{t : L(t)^2 > \frac{\lambda\pi A}{\log 2}\right\} \le \frac{\log 2}{\lambda},$$
$$\mu\left\{t : L(t)^2 \le \frac{\lambda\pi A}{\log 2}\right\} \ge \left(1 - \frac{1}{\lambda}\right)\log 2.$$

Both sets are restricted to $(r/2, r)$. If $A = 0$, the integrated inequality makes $L = 0$ almost everywhere and proves the assertion directly, without division by A.

Investigation 4.11 (Infinite Euclidean area)**.** Explain why an unbounded conformal domain causes no failure of the good-cut argument, and why replacing spherical area by Euclidean area can fail.

Solution. The pullback spherical area of an injective map is bounded by the total area 4π. Absolute continuity therefore applies to shrinking shells. The upper half-plane itself has infinite Euclidean area, and a shell approaching a boundary point sent to infinity may have image of infinite Euclidean area. A finite-area estimate cannot be obtained from that quantity. A stereographic change of coordinate repairs the geometry locally, whereas the spherical formulation works uniformly without having to guess which boundary direction is exceptional.

Chapter 5

Prime-end compactification and impressions

Source correspondence. Lyubich, The Carathéodory Boundary Theorem, Corollary 8.9 and Exercise 8.13.

5.1 Construction without a hidden boundary-continuity assumption

Take a disjoint copy of $\partial\mathbb{D}$ and adjoin it to Ω. For $\zeta \in \partial\mathbb{D}$, call the added point $P_f(\zeta)$. Give the resulting set the topology transported from $\overline{\mathbb{D}}$ by the bijection which is f on $\mathbb{D}$ and $\zeta \mapsto P_f(\zeta)$ on the circle. Denote this space by $\overline{\Omega}^C$, and its added boundary by $\partial_C\Omega$. At this stage the construction uses a conformal coordinate. It assumes no continuity of f into the physical closure. The comparison with small physical crosscuts will supply its geometric content.

Theorem 5.1 (Conformal compactification)**.** *The space $\overline{\Omega}^C$ is compact, metrizable, and homeomorphic to a closed disk. Its open subspace Ω has its original topology. The definition is independent, up to the unique identity-preserving homeomorphism, of the Riemann map used. Every conformal bijection of conformal disks extends to a homeomorphism of these compactifications.*

Proof. The first three assertions follow from transport of topology. To compare f with another Riemann map $\widetilde{f}$, observe that $g\widetilde{f}$ is a disk automorphism. Every disk automorphism has the form $e^{it}(z-c)/(1-\bar{c}z)$ with $|c|<1$. Its denominator does not vanish on the closed disk, and its inverse has the same form. Hence it extends to a circle-preserving homeomorphism of $\overline{\mathbb{D}}$. Conjugating this extension by the two transported bijections gives a homeomorphism which is the identity on Ω. Uniqueness follows because Ω is dense and the target is Hausdorff. The same argument, applied to $g' \circ h \circ f$, proves the statement for a conformal bijection $h : \Omega \to \Omega'$. $\square$

For completeness, the boundary-coordinate comparison has an explicit metric bound. If $m(z) = e^{it}(z-c)/(1-\bar{c}z)$, then

$$|m(z)-m(w)| = \frac{(1-|c|^2)|z-w|}{|1-\bar{c}z|\,|1-\bar{c}w|} \le \frac{1+|c|}{1-|c|}|z-w|, \qquad z,w \in \overline{\mathbb{D}}.$$

The inverse has the same type of bound. Thus a coordinate change preserves vanishing disk diameters quantitatively, as well as preserving the topology of the attached circle.

The theorem alone is sometimes called the ideal-boundary construction. Its stronger content for a planar domain is that the added circle is visible through shrinking physical crosscuts. The next results prove that connection and also explain the regularity in the chain convention.

Proposition 5.2 (Short representatives and cofinality)**.** *Every $P \in \partial_C\Omega$ has a regular landing-chain representative whose crosscut lengths tend to zero. Two regular landing chains represent the same added point if and only if they are cofinal. Their fjords, together with the added boundary points lying strictly on their fjord sides, form a neighborhood basis at the represented point.*

Proof. Write $P = P_f(\zeta)$, pass to the half-plane coordinate with $\zeta = 0$, and choose good semicircles from Theorem 4.6. Their half-disks are nested and shrink to 0, and their closures have pairwise disjoint endpoints on the real line. The images are landing crosscuts of length tending to zero. They are proper because conformal maps preserve properness. The basepoint is outside sufficiently small half-disks, so these are the required fjords.

In disk coordinates, the closures of the boundary intervals of a regular chain are nested, their diameters tend to zero, and their intersection is a single point ζ. Regularity puts ζ strictly inside each earlier boundary interval. Every fixed fjord then contains a disk neighborhood of ζ: its crosscut is a compact set disjoint from ζ, so a small enough cap misses it and lies on the correct side. Conversely the diameters of the fjords tend to zero, so they eventually lie in every disk neighborhood of ζ. These two statements show cofinality with the standard cap neighborhoods. Two chains with the same ζ are therefore cofinal. If their limits differ, disjoint disk neighborhoods show that they cannot be cofinal. Transport by f gives the stated neighborhood basis. □

The neighborhood-basis argument can be expressed by two opposite containments. For each regular chain there are $r_n > 0$ and $R_n \downarrow 0$ after replacing R_n by a decreasing upper bound, such that

$$\mathbb{D} \cap B(\zeta, r_n) \subset V_n \subset \mathbb{D} \cap B(\zeta, R_n).$$

The first radius comes from the positive distance of ζ from the closed crosscut and its position inside the boundary interval. For the second one may initially take $R_n = 2 \operatorname{diam} V_n$ and then take the supremum over later indices. Positivity of every r_n and convergence of R_n are the separate facts needed for cofinality.

Proposition 5.3 (An intrinsic null-chain criterion)**.** *Let (σ_n) be ordinary physical crosscuts with pairwise disjoint closures in the sphere, nested fjords $F_{n+1} \subset F_n$, and spherical diameters tending to zero. Then, after discarding finitely many initial crosscuts, their disk preimages form a regular chain and represent a unique point of $\partial_C\Omega$.*

Proof. Each endpoint of σ_n is the limit of a curve in Ω, so Corollary 4.5 gives a limit for its preimage. The two preimage endpoint limits are different: if they agreed, Lemma 4.7 would force the two physical endpoints to agree. Thus $g(\sigma_n)$ is an ordinary disk crosscut. The same lemma shows that distinct physical endpoints belonging to different crosscuts cannot give a shared disk endpoint. Interior disjointness follows from injectivity. Therefore the closed disk crosscuts are pairwise disjoint.

Theorem 4.4, applied to compact subarcs, gives $\operatorname{diam} g(\sigma_n) \to 0$. They leave every compact disk neighborhood of 0: otherwise some point on a subsequence would approach an interior point, and the small diameter would make both boundary endpoints approach that interior point, an impossibility. A sufficiently small crosscut close to $\partial\mathbb{D}$ cuts off a fjord contained in a comparably small boundary ball, by the observation following Proposition 3.2. Thus $\operatorname{diam} g(F_n) \to 0$. Nestedness of the fjords implies nestedness of their closed boundary intervals. Pairwise disjoint crosscut endpoints ensure strict containment of later intervals in earlier ones. The nested compact intervals have a single common point, and Proposition 5.2 identifies its regular cofinal class. □

This criterion uses only physical crosscuts and spherical diameter in its hypotheses. The short representatives of Proposition 5.2 are allowed coincident physical endpoints; that slightly larger convention avoids making a false assertion about the endpoints of an arbitrary finite-length conformal image. All compactification and extension theorems are proved for this explicitly specified convention. The classical ordinary-crosscut formulation can be used when the extra endpoint separation holds, as the preceding proposition shows. No change in the boundary circle follows merely from drawing a different representative.

5.2 Impressions, cluster sets and physical projection

For $P = P_f(\zeta)$, define its impression by

$$I(P) = \bigcap_{r>0} \overline{f(\mathbb{D} \cap B(\zeta, r))}^{\widehat{\mathbb{C}}}.$$

Equivalently take the intersection of the physical closures of any regular representing fjord chain. Cofinality makes the two intersections equal. The closures are nonempty compact connected sets and are nested, so their intersection is nonempty, compact and connected. It lies in $\partial\Omega$: an interior point has a compact disk-coordinate neighborhood separated from ζ.

Nested compactness also yields convergence toward the whole impression, even when that impression is not a point. For $K_n = \overline{F_n}^{\widehat{\mathbb{C}}}$,

$$I(P) \subset K_n, \qquad \lim_{n\to\infty} \sup_{w\in K_n} \operatorname{dist}_{\mathrm{sph}}(w, I(P)) = 0.$$

Otherwise points a fixed positive distance from $I(P)$ would have a convergent subsequence on the sphere. Nestedness would put its limit in every K_n and hence in $I(P)$, a contradiction. This is convergence to a compact set and does not assert that the diameters of the fjords vanish.

Proposition 5.4 (The impression is the full cluster set)**.** *A point b belongs to $I(P_f(\zeta))$ if and only if there are $z_n \in \mathbb{D}$ with $z_n \to \zeta$ and $f(z_n) \to b$. Consequently f has a continuous physical extension at ζ if and only if its impression is a singleton.*

Proof. The preceding cofinality argument identifies the impression with the intersection of the closed images of disk caps. This is exactly $C(f, \zeta)$ for the compact spherical target in Lemma 2.1. That lemma gives the sequential characterization, and Proposition 2.2 gives the equivalence with continuous extension. Thus the new geometric ingredient is the identification of fjord impressions with cap cluster sets; the compactness argument is reused from its canonical location. □

There need not be a physical projection $\overline{\Omega}^C \to \overline{\Omega}$ extending the identity. Such a projection exists continuously precisely when every impression is a singleton. Even then it need not be injective: different prime ends may project to the same slit point. In the opposite direction, a map from the physical closure to the prime-end closure would have to select one of those ends. Unless that choice is uniquely forced, the two closures cannot be identified by the identity on the interior.

Example 5.5 (A comb with a non-singleton impression)**.** Let

$$\Omega = (0,1)^2 \setminus \bigcup_{n\geq 2} (\{1/n\} \times (0, 7/10]).$$

Every deleted tooth is attached to the bottom side of the square in the closed complement. The teeth accumulate on the left side. The domain is open because the only accumulation of the

teeth away from individual teeth lies on that excluded side. It is connected: a point in any gap can first move vertically above height $7/10$, where all the gaps communicate. Its complement in the sphere is connected, since the outside of the square and all the teeth meet the bottom boundary. The standard planar simply-connectedness criterion therefore makes Ω a conformal disk.

Fix a root in the upper right portion. For $n \geq 5$, take the polygonal crosscut which goes from $(0, 7/10 + 1/n)$ horizontally to $(1/n, 7/10 + 1/n)$ and then vertically down to $(1/n, 7/10)$. It has length $2/n$, its interior lies in Ω, and its distinct endpoints lie on the left boundary and a tooth tip. These closed crosscuts are pairwise disjoint. Their fjords are

$$F_n = \Omega \cap ((0, 1/n) \times (0, 7/10 + 1/n)).$$

They are connected because their thin upper bands lie above all the tooth tips, and they are nested. The intrinsic null-chain criterion gives a single prime end P. Direct intersection of the physical closures gives

$$I(P) = \{0\} \times [0, 7/10].$$

For the inclusion from left to right, the horizontal widths and the excess heights tend to zero. For the reverse inclusion, every neighborhood of a point on that vertical segment meets one of the gaps with $x < 1/n$, for every fixed n. Thus each such point belongs to every $\overline{F}_n$. The impression is a whole segment although the crosscuts have lengths tending to zero. This is the precise failure of "short crosscut implies small physical fjord" without local connectivity.

The two scales in this example are therefore explicitly separated:

$$\ell_{\mathrm{Euc}}(\sigma_n) = \frac{2}{n} \longrightarrow 0, \qquad \operatorname{diam}_{\mathrm{Euc}} F_n \geq \frac{7}{10}, \qquad \operatorname{diam}_{\mathrm{sph}} I(P) \geq d_{\mathrm{sph}}(0, 7i/10) > 0.$$

The lower bounds follow from the endpoints of the vertical impression, which belong to the closure of every fjord; taking closure does not change diameter.

The complement is not locally connected at $(0, y)$ with $0 < y < 7/10$. In a ball of radius smaller than both y and $7/10 - y$, the nearby teeth are separated from the left-side part of the complement and from one another; their connections run down to the distant bottom side. Every relative neighborhood of $(0, y)$ includes points of arbitrarily close teeth, so no connected neighborhood can remain in that ball. This verifies the obstruction directly and agrees with Theorem 6.4. The example establishes a qualitative boundary phenomenon; no claim of a computable Riemann map for the comb is needed.

Investigation 5.6 (Checking the comb impression)**.** Why does every interior point of the vertical impression belong to every fjord closure, even though the fjords contain no points with $x = 0$?

Solution. Fix n and a height $0 < y < 7/10$. Choose a gap between consecutive teeth with horizontal coordinate smaller than both $1/n$ and an arbitrary $\eta > 0$. A point in that gap at height y belongs to F_n and lies within η of $(0, y)$. This proves membership in $\overline{F}_n$. The same argument, with heights approaching 0 or $7/10$, gives the two endpoints. Physical closure is taken separately at every stage before intersection; replacing it by an intersection of the open fjords would give the empty set and lose the boundary information.

Investigation 5.7 (The disk impression)**.** Compute all impressions for $\Omega = \mathbb{D}$ using both cap neighborhoods and a regular chain of semicircular crosscuts.

Solution. The closure of the cap at ζ is contained in $\overline{B(\zeta, r)}$, so its intersection over $r > 0$ is $\{\zeta\}$. Every regular chain is cofinal with these caps by Proposition 5.2, hence gives the same intersection. This checks that the construction has exactly one prime end for each ordinary disk boundary point; it also shows why the irregular nest in Example 3.4 must not be admitted as an additional class.

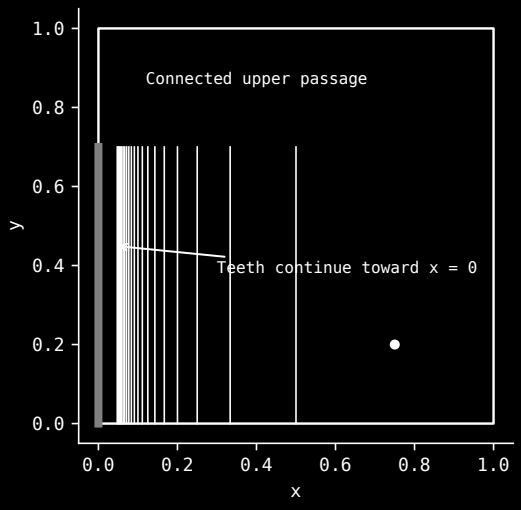


Figure 5.1: A finite prefix of the comb boundary in Example 5.5. The omitted teeth continue toward the left side. The illustrated finite prefix is a schematic of the infinite domain, not a numerical proof of its nonlocal connectivity or of the limiting prime-end impression. Those facts are established by the nested-fjord argument in the text.

Investigation 5.8 (Connectedness of an impression)**.** Give a direct proof that the intersection of nested nonempty compact connected subsets of a compact metric space is connected.

Solution. Suppose the intersection were contained in two disjoint open sets and met both. Choose the open sets with disjoint closures around the two compact parts of the alleged separation. The complement of their union is compact and misses the intersection. If every nested set met this complement, compactness would give a point of the intersection there. Therefore a late nested set lies in the union of the two open sets. It still meets both, because it contains the intersection, contradicting its connectedness. Nonemptiness is the finite-intersection property for nested compact sets.

Investigation 5.9 (A continuous extension can be many-to-one)**.** Show that continuous extension of a Riemann map does not imply that its boundary map is injective.

Solution. For the exterior disk coordinate w, the map $J(w) = (w + w^{-1})/2$ maps $|w| > 1$ conformally onto $\widehat{\mathbb{C}} \setminus [-1, 1]$ and extends continuously to the circle. On that circle $J(e^{it}) = \cos t$. Every point in $(-1, 1)$ has two preimages, while -1 and 1 have one each. Composing with disk inversion makes this a disk parametrization in the sphere. All impressions are singletons, but the boundary projection folds the circle onto the segment. The physical distinction between one point and two accesses accounts for the failure of injectivity.

Investigation 5.10 (Independence of a finite initial segment)**.** Show that deleting finitely many terms from a regular chain changes neither its cofinal class nor its impression, and explain why deleting infinitely many terms needs a cofinality condition.

Solution. Every retained term is an original term; every deleted initial term contains every sufficiently late retained term. This proves cofinality. The intersections of nested closures agree because an intersection of all later sets is already contained in every earlier one. An infinite subsequence with indices tending to infinity is also cofinal and causes no change. By contrast, a selection whose indices remain bounded might retain only an early fjord; its closure generally contains interior points and cannot represent the same impression. The issue is approach to arbitrarily late stages, not the mere cardinality of the retained list.

Chapter 6

Local connectivity and conformal boundary extension

Source correspondence. Lyubich, §8.2, the Carathéodory–Torhorst and Conformal Schönflies theorems.

6.1 From local connectedness to small connecting arcs

A space is locally connected if every point has a basis of connected open neighborhoods. For a compact metric continuum, this qualitative definition has a uniform consequence: nearby points can be joined inside a set of small diameter. Compactness, connectedness, path connectedness and local connectedness have distinct jobs in the following argument.

Lemma 6.1 (Uniform local arcs)**.** *Let K be a compact, connected, locally connected metric space. For every $\varepsilon > 0$ there is $\delta > 0$ such that any distinct $x, y \in K$ with $d(x, y) < \delta$ can be joined by an arc in K of diameter less than ε.*

Proof. For each $x \in K$, choose a connected relatively open neighborhood U_x whose closure has diameter less than ε. This is possible by first taking a sufficiently small ball and then a connected open neighborhood inside a still smaller ball. A finite subcover of these neighborhoods has a Lebesgue number $\delta > 0$. Thus the two-point set $\{x, y\}$ lies in some connected open U with small closure.

We give the path construction inside $\overline{U}$. Every connected open subset W of K can be covered by connected relatively open sets V of arbitrarily small diameter whose closures lie in W. Indeed local connectedness gives a small connected neighborhood of each point, and metric regularity lets its closure stay inside W. The overlap graph of this cover connects any set containing a specified first endpoint to any set containing a specified second endpoint. Otherwise the unions of the two graph classes would separate W into disjoint nonempty open subsets. Only a finite chain is needed between the two selected vertices of a connected graph.

Choose a finite such chain from x to y and select junction points in successive overlaps. Assign successive subintervals of $[0, 1]$ to these sets, with their endpoints mapped to the selected junction points. Repeat inside each assigned set, using a finite chain of smaller connected open sets with closures in the parent and diameters at most 2^{-n} at stage n. Subdivide further if necessary so that every parameter interval has length at most 2^{-n}. Previously assigned vertex values are retained. The assigned vertices form a dense subset of $[0, 1]$.

The resulting map on this dense subset is uniformly continuous. To verify this, fix a stage n. Two parameters closer than the minimum length of its finitely many intervals lie in either one interval or two adjacent intervals. All their later assigned values lie in the closures of the

corresponding parent sets. In the adjacent case those closures contain the common vertex value, so the distance between the two values is at most 2^{1-n}. Completeness of K extends the map to a continuous path on $[0,1]$. Every value belongs to $\overline{U}$, by construction. The path therefore has image of diameter less than ε. Apply the arc theorem stated at the beginning of Chapter 3 to extract an embedded arc between the distinct endpoints, without increasing its diameter. □

In the dense-vertex construction, let v denote the initially assigned map and let τ_n be the minimum length of a stage-n parameter interval. The uniform-continuity calculation used above is precisely

$$|s-t| < \tau_n \quad \Longrightarrow \quad d(v(s), v(t)) \le 2^{1-n}, \qquad s,t \text{ assigned vertices.}$$

For any target error choose n with 2^{1-n} below that error and then use the positive number τ_n. No lower bound on τ_n uniform in n is required for extension from the dense set.

The lemma supplies an arc but does not bound its length. A locally connected continuum may contain very long or nonrectifiable arcs in a small ball. Only diameter is needed for the separation argument, so imposing a rectifiability hypothesis here would unnecessarily weaken the boundary extension theorem.

Lemma 6.2 (Boundary local connectivity fills into the complement)**.** *If $\partial\Omega$ is locally connected, then $K = \widehat{\mathbb{C}} \setminus \Omega$ is locally connected.*

Proof. At an interior point of K a sufficiently small spherical ball is a connected neighborhood contained in K. Consider a point $b \in \partial K$ and use a plane coordinate on a small neighborhood of b. Given $\varepsilon > 0$, choose a connected relative neighborhood V of b in ∂K contained in $B(b, \varepsilon/2)$. Choose $\delta > 0$ so small that $\partial K \cap B(b, 2\delta) \subset V$ and $3\delta < \varepsilon/2$.

For each $x \in K \cap B(b,\delta)$ which is not already on the boundary, choose a nearest boundary point q_x. Its distance from x is at most $|x-b| < \delta$, so $q_x \in \partial K \cap B(b, 2\delta) \subset V$. The segment $[x, q_x]$ lies in K: before reaching a nearest boundary point, it cannot leave the interior component of K containing x. The union of V and all these segments is connected, lies in $B(b,\varepsilon)$, and contains $K \cap B(b,\delta)$. Thus b has arbitrarily small connected relative neighborhoods in K.

For completeness, connected neighborhoods rather than connected open neighborhoods suffice. In any open set $W \subset K$, take its component containing a point x. Every point of that component has a connected neighborhood contained in W, and that neighborhood stays in the same component. The component is therefore open. Components of open sets give the required basis, proving local connectedness. □

Lemma 6.3 (Small crosscuts cut off small fjords)**.** *Assume that $K = \widehat{\mathbb{C}} \setminus \Omega$ is locally connected. For every $\varepsilon > 0$ there is $\delta > 0$ such that a landing crosscut of spherical diameter less than δ, sufficiently close to $\partial\Omega$, has fjord diameter less than ε. The proximity requirement can be chosen uniformly to exclude the fixed basepoint a from the small enclosing ball.*

Proof. Take ε smaller, if necessary, than a fixed fraction of the spherical distance from a to $\partial\Omega$. Work in a spherical ball small enough that its complement is connected and its geometry admits a plane chart. Let p, q be the two endpoint values of the crosscut. If they are distinct, Lemma 6.1 joins them by an arc $\beta \subset K$ of arbitrarily small diameter once δ is sufficiently small. The crosscut and β meet only at their endpoints, because their interiors lie in Ω and K, respectively. Their union is a Jordan curve. If $p = q$, the closed image of the landing crosscut itself is a Jordan curve; no complementary arc is needed.

In both cases this Jordan curve lies in a small spherical ball disjoint from a. The Jordan side which does not meet the complement of that ball is contained in the ball: its complement is connected and disjoint from the curve. Both local sides of an interior point of the crosscut

contain points of Ω. Since the complementary arc is entirely in K, the two components of Ω minus the crosscut lie on the two sides of the Jordan curve. The side containing a is the large side. The fjord is therefore contained in the small ball, whose diameter was chosen below ε. □

In this argument let D be the diameter of the closed crosscut and B the diameter of its complementary arc, taking $B = 0$ in the coincident-end case. Since both pieces contain an endpoint p, their Jordan union lies in the spherical ball about p of radius $\max\{D, B\}$. At the small scales already required to exclude a, the estimate is

$$F \subset \overline{B}_{\mathrm{sph}}(p, \max\{D, B\}) \quad \Longrightarrow \quad \operatorname{diam}_{\mathrm{sph}} F \leq 2\max\{D, B\}.$$

This records why diameter of the complementary connection suffices; its arclength does not enter the bound.

The proof explains the role of local connectivity. A short crosscut can hide a long fjord when its two physical ends cannot be joined by a small arc in the complement. It is the small complementary connection, rather than shortness alone, which closes a local Jordan barrier.

6.2 The boundary extension equivalence

Theorem 6.4 (Carathéodory–Torhorst)**.** *For a conformal disk $\Omega \subset \widehat{\mathbb{C}}$, the following are equivalent:*

(i) $f : \mathbb{D} \to \Omega$ *extends continuously to* $\overline{f} : \overline{\mathbb{D}} \to \overline{\Omega}$ *in the spherical metric;*
(ii) $\partial\Omega$ *is locally connected;*
(iii) $K = \widehat{\mathbb{C}} \setminus \Omega$ *is locally connected.*

When these conditions hold, the boundary restriction of $\overline{f}$ is onto $\partial\Omega$, and every prime-end impression is a singleton. Neither injectivity of that restriction nor rectifiability of the physical boundary is included in this statement.

Proof. Assume (i). The circle image is exactly $\partial\Omega$. A boundary value cannot lie in Ω, since applying the continuous inverse g to an approaching interior sequence would give an interior disk limit. Conversely, if $b \in \partial\Omega$, choose $w_n \in \Omega$ tending to b and pass to a convergent subsequence of $g(w_n)$ in $\overline{\mathbb{D}}$. Its limit is on the circle and has image b.

We now prove directly that a continuous image of the circle is locally connected. Given $\eta > 0$, uniform continuity permits a finite partition of the circle into closed arcs whose images have diameter less than η. These images are compact and connected and cover the boundary. For a fixed boundary point b, take the union of all those finitely many sets which contain b. That union is connected and lies in $B(b, \eta)$. Every other set has positive distance from b; taking the minimum of finitely many positive distances shows that the union contains a relative neighborhood of b. Thus the boundary has a basis of connected neighborhoods and is locally connected. This proves (i)⇒(ii).

Lemma 6.2 proves (ii)⇒(iii). Assume (iii) and fix $\zeta \in \partial\mathbb{D}$. Proposition 5.2 supplies a regular chain at ζ whose physical crosscuts have lengths tending to zero. Their diameters tend to zero as well. Their fjords consequently have diameters tending to zero by Lemma 6.3. Their impression is a singleton, so Proposition 5.4 gives a continuous physical extension at ζ.

This gives a continuous limit from the open disk at every circle point. It also gives a continuous map on the whole closed disk. To check the only possible issue, let $\zeta_n \to \zeta$ on the circle. For each n, choose an interior z_n so close to ζ_n that $|z_n - \zeta_n| < 1/n$ and the spherical distance between $f(z_n)$ and the defined boundary value at ζ_n is less than $1/n$. The interior limit at ζ gives $f(z_n) \to \overline{f}(\zeta)$, hence the same convergence for the boundary values. Mixed interior and boundary sequences are handled in the same way. Thus (iii)⇒(i). The assertions about impressions and surjectivity were proved along the way. □

This proof follows the source's geometric mechanism but expands its short separation step into a small complementary arc and a Jordan barrier. The independent modulus argument in Chapter 4 supplies the inverse-map control. No general claim that an arbitrary continuous image of an arbitrary locally connected noncompact space is locally connected is needed; the finite compact cover of the circle is the exact argument used.

6.3 A quantitative form and its input requirements

Suppose that a function $\omega_K(t) \downarrow 0$ has been supplied such that every pair of different points of K at spherical distance at most t can be joined by an arc in K of diameter at most $\omega_K(t)$. Let

$$A(r) = \int_{\{1-r<|z|<1\}} (f^{\#})^2 \, \mathrm{d}A, \qquad L(r) = \left(\frac{\pi A(r)}{\log 2}\right)^{1/2}.$$

The finite-area calculation proves $A(r) \to 0$. Around each $\zeta \in \partial\mathbb{D}$ there is a crosscut on a circle of radius between $r/2$ and r whose physical length is at most $L(r)$. The small-Jordan-barrier proof then gives, for all sufficiently small r,

$$\operatorname{diam}_{\mathrm{sph}} f(\mathbb{D} \cap B(\zeta, r/2)) \le 2 \max\{L(r), \omega_K(L(r))\}.$$

The containment of the smaller cap in the selected fjord justifies use of $r/2$ on the left. The bound is uniform in ζ; the threshold also ensures that the enclosing ball misses a.

This is a usable quantitative implication when both A and ω_K have controlled bounds. Qualitative local connectivity supplies existence of an arc modulus but not an algorithm for evaluating one. Likewise finite area supplies a limit, not a computable rate from an unspecified description of f. The formula isolates the additional input needed for an effective boundary approximation. It does not manufacture a numerical error bar from a plotted polygon or a finite cloud of sampled boundary points.

6.4 Boundary-arc uniqueness and Jordan injectivity

Lemma 6.5 (Uniqueness on an open boundary arc)**.** *Let u be holomorphic on one side of a smooth circular boundary arc and continuous on the arc. If u is constant there, it is constant on a neighborhood on its holomorphic side, and hence on its connected domain.*

Proof. Subtract the constant and use a fractional linear coordinate taking a shorter subarc to an interval of the real line. We obtain a holomorphic function v on an upper half-neighborhood, continuous and zero on the interval. Define the reflected function on the lower half-neighborhood by $\widetilde{v}(z) = \overline{v(\overline{z})}$, and use v above the line. The two formulas agree continuously on the interval.

To prove holomorphicity across the interval, integrate around a triangle which crosses it. Cut the triangle along the parallel lines $\operatorname{Im} z = \pm\epsilon$. The integrals in the upper and lower parts vanish by Cauchy's theorem. The two new horizontal edges cancel in the limit because the reflected function is continuous. The remaining short edges tend to zero by boundedness on a compact neighborhood. Thus the integral around every sufficiently small triangle is zero; Morera's theorem gives holomorphicity across the interval. The extension vanishes on that interval, which now lies inside its domain, so the identity theorem makes it zero. Undo the coordinate and subtraction. This proves the source's boundary-arc uniqueness assertion without invoking a positive-measure boundary theorem. □

Theorem 6.6 (Conformal Schönflies theorem)**.** *If $J \subset \widehat{\mathbb{C}}$ is a Jordan curve and Ω is either component of its complement, then every conformal bijection $f : \mathbb{D} \to \Omega$ extends to a homeomorphism $\overline{\mathbb{D}} \to \overline{\Omega}$.*

Proof. The Jordan curve is locally connected, so Theorem 6.4 gives a continuous extension $\overline{f}$ onto the physical closure. It remains to prove injectivity on the boundary. Suppose two distinct circle points ζ_1, ζ_2 have the same physical image p. Join them by an ordinary crosscut c of the disk. Its image together with p is a Jordan curve Γ: the open image is embedded in Ω, while its two endpoints are the one point $p \notin \Omega$.

The set $J \setminus \{p\}$ is connected, since a circle minus one point is connected. It is disjoint from Γ, and so lies entirely on one side of Γ. The other side, say U, is disjoint from J and has points of Ω near the interior of $f(c)$. Since a connected set missing J lies in one Jordan component of the sphere minus J, it follows that $U \subset \Omega$. This is one component of $\Omega \setminus f(c)$ and corresponds under f to one disk fjord V.

The open circle arc bounding V is mapped by continuity into both J and $\overline{U}$. Their intersection is $\{p\}$. Hence $\overline{f}$ is constant on that open arc. In a local physical coordinate finite at p, Lemma 6.5 makes f constant, a contradiction. Therefore $\overline{f}$ is injective on the circle. Interior values cannot coincide with boundary values, and interior injectivity was already known. The continuous bijection from the compact closed disk to the Hausdorff physical closure is a homeomorphism. □

The argument separates two distinct uses of topology. The topological Schoenflies theorem supplied disk models for Jordan sides; it did not imply that the analytic map f has boundary values. Local connectivity supplied those values, and boundary-arc uniqueness then forced their injectivity. The result therefore does not assume the conformal conclusion as a prerequisite.

In a coordinate ψ with $\psi(p) = 0$, the decisive analytic step of the injectivity proof is the implication chain

$$\begin{aligned} \overline{f}(I) \subset J \cap \overline{U} = \{p\} &\implies (\psi \circ f)|_I = 0, \\ &\implies \psi \circ f \equiv 0 \text{ locally} \implies f \text{ is constant.} \end{aligned}$$

Here I is the nonempty open circle arc bounding V, and the middle implication is applied locally along a shorter arc before the identity theorem is used in the connected domain. It is constancy on an arc, not merely equality at its two endpoints, which creates the contradiction.

Investigation 6.7 (Local connectivity without a length bound)**.** Why does the boundary extension theorem apply to a Jordan curve of infinite length? Identify the part of the proof which would break if one replaced "small diameter" by "short arc" without justification.

Solution. A Jordan curve is homeomorphic to a circle, hence locally connected regardless of its length. Lemma 6.1 gives arcs of small diameter but does not claim that they have finite length. The Jordan-barrier argument uses only containment in a small ball, so it remains valid. Demanding a short complementary arc would insert an unproved and generally false rectifiability condition. The crosscuts coming from area do have short spherical length; the complementary boundary connections need only have small diameter. These are different parts of the construction.

Investigation 6.8 (A boundary map cannot collapse an arc)**.** Suppose a Riemann map has a continuous extension and two boundary points have the same value. Must the whole interval between them have that value?

Solution. No. For the slit example the circle values are $\cos t$, and t and $-t$ have the same value without constancy on either intervening arc. In fact a nonconstant conformal map cannot be constant on any nonempty open boundary arc, by Lemma 6.5. Thus its fibers may contain several points, but they have empty interior in the circle. This distinction is why equality of two endpoint values alone is insufficient for the Jordan injectivity proof; the proof used the connectedness of $J \setminus \{p\}$ to force constancy on an entire arc.

Investigation 6.9 (A quantitative arc modulus)**.** Assume $\omega_K(t) \le Ct^\alpha$ for $0 < t < t_0$, with $0 < \alpha \le 1$, and $A(r) \le Br^\beta$ with $\beta > 0$. Derive a boundary oscillation exponent from the preceding estimate.

Solution. We have $L(r) \le (\pi B/\log 2)^{1/2} r^{\beta/2}$. For small r, $\max\{L(r), CL(r)^\alpha\}$ is bounded by a constant times $r^{\alpha\beta/2}$, because $\alpha \le 1$. Therefore the spherical oscillation on a cap of radius $r/2$ is at most $C' r^{\alpha\beta/2}$, with C' depending only on the displayed constants and the small-scale threshold. This is a conditional Hölder estimate. The assumptions on the complementary arc modulus and the area tail must be established for the actual domain; local connectivity alone supplies neither exponent.

An explicit admissible constant follows by putting $C_0 = (\pi B/\log 2)^{1/2}$. Once $0 < r \le 1$ is below all the stated small-scale thresholds,

$$\begin{aligned} 2\max\{L(r), CL(r)^\alpha\} &\le 2\max\{C_0 r^{\beta/2}, CC_0^\alpha r^{\alpha\beta/2}\} \\ &\le 2\max\{C_0, CC_0^\alpha\}\, r^{\alpha\beta/2}. \end{aligned}$$

The last inequality uses $\beta/2 \ge \alpha\beta/2$ and $r \le 1$, which fixes the direction of comparison between the two powers.

Investigation 6.10 (A finite immersed curve)**.** Let Γ be the image of a smooth immersed circle with only transverse self-intersections, and let Ω be the unbounded complementary component, with ∞ adjoined. Describe its continuous exterior boundary map and the multiplicity at a point of Γ.

Solution. The image is a finite embedded graph with smooth edges. Finiteness follows because an immersion is locally injective uniformly on its compact parameter circle, while transverse intersections away from the diagonal are isolated in a compact set of parameter pairs. The boundary of the unbounded face is a union of finitely many closed edges and vertices, hence is locally connected. Filling the bounded faces gives a connected compact complement of Ω, and the domain is a conformal disk in the sphere. Theorem 6.4 gives continuous extension of its exterior uniformization to the circle, with range $\partial\Omega \subset \Gamma$. It need not cover edges of Γ hidden from the unbounded face.

At a point b of this finite graph, take a ball so small that it contains no other vertex and that its smooth incident arcs cut it into the usual finite local sectors. The sectors lying in Ω are exactly the components of $\Omega \cap B(b, r)$ for all sufficiently small r. Each such sector gives one local access to b, by a curve within the sector. Two sectors cannot give the same access, while two curves in one sector can be joined inside every smaller sector neighborhood. The angle–access correspondence proved in Theorem 8.8 therefore shows that the number of circle preimages of b is exactly this number of exterior sectors. If no sector belongs to Ω, both numbers are zero. At a smooth exposed edge there is one exterior sector; at an exposed crossing there may be more. The local sector count, rather than the number of parametrization visits of the original immersed curve, is the invariant.

Chapter 7

Naturality, tame ends and boundary-fixing maps

Source correspondence. Lyubich, Exercises 8.10 and 8.12 and Corollary 8.11.

A conformal compactification is automatically natural under conformal maps. A stronger fact is available for a homeomorphism of the physical closures, provided it maps the specified open domain onto the specified open domain. This qualification matters when a closure fills a slit: its topological interior can be larger than the original domain.

Theorem 7.1 (Naturality under a physical closure homeomorphism)**.** *Let $h : \overline{\Omega} \to \overline{\Omega'}$ be a homeomorphism of the physical closures with $h(\Omega) = \Omega'$. Its interior restriction extends uniquely to a homeomorphism $h_C : \overline{\Omega}^C \to \overline{\Omega'}^C$. No conformality or orientation hypothesis is required for this extension.*

Proof. Normalize disk coordinates at a and $h(a)$ and set $H = g' \circ h \circ f : \mathbb{D} \to \mathbb{D}$. Fix $\zeta \in \partial\mathbb{D}$. Choose a regular short landing-crosscut chain at ζ as in Proposition 5.2. Write its crosscuts in the physical domain as σ_n. Their spherical diameters tend to zero. Uniform continuity of h on the compact physical closure gives $\operatorname{diam} h(\sigma_n) \to 0$. The continuum estimate for g' then implies $\operatorname{diam} g'h(\sigma_n) \to 0$.

To expose the order of the two uniform choices, fix $\varepsilon > 0$. Choose $\eta > 0$ from the inverse-continuum theorem for g', and then $\delta > 0$ from uniform continuity of h. For each compact subarc $c \subset \sigma_n$ the resulting chain is

$$\operatorname{diam}_{\mathrm{sph}} c < \delta \implies \operatorname{diam}_{\mathrm{sph}} h(c) < \eta \implies \operatorname{diam} g'h(c) < \varepsilon.$$

Taking the supremum over endpoint pairs extends the bound to the whole crosscut. Connectedness is retained at both steps by continuity.

These are proper disk crosscuts. They eventually leave every compact subset of the disk, since the original physical crosscuts leave every compact subset of Ω and both interior maps are homeomorphisms. Every small proper disk crosscut lying near its boundary cuts off a small fjord on the side away from $H(0) = 0$. To verify this even when the two disk endpoints might agree, place the whole crosscut inside a small boundary ball. The connected set outside that ball lies on the root side, by separation, so the other component lies inside the ball. Therefore the images under H of the original cap neighborhoods have diameters tending to zero. Their nested closures have one circle point in common, which defines the limit $H(\zeta)$ from the entire open disk, not merely along one curve.

Repeating at every ζ and using the sequential argument in Theorem 6.4 produces a continuous extension of H to the closed disk. Apply the same reasoning to h^{-1}. The two extended maps compose to the identity on the dense open disk and hence on its closure. Thus they are inverse

homeomorphisms. Transport them to the prime-end compactifications. Uniqueness again follows from density and the Hausdorff property. □

The proof deliberately uses small connected sets. Uniform continuity of h alone does not make $g'hf$ uniformly continuous, since neither Riemann map was assumed to extend physically. The short-crosscut estimate and the inverse continuum lemma supply the missing argument.

Example 7.2 (Physical boundary fixing need not fix prime ends)**.** Let $\Omega = \widehat{\mathbb{C}} \setminus [-1, 1]$ and let $h(z) = \overline{z}$, with $h(\infty) = \infty$. Its physical closure is the whole sphere. The map h is a homeomorphism of that closure, preserves Ω, and fixes every physical boundary point. It interchanges the upper and lower approaches to every point of $(-1, 1)$. In the exterior Joukowski coordinate, its induced circle action is $e^{it} \mapsto e^{-it}$, which is not the identity. Thus a boundary-pointwise fixing assertion for unrestricted homeomorphisms is false. An orientation convention or a stronger hypothesis must be supplied before drawing a conclusion about the induced circle action.

This example addresses the unrestricted-homeomorphism reading of the source's boundary-fixing clause. It does not claim that an explicitly orientation-preserving version has been refuted. Rather than silently adding an unstated convention, the next result gives a sufficient condition with a complete proof. In the source's conjugation formula we write the map directions unambiguously as $H = g \circ h \circ f$; reversing f and g would produce an expression with the wrong domain.

Proposition 7.3 (Boundary-fixed isotopies fix the prime-end circle)**.** *Suppose $(h_s)_{0 \le s \le 1}$ is an isotopy of the physical closure, continuous jointly in (s, z), with h_0 the identity, $h_s(\Omega) = \Omega$, and $h_s(b) = b$ for every $b \in \partial\Omega$ and every s. Then the induced map of h_1 on $\partial_C\Omega$ is the identity.*

Proof. First consider a circle point ζ represented by a curve $\gamma : [0, 1) \to \Omega$ which lands physically at b and tends to $P_f(\zeta)$ in the prime-end compactification. For each t, the set $E_t = \{h_s(\gamma(t)) : 0 \le s \le 1\}$ is a compact continuum. Joint continuity on the compact parameter interval and the physical closure gives uniform convergence $h_s(\gamma(t)) \to b$ as $t \uparrow 1$. Thus $\operatorname{diam} E_t \to 0$. Theorem 4.4 gives $\operatorname{diam} g(E_t) \to 0$. Since $g(h_0\gamma(t)) \to \zeta$, it follows that $g(h_1\gamma(t)) \to \zeta$ as well. Naturality then says that the induced circle map fixes ζ.

The limit comparison in this step is the pair of estimates

$$\operatorname{diam}_{\mathrm{sph}} E_t \le 2 \sup_{0 \le s \le 1} d_{\mathrm{sph}}(h_s(\gamma(t)), h_s(b)) \longrightarrow 0,$$
$$|g(h_1(\gamma(t))) - \zeta| \le \operatorname{diam} g(E_t) + |g(\gamma(t)) - \zeta| \longrightarrow 0.$$

Joint continuity on the compact product gives the uniform limit in the first line, and $h_0 = \mathrm{id}$ supplies the comparison point in the second.

Such landing circle points are dense. To see this near an arbitrary circle point, use the short finite-length crosscuts of Theorem 4.6. Each of their endpoint directions is represented by a curve with a physical limit, and those directions approach the chosen circle point as the semicircles shrink. The circle homeomorphism induced by h_1 fixes this dense set; continuity makes it the identity everywhere. □

7.1 A noncuspidal tame end

Suppose a domain in the sphere has an end with a conformal collar $F : A(r_0, 1) \to A \subset \Omega$, where $0 < r_0 < 1$, and the outer circle corresponds to the end under consideration. The phrase "corresponds to the end" means that approaching this circle leaves every compact subset of the

end collar toward the specified complementary component, rather than toward the inner seam. This is a noncuspidal collar; a puncture has a different ideal completion and is not included by relabeling it.

Attach a copy of $|w| = 1$ to A using its annulus coordinate and leave the rest of the domain unchanged. Short boundary caps lie entirely in $A(r_0, 1)$, so the spherical area and good-crosscut proofs apply verbatim on those caps. The inverse-continuum argument also applies near the outer end: use a fixed circle $|w| = r_1$ with $r_0 < r_1 < 1$ as the root curve, and use radial segments from r_1 to an outer continuum. Its modulus lower bound is $|J|/\log(1/r_1)$; the same small-target logarithmic annulus gives the upper bound tending to zero. Continua sufficiently close to the specified end avoid the inner part of the collar, which is why the end qualification is needed.

For an outer continuum with coordinate radius bounded below by r_1, contained physically in $B(b, \delta)$ while the fixed root curve avoids $B(b, R)$, with $0 < \delta < R$, this collar calculation reads

$$\frac{|J|}{\log(1/r_1)} \le \mathcal{M} \le \frac{2\pi}{\log(R/\delta)} \quad \Longrightarrow \quad |J| \le \frac{2\pi \log(1/r_1)}{\log(R/\delta)} \longrightarrow 0.$$

The physical balls here are in one fixed finite coordinate and $\delta \downarrow 0$ with R fixed. The set J is the radial projection in the annular coordinate; the positive number $\log(1/r_1)$ is the exact replacement for the disk root constant.

If two conformal collars describe the same end, choose a smaller collar contained in their overlap. The coordinate transition is a conformal homeomorphism of an outer-end neighborhood. Apply the same short-crosscut and inverse-continuum argument to it and its inverse. It extends to an inverse pair of circle maps. Consequently the attached circle and its topology are independent of the chosen collar. In particular a statement about this prime-end circle does not depend on an arbitrary inner cutting curve. Impressions are formed by intersecting physical closures of its shrinking fjords, exactly as for a disk.

This construction is local at one specified tame end. It does not claim a circle for every end of an infinitely connected domain, nor identify all ends with isolated complementary components. A global compactification in that setting needs additional hypotheses and a separate end space. The collar calculation proves the particular extension requested in source Exercise 8.12 without importing a finite-type assumption for the entire domain.

Investigation 7.4 (Conjugation has the correct direction)**.** Let $f : \mathbb{D} \to \Omega$ and $h : \Omega \to \Omega$ be a homeomorphism. Write its disk conjugate, its inverse, and the effect of replacing f by $f \circ m$ for a disk automorphism m.

Solution. The disk conjugate is $H = f^{-1}hf$, its inverse is $f^{-1}h^{-1}f$, and the new conjugate is $m^{-1}Hm$. Each expression maps the disk to itself. If h extends as a physical closure homeomorphism, Theorem 7.1 extends H to the circle. A new disk coordinate merely conjugates that circle map by the boundary automorphism of m. Whether the induced map is the identity is therefore coordinate independent. The order of composition is forced by the domains, not by a convention for which letter denotes the Riemann map.

Investigation 7.5 (A twisted disk map which does extend)**.** Let $q : [0, 1] \to \mathbb{R}$ be continuous and let $h(re^{it}) = re^{i(t+q(r))}$. Determine its boundary action and give a boundary-fixed isotopy when $q(1) = 0$.

Solution. The map and its inverse are continuous on the closed disk, with boundary action $e^{it} \mapsto e^{i(t+q(1))}$. If $q(1) = 0$, the maps $h_s(re^{it}) = re^{i(t+sq(r))}$ form a jointly continuous isotopy fixing the boundary pointwise. Their induced prime-end maps are all the identity, in agreement with Proposition 7.3. Unlike the diverging twist in the earlier investigation, the rotation angle has a finite boundary limit. The criterion is a statement about the actual boundary behavior, not the size of the interior angular derivative.

Investigation 7.6 (The annular seam is not the ideal end)**.** In $A(r_0, 1)$ choose two inner seams $r_0 < r_1 < r_2 < 1$. Show that the prime-end circles obtained from $A(r_1, 1)$ and $A(r_2, 1)$ agree.

Solution. The identity is a conformal identification on their common outer collar $A(r_2, 1)$. Every sequence approaching $|w| = 1$ eventually lies in this common region, and the small cap neighborhoods are cofinal in the two collars. Their added points and their neighborhood bases therefore agree. Changing the seam removes a compact annular band from the collar; it does not change its end. By contrast, exchanging inner and outer boundary components would describe the other annular end and must be recorded as such.

Investigation 7.7 (Images of impressions under closure homeomorphisms)**.** Under the hypotheses of Theorem 7.1, prove $I(h_C(P)) = h(I(P))$.

Solution. If $b \in I(P)$, choose interior points converging to P in the prime-end topology and to b physically. Continuity of h_C and h sends them to a sequence converging to $h_C(P)$ and $h(b)$, respectively, so $h(b) \in I(h_C(P))$. This proves one inclusion. Apply the same argument to h^{-1} to obtain the reverse inclusion. The formula preserves singleton impressions, but it does not choose an individual prime end merely from a physical point belonging to several impressions. It is therefore consistent with the conjugation example, which permutes ends while fixing their singleton physical images.

Chapter 8

Accesses, landing curves, and the Lindelöf principle

Source correspondence. Lyubich, §8.3, Lindelöf Theorem, Exercise 8.16, Corollary 8.17, and Lemma 8.18.

The ideal circle records ways of approaching a domain, whereas its physical boundary records limiting locations. These records need not coincide. A slit has two sides, and approaching an interior point of the slit from its upper side is a different operation from approaching from its lower side. Both operations have the same limiting complex number. The purpose of this chapter is to distinguish these operations precisely and then to show why the conformal radial curves detect all accessible locations.

Throughout this chapter, $U \subset \widehat{\mathbb{C}}$ is a conformal disk, with a complement containing at least two points, and $f : \mathbb{D} \to U$ is conformal. Limits and diameters on the sphere use its usual spherical metric. In a fixed finite coordinate neighbourhood the Euclidean and spherical metrics give the same limits. A curve is a continuous map, and its image need not be simple unless this is stated. A landing curve $\gamma : [0, 1) \to U$ has a limit $b \in \partial U$ as $t \uparrow 1$.

8.1 A local definition of an access

Definition 8.1 (Accessible point and access)**.** A boundary point b is accessible if a curve in U lands at b. Two curves landing at b define the same access if, for every sufficiently small spherical ball $B(b, \varepsilon)$, their sufficiently late tails belong to the same connected component of $U \cap B(b, \varepsilon)$. An access is an equivalence class under this relation.

Each tail is connected and is eventually contained in the ball, so it belongs to one component. Shrinking the ball merely refines the component. Reflexivity and symmetry are immediate. For transitivity, choose late tails of three curves in the ball. If the first and second occupy one component and the second and third occupy one component, the component containing the second is common to all three. Thus the definition really gives an equivalence relation. The choice of spherical balls is immaterial: any nested neighbourhood basis at b gives the same relation, by containment between sufficiently small neighbourhoods.

This definition is especially useful when a boundary has many branches. It asks whether two approaches can still be connected close to their common endpoint. It does not require their images to remain close pointwise, nor does it identify approaches merely because their endpoints coincide.

Writing the two curves as γ_1, γ_2, the tail quantifiers, for a sufficiently small $\varepsilon_0 > 0$, are explicitly

$$\gamma_1 \sim_b \gamma_2 \quad \Longleftrightarrow \quad \begin{array}{c} \forall \varepsilon \in (0, \varepsilon_0)\ \exists T < 1\ \exists V \text{ a component of } U \cap B(b, \varepsilon) : \\ \gamma_1([T, 1)) \cup \gamma_2([T, 1)) \subset V. \end{array}$$

The parameter T and component V may depend on ε.

Proposition 8.2 (Interpretation by homotopies)**.** *In a conformal disk, the access relation is equivalently described by homotopies of landing curves whose approach to the endpoint is uniform in the homotopy parameter. Starting points may move within U. More precisely, after adjoining the endpoint b, the homotopy is continuous on the closed parameter square, maps its endpoint edge to b, and maps the rest of each curve into U.*

Proof. A homotopy with this property maps a sufficiently thin strip adjacent to the endpoint edge into any prescribed ball about b, by uniform continuity on the compact square. Each transverse segment of that strip connects the two curves within the ball. Their tails therefore belong to the same component.

For the converse, choose a spherical coordinate chart whose omitted point is a point of $\widehat{\mathbb{C}} \setminus U$ different from b. In this chart U is a simply connected plane domain and b is finite. Small Euclidean balls may replace the spherical balls. Each component of $U \cap B(b, \varepsilon)$ is simply connected. One way to verify this is to take a Jordan curve in such a component. Its bounded interior lies in U, because U is simply connected, and lies in the ball, because the ball is convex. Hence the interior lies in the same component. The Jordan-curve criterion for simple connectivity proves the assertion.

Choose a decreasing sequence $\varepsilon_n \downarrow 0$ and increasing parameters $t_n \uparrow 1$ so that both curve tails after t_n belong to a common component V_n of $U \cap B(b, \varepsilon_n)$. The choices can be made with $V_{n+1} \subset V_n$: both components contain a sufficiently late common tail of either curve. Join the two curve points at t_n by a path in V_n. The joining paths at levels n and $n+1$, together with the two intervening curve segments, form a loop in V_n. Simple connectivity fills this loop by a continuous disk in V_n. Regard that disk as a homotopy on the strip between t_n and t_{n+1}. The fillings agree on their prescribed joining edges, so they paste to a homotopy on all the late strips. Its images approach b uniformly, because the nth strip lies in $B(b, \varepsilon_n)$. The remaining initial strip can be filled in U, using its simple connectivity. Adjoining the endpoint edge gives the required continuous homotopy. If $H(s, t)$ denotes this pasted homotopy in the chosen planar coordinate, nesting of the balls gives the endpoint continuity estimate directly:

$$\sup_{\substack{0 \le s \le 1 \\ t_n \le t < 1}} |H(s, t) - b| \le \varepsilon_n \longrightarrow 0.$$

□

The uniformity clause is substantive. A family of curves may each land at b while the locations where they enter a small ball escape to later and later parameters as the family varies. Such a family does not by itself give a homotopy continuous at the endpoint edge. The local-component definition avoids this ambiguity.

8.2 A finite-area estimate for bounded conformal maps

The proof of landing uses a quantitative analytic fact. It is weaker than a pointwise bound on the derivative, but stronger than the mere existence of a radial subsequence.

Lemma 8.3 (Vanishing rescaled derivative)**.** *Let $g : \mathbb{H} \to \mathbb{C}$ be bounded and conformal. For every fixed $A < \infty$,*

$$\sup_{|x| \le Ay} y|g'(x+iy)| \longrightarrow 0 \qquad (y \downarrow 0).$$

More generally the same conclusion holds for a holomorphic g whenever $\int_{\mathbb{H}} |g'|^2 \, \mathrm{d}A < \infty$.

Proof. For a conformal map, change of variables gives

$$\int_{\mathbb{H}} |g'(w)|^2 \, \mathrm{d}A(w) = \operatorname{area}(g(\mathbb{H})) < \infty,$$

since the image is bounded. If $w = x + iy$, the disk $B(w, y/2)$ lies in $\mathbb{H}$. The mean inequality for the nonnegative subharmonic function $|g'|^2$ gives

$$y^2|g'(w)|^2 \le \frac{4}{\pi} \int_{B(w,y/2)} |g'(\zeta)|^2 \, \mathrm{d}A(\zeta).$$

For $|x| \le Ay$, these disks are contained in $\{\zeta \in \mathbb{H} : |\zeta| \le (A+2)y\}$. The integral over this shrinking set tends to zero by the absolute continuity of the integral of an integrable function. The estimate is uniform in x in the stated range. This proof uses no regularity of the image boundary. □

The factor y is essential. A derivative can diverge near a corner, and indeed it will do so in the slit examples below. The conclusion says that an interval of Euclidean length comparable to its height has an image of vanishing length when it approaches the boundary nontangentially.

Lemma 8.4 (Good semicircles at every dyadic scale)**.** *Let $g : \mathbb{H} \to \mathbb{C}$ be conformal and bounded. There are radii $r_n \in (2^{-n-1}, 2^{-n})$ such that the image of the open semicircle $S_{r_n} = \{r_n e^{it} : 0 < t < \pi\}$ has finite length L_n, with $L_n \to 0$. In particular $1 < r_n/r_{n+1} < 4$.*

Proof. Write $L(r) = \int_0^\pi |g'(re^{it})| r \, \mathrm{d}t$ whenever the integral is finite. Cauchy–Schwarz yields

$$L(r)^2 \le \pi r \int_0^\pi |g'(re^{it})|^2 r \, \mathrm{d}t.$$

Integrating with respect to $\mathrm{d}r/r$ over $(s, 2s)$ gives

$$\int_s^{2s} L(r)^2 \frac{\mathrm{d}r}{r} \le \pi \int_{\{s<|w|<2s\} \cap \mathbb{H}} |g'(w)|^2 \, \mathrm{d}A(w).$$

Consequently some radius in this interval satisfies

$$L(r)^2 \le \frac{\pi}{\log 2} \int_{\{s<|w|<2s\} \cap \mathbb{H}} |g'(w)|^2 \, \mathrm{d}A(w).$$

Take $s = 2^{-n-1}$. The right side tends to zero, because the total integral is finite. The interval choices give the asserted ratio bound. A finite-length open arc is Cauchy at each endpoint, so its image has limits there; its diameter is at most its length. □

One radius is selected independently in each dyadic interval. These choices give a factor of four between consecutive selected radii, not automatically a factor of two. The factor of four is sufficient for the landing proof. There is therefore no reason to impose a stronger spacing claim without an additional selection argument. This is a small example of why an apparently harmless quantitative detail must be tracked through a proof.

8.3 The landing theorem, including unbounded domains

Theorem 8.5 (Lindelöf landing principle)**.** *Suppose $\delta : [0,1) \to \mathbb{D}$ lands at $\xi \in \partial\mathbb{D}$ and $f(\delta(t)) \to b \in \partial U$. Then*

$$f(r\xi) \longrightarrow b \qquad (r \uparrow 1).$$

The image of the radius and the given image curve define the same access to b.

Proof. First suppose the image is bounded. A Möbius map from $\mathbb{H}$ to $\mathbb{D}$ can be chosen to send 0 to ξ and the positive imaginary axis to the diameter ending at ξ. It is enough to consider a bounded conformal map $g : \mathbb{H} \to \mathbb{C}$ and a curve tending to 0 whose image tends to b.

Choose the good semicircles of Lemma 8.4. The given curve crosses each sufficiently small semicircle. Moreover it has a crossing parameter $t_n \to 1$: every initial compact part of the curve has positive distance from 0. Choose a crossing after any such initial part. Its image tends to b. Since the entire image semicircle has diameter at most $L_n \to 0$, it follows that

$$g(ir_n) \longrightarrow b.$$

For $r_{n+1} \le y \le r_n$, integrate along the vertical segment:

$$|g(iy) - g(ir_n)| \le \int_{r_{n+1}}^{r_n} |g'(iv)| \, \mathrm{d}v \le \left(\sup_{0<v\le r_n} v|g'(iv)| \right) \log 4.$$

Lemma 8.3 makes the last quantity tend to zero. This fills the gaps between the selected heights and proves the full radial limit. A subsequence alone would not have sufficed.

For a general spherical domain we now give an explicit bounded reduction. Choose a complementary point $a \neq b$ and a Möbius map M taking b to 0 and a to ∞. The simply connected domain $M(U)$ omits 0, so it admits a holomorphic square root s. That square root is injective: equality of its values implies equality after squaring. Its image V contains no pair of opposite points, since such a pair would give two points of $M(U)$ with the same square and contradict the chosen single-valued branch. Choose $v_0 \in V$ and $\eta > 0$ with $B(v_0, \eta) \subset V$. Then $B(-v_0, \eta)$ is disjoint from V. Thus

$$h(z) = \frac{1}{s(M(z)) + v_0}$$

is a bounded conformal map on U, with bound $1/\eta$. As $z \to b$ in U, the modulus of $s(M(z))$ tends to zero, so $h(z) \to 1/v_0$. The bounded case applied to $h \circ f$ shows $(h \circ f)(r\xi) \to 1/v_0$. The inverse expression

$$R(w) = M^{-1}((1/w - v_0)^2)$$

is a rational map on the sphere and is continuous there. Since $R \circ h$ is the identity on U, it follows that $f(r\xi) \to b$.

It remains to verify the access assertion. In the bounded model, the good semicircle connects a late point of the original curve to a point of the radial curve, and its image lies in an arbitrarily small neighbourhood of $1/v_0$ for all sufficiently large n. Applying the continuous map R makes this a connecting path in an arbitrarily small neighbourhood of b. Both landing curves have their subsequent tails in the same small ball. The connecting path therefore puts these tails in one component of the intersection with U. Definition 8.1 gives equality of accesses. □

The bounded reduction is not a claim that every conformal disk is a bounded plane domain in a Möbius coordinate. An exterior slit cannot be made bounded by merely omitting a point of its slit boundary. The square root separates two sides before the reciprocal makes the image bounded. The final rational expression is used only to transfer limits back to the original sphere; it is not asserted to be globally injective.

8.4 Uniform approach inside a Stolz region

Definition 8.6 (Stolz region)**.** For $\xi \in \partial\mathbb{D}$ and $A > 1$, set

$$S_A(\xi) = \{z \in \mathbb{D} : |z - \xi| \le A(1 - |z|)\}.$$

A nontangential limit is a limit uniform over each fixed such region as its points approach ξ. Uniformity is not required simultaneously over all A.

Theorem 8.7 (A landing radius controls every fixed Stolz region)**.** *If $f(r\xi) \to b$, then $f(z) \to b$ uniformly for $z \to \xi$ in $S_A(\xi)$, for each finite $A > 1$.*

Proof. Apply the same bounded reduction as in Theorem 8.5, now using the landing radius as the given curve. After changing to a half-plane coordinate, a fixed Stolz region lies near 0 inside a cone $|x| \le C_A y$. For its bounded conformal map g, join $x + iy$ to iy by a horizontal segment. Every point on that segment has height y, and its real part has modulus at most $C_A y$. Consequently

$$|g(x + iy) - g(iy)| \le C_A \sup_{|u| \le C_A y} y|g'(u + iy)| \longrightarrow 0$$

by Lemma 8.3. The radial value $g(iy)$ has its known limit, so the entire cone has that limit. The conversion between a disk Stolz region and a half-plane cone follows from the explicit Möbius formula, whose derivative at the boundary point is finite and nonzero. For example, put $\zeta = \overline{\xi}z$ and $w = i(1 - \zeta)/(1 + \zeta) = x + iy$. Then, near ξ,

$$y = \frac{1 - |z|^2}{|1 + \overline{\xi}z|^2}, \qquad \frac{|x|}{y} = \frac{2|\operatorname{Im}(\overline{\xi}z)|}{1 - |z|^2},$$
$$\frac{|x|}{y} \le \frac{2|z - \xi|}{(1 - |z|)(1 + |z|)} \le \frac{2A}{1 + |z|} \le 2A.$$

Finally apply the uniform continuity of the rational map R on the compact sphere. □

This theorem proves Exercise 8.16 in the source at the stated level of generality. It does not assert unrestricted continuity at the ideal boundary point. Tangential approaches can explore parts of an impression that no fixed Stolz region sees. Singleton impressions and full boundary continuity belong to the stronger hypotheses developed in the preceding prime-end chapters.

8.5 Accessible points and angles

Theorem 8.8 (An angle for each access)**.** *Let γ be any curve in U landing at $b \in \partial U$. There is a unique $\xi \in \partial\mathbb{D}$ such that the radial curve $f(r\xi)$ lands at b with the same access as γ. Two landing curves have the same inverse-map limit if and only if they land at the same point with the same access.*

Proof. By the inverse-map landing result, Corollary 4.5, the curve $f^{-1} \circ \gamma$ lands at some $\xi \in \partial\mathbb{D}$. Theorem 8.5 gives a radial curve with the required endpoint and access. If two curves have the same inverse-map limit, applying that theorem to each gives the same radial curve; both its endpoint and its access are unique, so the endpoints and accesses coincide.

Conversely suppose two curves have endpoint b and the same access. For every small ε, late points on the curves can be joined by a path in $U \cap B(b, \varepsilon)$. The image of that path is a continuum of spherical diameter at most 2ε. The uniform continuity on continua of Theorem 4.4 says that its inverse image under f has diameter tending uniformly to zero as $\varepsilon \downarrow 0$. Choose the joined points successively farther along the two curves. Their inverse images converge to their

respective boundary limits, and their distance tends to zero. The two limits are therefore equal. In particular two different angles cannot give the same access. In quantitative form, let x_n, y_n be joined target points in balls of radii $\varepsilon_n \downarrow 0$, and let $\omega(\delta) \to 0$ be the inverse-continuum diameter bound from Theorem 4.4. For their respective inverse limits ξ_1, ξ_2,

$$|\xi_1 - \xi_2| \le |\xi_1 - f^{-1}(x_n)| + \omega(2\varepsilon_n) + |f^{-1}(y_n) - \xi_2| \longrightarrow 0.$$

□

The theorem combines the content of source Corollary 8.17 and Lemma 8.18. Its direction from an access to an angle uses the small continuum theorem. Its direction from an angle to an access uses the finite-area landing argument. Neither direction follows merely by identifying the ideal circle with the set of physical boundary points.

8.6 Cross-cuts made from rays and an equipotential

A Green cross-cut, relative to the chosen centre $f(0)$, is the image of two radial segments and a circular arc in the disk. More explicitly, choose distinct angles $\theta_- < \theta_+ < \theta_- + 2\pi$ and $0 < s < 1$. Use the radial segments from $e^{i\theta_-}$ to $se^{i\theta_-}$ and from $se^{i\theta_+}$ to $e^{i\theta_+}$, together with the circle arc $se^{i\theta}$, $\theta_- \le \theta \le \theta_+$. Its fjord is the annular sector

$$G(s; \theta_-, \theta_+) = \{re^{i\theta} : s < r < 1,\ \theta_- < \theta < \theta_+\}.$$

The image is a landing cross-cut whenever both endpoint rays land. Its two physical endpoints may coincide, but their accesses remain distinct because their angles are distinct.

Proposition 8.9 (Green replacement and cofinal Green chains)**.** *A landed cross-cut whose endpoint accesses are distinct can be replaced by a Green cross-cut with those same endpoint accesses. Moreover every prime end has a representative nested chain of Green fjords with landed endpoint rays. The assertion about a representative chain means cofinality of nests, not equality of an arbitrary original fjord with its Green replacement.*

Proof. Take inverse images of the two endpoint tails of the given cross-cut. They land at disk boundary points by Corollary 4.5. The angles are distinct by Theorem 8.8. That theorem also says that the corresponding radial images land with the prescribed accesses. Joining their points on any circle $|z| = s$ by either selected circle arc gives the required Green cross-cut. One chooses the arc whose boundary interval describes the desired side. This construction preserves endpoints and accesses; no assertion of equality of the two bounded regions has been made.

For the chain statement, work in the disk compactification. The regular representative chain supplied by Proposition 5.2 has later closed boundary intervals inside earlier open intervals; this excludes a fixed endpoint shared by an irregular shrinking nest. Its ordinary fjords representing an ideal point ξ give a neighbourhood basis at ξ, with nested boundary intervals containing ξ and diameters tending to zero. Landing angles are dense. To see this from the preceding geometric development, apply the shrinking-cross-cut construction in any small boundary interval. Its finite-length image cross-cut has two landed endpoint tails. Lindelöf then makes the radial images at those endpoint angles land, and both endpoints can be chosen inside the prescribed interval.

Choose two such landing angles on opposite sides of ξ in a small boundary interval belonging to a prescribed fjord. By moving their circle level s sufficiently close to one, their entire Green fjord lies inside the prescribed ordinary fjord: the chosen closed boundary subinterval avoids that fjord's cross-cut endpoints, and compactness separates it from the interior cross-cut. Make this choice successively, each time inside the previous Green fjord as well as the next ordinary fjord, and with angular width tending to zero and $s \uparrow 1$. This produces a nested Green chain

subordinate to the original chain. Conversely each chosen Green fjord contains the intersection of a sufficiently small disk about ξ with $\mathbb{D}$. A sufficiently late original fjord, whose disk-coordinate diameter tends to zero at ξ, is therefore contained in it. The nests are cofinal and represent the same prime end. Conformal images preserve all these containments. □

This completes the Green-cross-cut observation following source Lemma 8.18. A Green chain supplies a useful coordinate description of an approach even when its physical impression is not a singleton. Replacing one cross-cut is a finite geometric operation; representing a prime end requires the cofinal nesting argument as well.

Investigation 8.10 (A curve may revisit an old neighbourhood)**.** In the proof of Theorem 8.5, explain why a crossing of each small semicircle can be chosen at a parameter tending to one, even when the curve is not simple and crosses a semicircle many times.

Solution. Fix $T < 1$. The continuous curve on $[0, T]$ is compact and lies in the open half-plane, so its distance from 0 has a positive minimum m_T. Every semicircle with radius less than m_T is missed by this initial segment. Since the full curve approaches 0, continuity of its modulus forces a crossing after T whenever its initial modulus exceeds that radius. Thus any choice of such a crossing is eventually later than every $T < 1$. Injectivity is unnecessary. The same compactness argument handles an arbitrary reparametrization that still has its endpoint at $t = 1$.

Investigation 8.11 (Why a radial subsequence is insufficient)**.** Give a continuous function on $(0, 1)$ that converges to zero along 2^{-n} but has no limit at zero. Identify the extra estimate that prevents this behaviour in the Lindelöf proof.

Solution. The function $q(y) = \sin(2\pi \log_2 y)$ vanishes at every 2^{-n}. At $y = 2^{-n+1/4}$ it equals one, so it has no limit. The Lindelöf proof does not infer a full limit from selected good heights. It bounds the oscillation between consecutive heights by $\log 4 \sup_{v \le r_n} v|g'(iv)|$, which tends to zero. For the example, $y|q'(y)|$ does not tend to zero. This identifies the exact role of the finite-area hypothesis in filling the gaps.

Investigation 8.12 (Two accesses to the same point)**.** Let $U = \widehat{\mathbb{C}} \setminus [-1, 1]$ and $b = 0$. Show directly that curves approaching 0 from the upper and lower half-planes define different accesses, while any two such curves eventually in the upper component define the same access.

Solution. For $0 < \varepsilon < 1$, the disk $B(0, \varepsilon)$ loses its full horizontal diameter when intersected with U. What remains has exactly two components, its upper and lower half-disks. Curves in opposite components cannot be connected in that intersection. Curves eventually in the upper component have tails in the same component for every sufficiently small ε, and hence are equivalent by definition. The first assertion concerns two classes, not two physical endpoints. The explicit angle representatives will be computed in Chapter 10.

Investigation 8.13 (The endpoint of a slit)**.** For the same U, determine the number of accesses to $b = 1$ and explain why the answer differs from that at 0.

Solution. For $0 < \varepsilon < 1$, the ball about 1 loses only the radius extending leftward from its centre. Its intersection with U is connected and indeed simply connected: in polar coordinates centred at 1 it is $0 < r < \varepsilon$, $-\pi < \theta < \pi$. Every landing curve eventually lies in this one component. All such curves define one access. Upper and lower approaches can turn around the right side of the tip while remaining in an arbitrarily small ball. At an interior point of the slit the removed diameter prevents that connection.

Chapter 9

Exterior uniformization and its normalization

Source correspondence. Lyubich, §8.3 and Corollary 8.15; the leading coefficient at infinity is retained explicitly.

External rays attach the ideal-circle description to a compact set seen from infinity. The coefficient at infinity must be kept in this construction. Removing it by notation would amount to changing the physical scale of the compact set.

9.1 Full compact sets and the coefficient at infinity

Let $K \subset \mathbb{C}$ be a nondegenerate compact connected set whose complement in the sphere is simply connected. Such a set is called a full continuum or hull here. Nondegenerate means that it has more than one point. The domain $U = \widehat{\mathbb{C}} \setminus K$ contains ∞ and is a conformal disk. A Riemann map sending ∞ to the centre of the unit disk, followed by inversion, gives a conformal map

$$B : \mathbb{C} \setminus K \longrightarrow \{w \in \mathbb{C} : |w| > 1\}.$$

At infinity it has a simple pole. A rotation in the target fixes its leading coefficient to be positive, giving

$$B(z) = \frac{z}{c} + b_0 + O(z^{-1}), \qquad c > 0. \tag{9.1}$$

Equivalently its inverse has expansion

$$F(w) = cw + c_0 + c_1 w^{-1} + c_2 w^{-2} + \cdots .$$

The constant terms in these two expansions are linked by composition:

$$B(F(w)) - w = \frac{c_0}{c} + b_0 + O(w^{-1}) = 0 \quad \Longrightarrow \quad b_0 = -\frac{c_0}{c}.$$

We call c the conformal capacity of K, denoted $\operatorname{cap}(K)$. This is the usual logarithmic-capacity normalization for full continua; the present chapter needs the displayed conformal definition and not an unproved equivalence with an energy minimization definition.

Proposition 9.1 (Uniqueness and scaling)**.** *The normalized map B is unique. If $\alpha \neq 0$ and $\beta \in \mathbb{C}$, then*

$$\operatorname{cap}(\alpha K + \beta) = |\alpha| \operatorname{cap}(K), \qquad B_{\alpha K + \beta}(z) = \frac{\alpha}{|\alpha|} B_K\left(\frac{z - \beta}{\alpha}\right).$$

Proof. Two maps with the prescribed range and the same point at infinity differ by an automorphism of the exterior disk fixing infinity. Inversion turns this into a disk automorphism fixing zero, which is a rotation. Positivity of the coefficient at infinity forces that rotation to be the identity. For the transformed set, the displayed formula maps its complement conformally onto the exterior disk, because its prefactor has modulus one. Its leading coefficient is $\alpha/(|\alpha|\alpha c) = 1/(|\alpha|c)$, which is positive. Uniqueness therefore identifies it with the normalized map, and its leading coefficient proves the capacity identity. □

The normalized map for a rotated hull must rotate the target angle in the same direction as the hull. The coefficient at infinity checks that choice without any angle convention. In particular translations preserve capacity, and dilation by a positive factor multiplies capacity by that factor. A formula such as $B(z) \sim z$ is therefore valid only after the capacity has been normalized to one. The source's normalization in §8.3 requires this restriction; it is not available for a general hull.

9.2 Rays and equipotentials as actual curves

Write angles in radians in this chapter. For $r > 1$ and $\theta \in \mathbb{R}/(2\pi\mathbb{Z})$ define

$$R_\theta(r) = F(re^{i\theta}), \qquad E_r = F(\{|w| = r\}).$$

Each E_r is a simple analytic closed curve, because F is conformal on a neighbourhood of the circle. Each ray is an analytic simple curve for $r > 1$. The ray curves and level curves fill $\mathbb{C} \setminus K$ and intersect orthogonally. To verify orthogonality, their tangent vectors are respectively $F'(w)e^{i\theta}$ and $F'(w)ire^{i\theta}$; their ratio is ir, a purely imaginary nonzero number. Thus the tangent directions differ by a right angle.

The scalar function

$$g_K(z) = \log|B(z)| \tag{9.2}$$

is positive and harmonic on $\mathbb{C} \setminus K$. Locally choose a logarithm of B; its real part is g_K, and different choices change only the imaginary part by a multiple of 2π. Its gradient is nonzero because $B'/B \neq 0$. The equipotential E_r is exactly the level set $g_K = \log r$. The expansion at infinity gives

$$g_K(z) = \log|z| - \log \operatorname{cap}(K) + O(|z|^{-1}).$$

The Cauchy–Riemann equations for a local logarithm also give the coordinate form of the gradient:

$$(g_K)_x - i(g_K)_y = \frac{B'}{B}, \qquad |\nabla g_K| = \left|\frac{B'}{B}\right| > 0.$$

The logarithm is local even though its real part is global. With E_r parametrized by $F(re^{i\theta})$, its differential has period

$$\int_{E_r} \frac{B'(z)}{B(z)}\,\mathrm{d}z = \int_0^{2\pi} \frac{ire^{i\theta}}{re^{i\theta}}\,\mathrm{d}\theta = 2\pi i.$$

The formula is meaningful with physical units only after the logarithm is applied to a dimensionless ratio. Here B is dimensionless and z/c is dimensionless, so the expansion has that interpretation.

Proposition 9.2 (All external rays land for a locally connected hull)**.** *If K is locally connected, every R_θ has a limit in ∂K as $r \downarrow 1$. The landing map $\theta \mapsto \ell(\theta)$ is continuous and onto ∂K. It need not be injective.*

Proof. Apply the Carathéodory–Torhorst theorem, Theorem 6.4, to the exterior disk after inversion and to U as a spherical conformal disk. Its complementary continuum is the locally connected set K. The inverse uniformization extends continuously to the ideal circle, yielding

the limits and their continuity. Every physical boundary point is the limit of points of U. Their inverse images have a subsequence converging to the closed disk. That limit cannot be an interior point, since the original points approach the boundary. Continuity of the extended map then places the given boundary point in the image of the circle. Injectivity requires stronger topology, as the slit model will demonstrate. □

Without local connectivity, a particular ray can still land, and every accessible point still has a landing ray by Theorem 8.8. The implication in Proposition 9.2 concerns all angles and the continuous dependence of their landing locations. It must not be reversed from the mere existence of some landing rays.

9.3 The circular conductor as a normalization control

For $K = \{z : |z - z_0| \le a\}$ with $a > 0$, the normalized exterior map is

$$B(z) = \frac{z - z_0}{a}, \qquad F(w) = z_0 + aw, \qquad \operatorname{cap}(K) = a.$$

The rays are straight half-lines from z_0, the equipotentials are concentric circles, and $g_K(z) = \log(|z - z_0|/a)$. The landing map is $z_0 + ae^{i\theta}$, a homeomorphism. This example tests three separate normalizations: the exterior target has radius one, the leading coefficient is $1/a$, and g_K vanishes on the conductor. Setting all three leading quantities equal to one for an arbitrary a would be inconsistent.

If z has units of length, capacity also has units of length. A numerical value for capacity is therefore incomplete without the length unit or an explicit nondimensionalization. By contrast, the angle and the potential level $\log r$ are dimensionless. These conventions become essential when the same conformal geometry is used to derive a flux or an electrical capacitance per unit axial length.

Investigation 9.3 (A translated and rotated disk)**.** Let $K = \{z : |z - (2 + i)| \le 3\}$. Find its normalized map, capacity, ray at angle $\pi/3$, and equipotential at level $g_K = 2$.

Solution. The map is $B(z) = (z - 2 - i)/3$ and the capacity is 3 in the chosen length unit. The ray is $2 + i + 3re^{i\pi/3}$, $r > 1$. The level $g_K = 2$ is the circle $|z - 2 - i| = 3e^2$, because $\log|B| = 2$ means $|B| = e^2$. Rotating this disk about its centre changes neither the set nor the normalized map. Rotating the entire configuration about the origin rotates the centre and the rays, while preserving the positive real coefficient of z in the normalized formula.

Investigation 9.4 (Capacity normalization is an actual scaling)**.** Suppose K has capacity $c \neq 1$. Can a rotation of the target exterior disk turn $B(z) = z/c + O(1)$ into a map asymptotic to z? Give the change of physical coordinates that does permit this normalization.

Solution. A target rotation multiplies the leading coefficient by a complex number of modulus one, so it cannot change its modulus $1/c$. Put $\widetilde{z} = z/c$ and $\widetilde{K} = K/c$. Then $\widetilde{B}(\widetilde{z}) = B(c\widetilde{z})$ has leading coefficient one and maps the complement of $\widetilde{K}$ onto the unit exterior. This scales the hull itself. It changes every physical length by $1/c$, while leaving the conformal angle coordinate and the dimensionless potential levels intact.

Investigation 9.5 (Why positivity of the potential is not enough)**.** Let $v(z) = \log|B(z)| + C$ for a real constant C. Determine which of the ray foliation, the gradient, the level labels, and the zero level on the conductor changes when C changes.

Solution. The gradient is unchanged, so its integral curves and the orthogonal ray foliation are unchanged. The geometric family of level curves is also unchanged, but its labels shift

from t to $t + C$. The boundary value becomes C wherever the original potential tends to zero. Thus a potential difference or a field cannot detect this additive constant, whereas a prescribed zero-potential conductor can. Capacity is read from the specifically normalized expansion of g_K, not from an arbitrarily shifted harmonic function.

Investigation 9.6 (A degenerate hull is outside this normalization)**.** Explain why $K = \{0\}$ is excluded. Show that no conformal bijection from $\mathbb{C} \setminus \{0\}$ to $\{|w| > 1\}$ has the stated behaviour.

Solution. The sphere complement of a point is conformally the plane, not the disk. If the indicated exterior map existed, its reciprocal would be a bounded holomorphic function on the punctured plane. The singularity at zero would be removable by boundedness. It would then extend to a bounded entire function and hence be constant by Liouville's theorem, contrary to bijectivity. The positive capacity coefficient used here belongs to nondegenerate full continua; treating the point as a limiting conductor requires a separate degenerating limit.

Chapter 10

A slit resolved into its two sides

The segment $K_a = [-a, a]$, $a > 0$, provides a complete model in which the physical boundary is locally connected but is not a Jordan curve. Its exterior map can be derived algebraically, its prime ends can be counted locally, and its boundary concentrations can be calculated exactly. These three descriptions will be checked against one another.

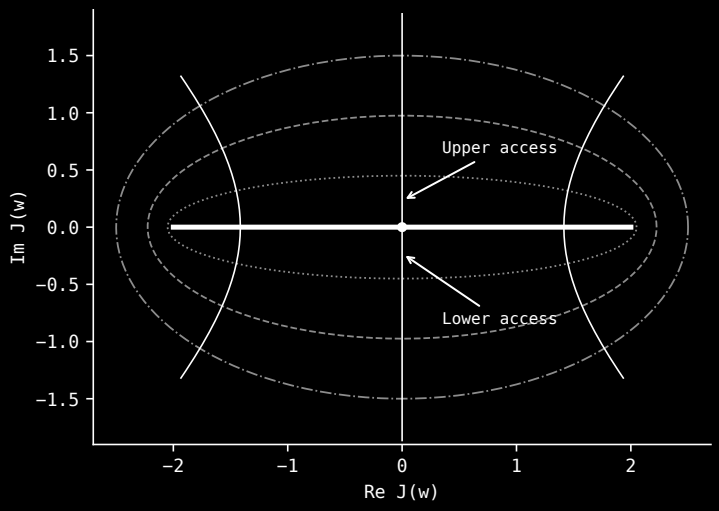


Figure 10.1: External rays and equipotentials for $F(w) = w + w^{-1}$, whose slit is $[-2, 2]$. The equipotentials are the images of $|w| = 1.25, 1.6, 2$; each displayed ray is the image of a fixed angle. The sampled curves illustrate the exact parametrization $x = 2\cosh t \cos\theta$, $y = 2\sinh t \sin\theta$ and do not constitute a numerical boundary enclosure.

10.1 The Joukowski map and its inverse branch

Proposition 10.1 (Exterior uniformization of a segment)**.** *The map*

$$F_a(w) = \frac{a}{2}(w + w^{-1}), \qquad |w| > 1,$$

is conformal onto $\mathbb{C} \setminus [-a, a]$*. Its inverse is*

$$B_a(z) = \frac{z + \sqrt{z^2 - a^2}}{a},$$

where the branch is characterized by $\sqrt{z^2 - a^2}/z \to 1$ *at infinity. Consequently* $\operatorname{cap}([-a, a]) = a/2$*.*

Proof. The derivative is $F_a'(w) = (a/2)(1-w^{-2})$, which has no zeros for $|w| > 1$. If $F_a(w) = F_a(v)$, then

$$(w - v)\left(1 - \frac{1}{wv}\right) = 0.$$

The second factor cannot vanish when both moduli exceed one, so the map is injective. Its inverse equation is $w^2 - (2z/a)w + 1 = 0$. The product of the two roots is one. A root lies on the unit circle precisely when $z = (a/2)(e^{i\theta} + e^{-i\theta}) = a\cos\theta \in [-a, a]$. For z off this segment, neither root lies on the unit circle, and their product implies that exactly one has modulus greater than one. This proves surjectivity and selects the inverse branch. The inverse is holomorphic by the nonvanishing derivative already established. Solving the quadratic gives the displayed square-root expression, with its sign fixed at infinity. Finally $F_a(w) = (a/2)w + O(w^{-1})$, so its leading coefficient is $a/2$. The same algebra locates the two boundary critical points exactly:

$$F_a(w) - a = \frac{a}{2w}(w - 1)^2, \qquad F_a(w) + a = \frac{a}{2w}(w + 1)^2.$$

Thus the quadratic contact at the two tips already appears before any asymptotic expansion is made. □

The branch specification cannot be replaced everywhere by a library's principal square root of the number $z^2 - a^2$. For a large negative real z, the required square root is negative, asymptotic to z, whereas the principal square root of the positive real number $z^2 - a^2$ is positive. Using the latter would select the root inside the unit circle and destroy the exterior inverse. The holomorphic branch is selected by continuation in the slit domain and its condition at infinity.

For stable evaluation far from the slit one can also use the identity

$$B_a(z)\,\frac{z - \sqrt{z^2 - a^2}}{a} = 1.$$

It follows from the difference of squares. This identity is useful as an algebraic check of branch and reciprocal pairing, but evaluating the small factor by subtracting two nearly equal large numbers can lose accuracy. The identity alone is not a rounding-error enclosure.

10.2 Ellipses, hyperbolas, and exact landing

Set $w = e^{t+i\theta}$ with $t > 0$. Direct expansion gives

$$x = a\cosh t\cos\theta, \qquad y = a\sinh t\sin\theta. \tag{10.1}$$

Let $Z(t, \theta) = x + iy$. Differentiating both coordinates gives the orthogonal metric and its area factor, for $t > 0$:

$$Z_\theta = iZ_t, \quad |Z_t|^2 = |Z_\theta|^2 = a^2(\sinh^2 t + \sin^2\theta),$$
$$\mathrm{Re}(Z_t\overline{Z_\theta}) = 0, \qquad \det\frac{\partial(x, y)}{\partial(t, \theta)} = a^2(\sinh^2 t + \sin^2\theta) > 0.$$

For fixed t, this is the ellipse

$$\frac{x^2}{a^2\cosh^2 t} + \frac{y^2}{a^2\sinh^2 t} = 1,$$

with foci at $\pm a$, since $a^2\cosh^2 t - a^2\sinh^2 t = a^2$. For fixed θ with $\sin\theta\cos\theta \neq 0$, elimination of t gives the corresponding branch of the confocal hyperbola

$$\frac{x^2}{a^2\cos^2\theta} - \frac{y^2}{a^2\sin^2\theta} = 1.$$

Its signs and branch are still prescribed by (10.1); the squared equation alone would include additional branches. For $\theta = 0$ or π the ray lies on the real axis beyond a tip, and for $\theta = \pi/2$ or $3\pi/2$ it lies on the positive or negative imaginary axis.

As $t \downarrow 0$,

$$F_a(e^{t+i\theta}) \longrightarrow a\cos\theta.$$

For $x \in (-a, a)$, the equation $x = a\cos\theta$ has exactly two solutions modulo 2π, one with positive sine and one with negative sine. Their ray images have respectively positive and negative imaginary parts. They therefore give the two accesses to the interior of the slit. At a there is only the angle zero, and at $-a$ only the angle π. The local component count from the preceding chapter agrees exactly with this angle count. The landing map is a continuous surjection of a circle onto an interval, and its failure of injectivity is not a failure of continuity.

Proposition 10.2 (Different landing rates at a tip and in a side)**.** *For fixed θ and $t \downarrow 0$,*

$$F_a(e^{t+i\theta}) - a\cos\theta = ia\sin\theta\, t + \frac{a}{2}\cos\theta\, t^2 + O(t^3).$$

Thus the leading displacement is linear in t at every non-tip angle, but quadratic at $\theta = 0, \pi$. On the real axis beyond the right tip,

$$g_{K_a}(a+s) = \operatorname{arcosh}(1 + s/a) = \sqrt{2s/a} + O((s/a)^{3/2}) \qquad (s \downarrow 0).$$

Proof. Expand $\cosh t = 1 + t^2/2 + O(t^4)$ and $\sinh t = t + O(t^3)$ in (10.1). At $\theta = 0$, $s = a(\cosh t - 1) = at^2/2 + O(at^4)$. Since $t > 0$, inversion gives $t = \sqrt{2s/a}(1 + O(s/a))$, and $g_{K_a} = t$ by definition. The same reasoning applies at the left tip after reflection. □

This is a local conditioning statement. A small potential increment near a tip corresponds to a quadratic physical displacement; recovering the potential from the displacement introduces a square root. It is not legitimate to assume a nonzero limiting derivative of the boundary map at every ideal angle. The derivative vanishes at the two tip angles.

10.3 Landing-angle measure and the arcsine law

Assign normalized uniform measure $\mathrm{d}\theta/(2\pi)$ to the ideal circle, and push it forward by $x = a\cos\theta$. For an integrable function q on the segment with respect to this pushed-forward measure, change of variables separately on the upper and lower semicircles gives

$$\frac{1}{2\pi}\int_0^{2\pi} q(a\cos\theta)\ \mathrm{d}\theta = \frac{1}{\pi}\int_{-a}^{a} \frac{q(x)}{\sqrt{a^2 - x^2}}\ \mathrm{d}x. \tag{10.2}$$

The formula is initially immediate for continuous q. The two sides then define finite Borel measures agreeing on continuous test functions, and hence the same measure. This last assertion follows, for example, by approximating indicators of closed intervals from above with decreasing continuous piecewise linear functions, then using the monotone-class argument for the Borel sets they generate. Equality for indicators gives equality for simple functions and then for nonnegative measurable q by monotone convergence. Integrable complex q follows by decomposing its real and imaginary positive and negative parts; the completed measures give the same conclusion for their measurable representatives. Each side of the slit contributes half of the displayed density. When physical points are recorded without their side, both contributions must be added.

The density diverges at the tips but is integrable. For $0 < \varepsilon < 2a$, the measure of the interval $[a - \varepsilon, a]$ is exactly

$$\frac{1}{\pi}\arccos(1 - \varepsilon/a) = \frac{1}{\pi}\sqrt{2\varepsilon/a} + O((\varepsilon/a)^{3/2}). \tag{10.3}$$

The first equality follows by finding the two short angular intervals adjacent to angle zero; the second follows by inverting the cosine expansion. In particular the singleton tip has mass zero. A divergent density does not imply an atom. The distinction is important when a plot of the density places a very large value in its first numerical bin.

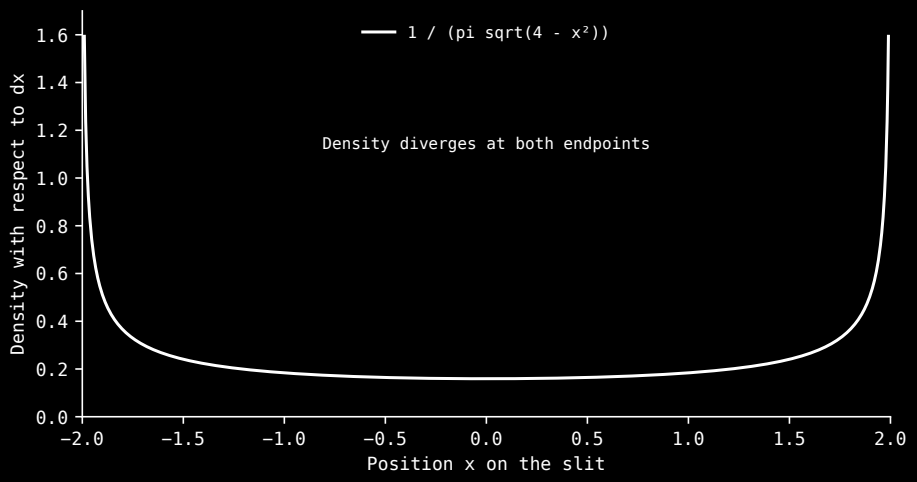


Figure 10.2: The density $1/(\pi\sqrt{4-x^2})$ for the landing-angle measure on $[-2,2]$. The displayed samples lie strictly inside the segment. The endpoint divergence is integrable, and each singleton endpoint has zero measure; no finite sampled peak is an endpoint value.

The general definition and invariance properties of harmonic measure are developed in the radial-limit chapters. Here the pushforward is an explicit calculation independent of that terminology. Its later identification with normalized potential flux will provide a second calculation of the same measure and check the factor of two contributed by the two sides.

10.4 Boundary data on a slit: physical values and side values

A continuous function q on the physical segment pulls back to $Q(\theta) = q(a\cos\theta)$, which obeys $Q(\theta) = Q(2\pi - \theta)$. An arbitrary continuous function on the ideal circle need not have this symmetry. It can prescribe different values on the upper and lower sides of an interior physical point. This is a valid boundary condition on the prime-end boundary, but it is not a single-valued continuous condition on the physical segment.

For example, $Q(\theta) = \sin\theta$ has opposite signs on the two sides and vanishes at the two tips. It defines continuous ideal boundary data. At a physical point $x \in (-a, a)$ the two prescribed values are $\pm\sqrt{1-(x/a)^2}$. There is no continuous physical function q whose pullback is Q. The obstruction is exactly the failure of Q to be constant on the fibres of the landing map. If a numerical solver merges the two sides into one list of physical nodes without retaining side labels, it cannot represent this boundary condition correctly. More explicitly, for $-a < x < a$ the two side values induced by Q are

$$q_+(x) = Q(\arccos(x/a)), \qquad q_-(x) = Q(2\pi - \arccos(x/a)).$$

Equality of these expressions is the fibre condition; taking their limits at $x = \pm a$ also records the continuity requirement at the tips.

Investigation 10.3 (Check the inverse on both real half-axes)**.** For $z > a$ and $z < -a$, determine the sign of the required square root in $B_a(z)$ and verify $|B_a(z)| > 1$ in both cases.

Solution. For $z > a$, the branch is $+\sqrt{z^2 - a^2}$, so $B_a(z) = (z+\sqrt{z^2 - a^2})/a > 1$. For $z < -a$, the branch is $-\sqrt{z^2 - a^2}$ with the radical on the right positive, hence $B_a(z) = (z-\sqrt{z^2 - a^2})/a < -1$. In each case the other quadratic root is its reciprocal and lies inside the unit disk. This verifies the branch through a global range property, not merely through a symbolic square-root identity.

Investigation 10.4 (The capacity of a segment of prescribed length)**.** A straight conducting segment has endpoints $p \neq q$. Compute its conformal capacity and explain why its angle does not enter the answer.

Solution. Its length is $L = |q - p|$. It is a translation and rotation of $[-L/2, L/2]$, whose capacity is $(L/2)/2 = L/4$ by Proposition 10.1. Translations and rotations preserve capacity by Proposition 9.1. The result is a length, not an electrical capacitance; conversion to an electrical quantity requires a surrounding conductor, a material parameter, and specified voltage boundary conditions.

Investigation 10.5 (A weighted moment without a singular integral)**.** Evaluate the first and second moments of the density in (10.2), and compute the total measure of $[0, a]$.

Solution. Using $x = a\cos\theta$, the first moment is $a(2\pi)^{-1}\int_0^{2\pi}\cos\theta\,\mathrm{d}\theta = 0$. The second is $a^2(2\pi)^{-1}\int_0^{2\pi}\cos^2\theta\,\mathrm{d}\theta = a^2/2$. The preimage of $[0, a]$ is the set of angles with nonnegative cosine, of total angular length π, so its measure is $1/2$. This route automatically treats the endpoint singularities and avoids assigning finite point values to an unbounded density.

Investigation 10.6 (Which ideal data descend to a physical boundary?)**.** Show that a continuous 2π-periodic function Q is of the form $q(a\cos\theta)$ for a continuous q on $[-a, a]$ if and only if $Q(\theta) = Q(2\pi - \theta)$ for all θ.

Solution. Necessity follows because the cosine has that symmetry. For sufficiency, define $q(x) = Q(\arccos(x/a))$ using $\arccos : [-1, 1] \to [0, \pi]$. This is continuous, including both endpoints. Every angle is either in $[0, \pi]$ or has the same cosine as its reflected angle in that interval. The assumed symmetry therefore gives $Q(\theta) = q(a\cos\theta)$ for all angles. No differentiability is needed. The test is precisely constancy on the two-point fibres, together with continuity at the one-point fibres at the tips.

Investigation 10.7 (Angle resolution near a tip)**.** Equally spaced ideal angles have spacing $h = 2\pi/N$. Determine the distance from a to the landing point at angle h, and compare it with the distance between landing points near angle $\pi/2$.

Solution. The tip distance is $a(1 - \cos h) = ah^2/2 + O(ah^4)$, of order aN^{-2}. Near $\pi/2$, the derivative of $a\cos\theta$ has magnitude a, so one angular step gives distance $ah + O(ah^2)$, of order aN^{-1}. Uniform angle sampling is therefore nonuniform in physical arclength. It clusters quadratically near the tips, exactly where the pushforward density is largest. This clustering is geometric and does not itself certify the numerical accuracy of a field computed there.

Chapter 11

Length, exceptional sets, and differentiation

The final appendix of the source changes the question. A boundary need not be locally connected, and the conformal map need not have a continuous extension to the whole closed disk. Nevertheless, one can ask whether a typical direction has a limit. The word "typical" will mean outside a set of zero angular length; it does not mean outside a finite set, outside a countable set, or outside a set that is negligible for every measure on the geometric boundary. This chapter develops the real analysis needed to make that distinction precise. The subsequent arguments are classical. Their purpose here is to supply the proofs omitted in the source appendix, not to claim a new Fatou theorem.

We use the circle in radian coordinates,

$$\mathbb{T} = \mathbb{R}/(2\pi\mathbb{Z}), \qquad \zeta(t) = e^{it}, \qquad \mathrm{d}m(t) = \frac{\mathrm{d}t}{2\pi}.$$

Thus $m(\mathbb{T}) = 1$. A source angle $\theta \in \mathbb{R}/\mathbb{Z}$ corresponds to $t = 2\pi\theta$. Multiplication of a measure by 2π changes numerical lengths but changes neither null sets nor the meaning of almost everywhere. All integrals over $\mathbb{T}$ below use m unless another measure is shown. Write $d(s,t) = \min_{k\in\mathbb{Z}} |s - t + 2\pi k|$ for angular distance.

11.1 The measure and integration boundary

For completeness, the elementary measure facts used below are recorded with their construction. A countable family of open arcs covers a set E; the infimum of the sums of their normalized lengths is its outer measure $m^*(E)$. The empty family gives $m^*(\varnothing) = 0$, inclusion gives monotonicity, and combining covers with total excess less than $\varepsilon 2^{-j}$ proves countable subadditivity. A set E is measurable when, for every set A,

$$m^*(A) = m^*(A \cap E) + m^*(A \setminus E).$$

The reverse inequality is automatic, so the content is the inequality from left to right. Splitting every covering arc at the endpoints of a fixed arc shows that arcs are measurable: the finitely many splitting endpoints have outer measure zero, since each admits covers of arbitrarily short total length. Applying the splitting identity successively proves closure under finite unions and complements. For pairwise disjoint measurable E_j, the successive identities give

$$m^*(A) \geq \sum_{j=1}^{n} m^*(A \cap E_j) + m^*\left(A \setminus \bigcup_{j\geq 1} E_j\right).$$

Let n increase and combine this with subadditivity for $A \cap \bigcup_j E_j$. This proves measurability of the countable union and countable additivity of $m = m^*$. Arbitrary countable unions reduce to the disjoint case by taking successive differences. Subsets of outer-measure-zero sets satisfy the splitting identity too. This is the completed length measure used in the book; Borel sets are measurable because the open arcs generate the topology.

The normalized measure of an arc is its prescribed length. For the lower bound, a countable open cover of a compact subarc has a finite subcover. The sum of the covering lengths is at least the length of the subarc, by ordering the endpoints and adding the lengths of the intervals between them. Increase the compact subarc to the original arc. The upper bound is obtained by covering with a slightly longer arc. This also proves $m(\mathbb{T}) = 1$.

Lemma 11.1 (Regular approximation)**.** *For every measurable $E \subset \mathbb{T}$ and every $\varepsilon > 0$ there are a compact set K and an open set O with*

$$K \subset E \subset O, \qquad m(O \setminus K) < \varepsilon.$$

Consequently, finite linear combinations of indicators of arcs approximate integrable functions in L^1, and continuous functions approximate them in L^1. Continuous functions also approximate square-integrable functions in L^2.

Proof. Choose an open-arc cover of E whose total length is below $m(E) + \varepsilon/2$. Its union O satisfies $m(O \setminus E) < \varepsilon/2$. Apply the same construction to the complement of E and take a complement to obtain compact $K \subset E$ with $m(E \setminus K) < \varepsilon/2$.

Here is the approximation argument in detail. For a nonnegative measurable f, first replace it by $\min(f, N)$ and then round its values downward to multiples of $1/N$. The resulting finite-valued measurable functions increase to f if one instead chooses dyadic truncations and dyadic meshes. For an integrable complex function, perform this truncation and rounding on real and imaginary parts, positive and negative parts separately. Integrability makes the discarded tails small; the rounding error is uniformly small on a space of measure one. Thus measurable simple functions are dense in L^1. The same reasoning applied to the squared error gives density in L^2. For each indicator 1_E, choose $K \subset E \subset O$ as above. Compactness gives a finite union of arcs V with $K \subset V \subset O$, so $\|1_E - 1_V\|_1 \le m(O \setminus K)$ and the squared L^2 error has the same bound. Finally the function

$$q(t) = \frac{d(t, \mathbb{T} \setminus O)}{d(t, \mathbb{T} \setminus O) + d(t, K)}$$

is continuous, equals one on K, equals zero outside O, and lies between zero and one. The denominator is positive because the disjoint closed sets K and $\mathbb{T} \setminus O$ have positive distance. Empty sets and the whole circle are handled by constant functions. The difference $q - 1_E$ is supported in $O \setminus K$, giving the asserted approximations. For the same cutoff q, the error estimate in both required norms is

$$\|q - 1_E\|_p^p = \int_{O \setminus K} |q - 1_E|^p \, \mathrm{d}m \le m(O \setminus K) < \varepsilon, \qquad p \in \{1, 2\}.$$

□

For a nonnegative simple function $s = \sum_j c_j 1_{E_j}$, with disjoint measurable sets and $c_j \ge 0$, set $\int s \, \mathrm{d}m = \sum_j c_j m(E_j)$. For a nonnegative measurable f, define its integral as the supremum of the integrals of such $s \le f$. Integrable means $\int |f| \, \mathrm{d}m < \infty$; complex integrals are obtained by integrating the four real nonnegative parts. Two functions that agree outside a null set represent the same integrable function. Pointwise assertions, however, require a chosen representative. The distinction will matter when a boundary trace is identified at its Lebesgue points.

Lemma 11.2 (Convergence and size estimates)**.** *The integral just defined has the following properties.*

1. *If $0 \le f_n \uparrow f$, then $\int f_n \to \int f$.*
2. *If $f_n \ge 0$, then $\int \liminf_n f_n \le \liminf_n \int f_n$.*
3. *If $f_n \to f$ almost everywhere and $|f_n| \le g$ for an integrable g, then $\int |f_n - f| \to 0$.*
4. *For $f \in L^1$ and $\lambda > 0$, $m\{|f| > \lambda\} \le \|f\|_1/\lambda$.*
5. *If $f, g \in L^2$, then $|\int f\overline{g}\,\mathrm{d}m| \le \|f\|_2\|g\|_2$.*

Proof. For the first assertion, monotonicity bounds the limit above by $\int f$. Given a nonnegative simple $s \le f$ and $0 < c < 1$, the sets on which $f_n \ge cs$ increase to the support of s, apart from its zero level. Countable additivity implies continuity of measure for increasing sets: write their union as the disjoint union of successive differences. Hence $\liminf \int f_n \ge c \int s$. Take the supremum over s, then let $c \uparrow 1$. For the second assertion put $h_n = \inf_{k \ge n} f_k$; these functions increase to the lower limit, and $\int h_n \le \inf_{k \ge n} \int f_k$. For the third, apply the second assertion to $2g - |f_n - f|$, after removing the null set where convergence or domination fails. This gives $2\int g \le 2\int g - \limsup \int |f_n - f|$. The fourth follows from $|f| \ge \lambda 1_{\{|f| > \lambda\}}$, with a limiting argument if desired at the strict inequality. For the fifth, $\int |f - tg|^2 \ge 0$ for every complex t. Minimizing this quadratic in t proves the claim when $\|g\|_2 > 0$; the zero case is immediate. Explicitly, with $c = \int f\overline{g}\,\mathrm{d}m$ and $\|g\|_2 > 0$,

$$0 \le \left\| f - \frac{c}{\|g\|_2^2} g \right\|_2^2 = \|f\|_2^2 - \frac{|c|^2}{\|g\|_2^2} \quad \Longrightarrow \quad |c|^2 \le \|f\|_2^2 \|g\|_2^2.$$

□

The second assertion is Fatou's lemma for integrals. It is different from Fatou's boundary theorem for holomorphic functions. The latter requires the rest of the present development; it does not follow simply by naming the former. We will use the integral lemma again in the boundary uniqueness argument, where a family of logarithms is nonnegative but not dominated.

We also need interchange of two nonnegative integrals on a rectangle or a product of circles. Construct product area by covers with rectangles and products of their side lengths, exactly as length was constructed by arc covers; splitting at horizontal and vertical sides proves the rectangle identities. For an indicator of a rectangle, the two iterated integrals and the product-area integral agree by direct multiplication of lengths. They therefore agree for finite unions of rectangles, after disjoint subdivision.

Here are the extension details. Let $\mathcal{A}$ be that algebra of sets. The class $\mathcal{C}$ of Borel sets whose section integrals are measurable and whose two iterated integrals agree with their area is closed under increasing unions, by monotone convergence. It is closed under decreasing intersections as well, by applying dominated convergence to indicators on the finite containing rectangle. The elementary monotone-class argument shows that any such class containing $\mathcal{A}$ contains its generated σ-algebra. To verify the argument rather than assume it, let $\mathcal{M}$ be the smallest class closed under monotone limits and containing $\mathcal{A}$. The class of sets whose complements lie in $\mathcal{M}$ is a monotone class containing $\mathcal{A}$, so $\mathcal{M}$ is closed under complements. For fixed $E \in \mathcal{A}$, the sets F with $E \cap F \in \mathcal{M}$ form another monotone class containing $\mathcal{A}$; hence they include $\mathcal{M}$. Now fix $F \in \mathcal{M}$ and repeat with the roles reversed. This shows that $\mathcal{M}$ is closed under finite intersections. Complements give finite unions, and an arbitrary countable union is the increasing limit of its finite partial unions. Thus $\mathcal{M}$ is a σ-algebra, proving the assertion. Applied to $\mathcal{C}$, this proves the section and integration identities for Borel sets.

A Borel null set has sections of zero length outside a null set, since its nonnegative section integral has integral zero. Subsets of such a set therefore do not alter the iterated integrals outside a null set of sections, using the completeness of length measure. This handles the completed product measure. Monotone approximation by simple functions now proves interchange for

nonnegative measurable functions; an absolutely integrable complex function follows by its four nonnegative real parts. This is the form of Tonelli–Fubini used below. It does not permit an unjustified exchange for a signed expression whose absolute integrability has not been checked.

11.2 Completeness without a functional-analysis black box

For $1 \le p < \infty$, let $\|f\|_p = (\int |f|^p \, \mathrm{d}m)^{1/p}$, identifying functions equal almost everywhere. We need completeness only for $p = 1, 2$. The triangle inequality for $p = 1$ is immediate. For $p = 2$, expand $|f + g|^2$ and use Cauchy–Schwarz to get $\|f + g\|_2 \le \|f\|_2 + \|g\|_2$.

Lemma 11.3 (L^1 and L^2 completeness)**.** *Every Cauchy sequence in $L^p(\mathbb{T})$, for $p = 1$ or $p = 2$, has a limit in that norm. Every norm-convergent sequence has a subsequence converging pointwise almost everywhere.*

Proof. From a Cauchy sequence choose a subsequence g_j with $\|g_{j+1} - g_j\|_p \le 2^{-j}$. Because $m(\mathbb{T}) = 1$, Cauchy–Schwarz gives $\|h\|_1 \le \|h\|_2$, so in both cases

$$\int \sum_{j=1}^{\infty} |g_{j+1} - g_j| \, \mathrm{d}m \le \sum_{j=1}^{\infty} 2^{-j} < \infty.$$

The first convergence theorem just proved justifies the interchange. The sum is finite almost everywhere, for a nonnegative function infinite on a set of positive measure has infinite integral. Thus g_j converges almost everywhere to a measurable function g. For each j, the triangle inequality for finite sums and Fatou's integral lemma give

$$\|g - g_j\|_p \le \sum_{k=j}^{\infty} 2^{-k}.$$

Indeed raise the finite-tail estimate to the power p, apply the lemma, and take the pth root. This also proves $g \in L^p$. The original Cauchy sequence converges to g by comparing it with a late g_j. If $f_n \to f$ in norm, choose n_j with $\|f_{n_j} - f\|_p^p < 2^{-2j}$. The size estimate applied to $|f_{n_j} - f|^p$ shows that the sets $\{|f_{n_j} - f| > 2^{-j/p}\}$ have summable measures. The measure of their union for $j \ge N$ tends to zero as $N \to \infty$, so almost every point belongs to only finitely many of them. At such a point $f_{n_j} \to f$. The exceptional-set calculation for this chosen subsequence is

$$m\left(\bigcup_{j \ge N} \{|f_{n_j} - f| > 2^{-j/p}\} \right) \le \sum_{j \ge N} 2^{-j} = 2^{1-N} \longrightarrow 0.$$

It concerns the selected indices n_j, without asserting convergence of the full original sequence at every point. □

The subsequence conclusion does not give convergence along every radius. That missing step is precisely why a norm limit of boundary circles is not already a proof of Fatou's theorem. We will identify the limiting function and then prove that its Poisson averages converge at every Lebesgue point.

11.3 A covering estimate and the maximal function

For $0 < h \le \pi$, put $I(t, h) = \{s : d(s, t) < h\}$, interpreting $I(t, \pi)$ as the full circle up to one point. Define

$$Mf(t) = \sup_{0<h\le\pi} \frac{1}{m(I(t,h))} \int_{I(t,h)} |f(s)| \, \mathrm{d}m(s).$$

For fixed h, the integral varies continuously with t. To check this, first use an arc-step approximation to $|f|$; for an indicator of an arc, the overlap length with a translated arc is continuous. The approximation error in the integral is at most the L^1 error, uniformly in t. Consequently $\{Mf > \lambda\}$ is open, even though the supremum is over uncountably many radii.

Lemma 11.4 (Finite arc covering)**.** *Given a finite family of arcs, one can choose pairwise disjoint members $I_1, \dots, I_N$ so that the union of the original family is contained in the union of their threefold concentric enlargements. The length of a threefold enlargement is at most three times the original length, with length capped by the full circle.*

Proof. Choose a longest remaining arc, retain it, and discard all arcs intersecting it. Repeat until none remain. Every discarded arc has radius no larger than the radius h of the retained arc it meets. Its center is at distance at most $2h$ from the retained center, so all its points are at distance at most $3h$ from that center. If $3h \geq \pi$ the enlargement is the full circle and the conclusion still holds. Retained arcs are disjoint by construction. This finite argument avoids any assertion about selecting a largest member from an infinite family. □

Theorem 11.5 (Weak maximal estimate)**.** *For every $f \in L^1(\mathbb{T})$ and every $\lambda > 0$,*

$$m\{Mf > \lambda\} \leq \frac{3\|f\|_1}{\lambda}.$$

In particular $Mf < \infty$ almost everywhere.

Proof. Let K be a compact subset of the open set $\{Mf > \lambda\}$. For every $t \in K$, select an arc centered at t on which the average of $|f|$ exceeds λ. A finite collection covers K. Select the disjoint subcollection from Lemma 11.4. Then

$$m(K) \leq 3 \sum_j m(I_j) < \frac{3}{\lambda} \sum_j \int_{I_j} |f| \, \mathrm{d}m \leq \frac{3\|f\|_1}{\lambda}.$$

Regular approximation allows the compact sets to approach the measure of the open set. Finally $\{Mf = \infty\} \subset \{Mf > N\}$ for every integer N, whose measures tend to zero. □

11.4 Lebesgue points

Definition 11.6. A point t is a Lebesgue point of a representative $f \in L^1$ when $f(t)$ is finite and

$$\lim_{h \downarrow 0} \frac{1}{m(I(t,h))} \int_{I(t,h)} |f(s) - f(t)| \, \mathrm{d}m(s) = 0.$$

Theorem 11.7 (Differentiation of integrable data)**.** *Almost every point of $\mathbb{T}$ is a Lebesgue point of $f \in L^1$.*

Proof. Let $D_f(t)$ be the upper limit of the averages in the definition. A continuous g has $D_g(t) = 0$ at every point by uniform continuity. The triangle inequality gives

$$D_f(t) \leq M(f - g)(t) + |f(t) - g(t)|.$$

For $\eta > 0$, the maximal estimate and the elementary size estimate imply

$$m\{D_f > \eta\} \leq \frac{6\|f - g\|_1}{\eta} + \frac{2\|f - g\|_1}{\eta} = \frac{8\|f - g\|_1}{\eta}.$$

Continuous approximation makes the right side arbitrarily small. Therefore $\{D_f > \eta\}$ is null for each $\eta > 0$; taking the union for $\eta = 1/n$ proves $D_f = 0$ almost everywhere. Measurability

causes no hidden issue: local integrals are measurable in t, their dependence on $h > 0$ is continuous, and suprema over rational radii suffice. The values $f(t)$ are finite almost everywhere by integrability. □

This is the centered-circle version of the differentiation theorem. A primary modern account of the maximal-estimate method is Tao's real-analysis notes [3]. Our normalization, finite arc selection and the displayed constants have been fixed here so that later estimates can be checked directly. The exact constant 3 is not asserted to be optimal; its finiteness is what the convergence proof uses.

11.5 Solved investigations: measure and limits

Investigation 11.8 (A dense exceptional set)**.** Construct a dense null subset of the circle. Explain why removing it is compatible with an almost-everywhere conclusion but not with a statement about every open arc being free of exceptions.

Solution. Let $E = \{2\pi q \pmod{2\pi} : q \in \mathbb{Q}\}$. It is countable and dense. Enumerate it as $t_1, t_2, \ldots$. For each $\varepsilon > 0$, cover t_j by an arc of normalized length at most $\varepsilon 2^{-j}$. Then $m(E) \le \varepsilon$, and arbitrariness gives $m(E) = 0$. Every nonempty open arc nevertheless contains an element of E. Thus measure zero gives no positive distance from the exceptional set. An algorithm that samples a dense countable grid may hit only points in a prescribed null set; density of a numerical sample does not replace an almost-everywhere theorem or test its exceptional set.

Investigation 11.9 (From differentiation to density)**.** Show that almost every point of a measurable set E has density one in E, and almost every point of its complement has density zero in E.

Solution. Apply Theorem 11.7 to 1_E. At a point of E where the theorem holds, its local mean difference from 1 is $1 - m(E \cap I)/m(I)$, so this expression tends to zero. At a point outside E, the mean difference from 0 is $m(E \cap I)/m(I)$, so it tends to zero. The exceptional set is one null set for the chosen representative. Changing E by a null set changes no local integrals, although it may change membership of individual exceptional points. This is a concrete reason to formulate density conclusions with an almost-everywhere qualifier even when E itself is geometrically explicit.

Investigation 11.10 (Norm convergence is not full pointwise convergence)**.** Construct $f_n \to 0$ in $L^1(\mathbb{T})$ such that $f_n(t)$ fails to converge at every point when suitable half-open representatives are used.

Solution. At level k, partition $[0, 2\pi)$ into 2^k half-open equal arcs and list their indicators in order. Concatenate the lists for $k = 1, 2, 3, \ldots$. Every function in the level-k block has L^1 norm 2^{-k}, so the sequence tends to zero in L^1. Every point belongs to exactly one arc at each level, hence the sequence equals one there infinitely often. It also equals zero infinitely often, since each level has at least two arcs. Thus there is no pointwise limit. This example explains why the later L^2 construction of a boundary function must be followed by a Poisson convergence theorem. It also shows why the subsequence in Lemma 11.3 cannot generally be omitted. An explicit indexing of this construction is, for $k \ge 1$ and $0 \le j < 2^k$,

$$f_{2^k-1+j}(t) = 1_{[2\pi j/2^k,\, 2\pi(j+1)/2^k)}(t), \qquad \|f_{2^k-1+j}\|_1 = 2^{-k},$$
$$\liminf_{n\to\infty} f_n(t) = 0, \qquad \limsup_{n\to\infty} f_n(t) = 1 \qquad (0 \le t < 2\pi).$$

Investigation 11.11 (A quantitative exceptional set)**.** Suppose g is continuous and $\|f - g\|_1 \le \varepsilon$. Bound the measure of points where either some centered average of $|f - g|$ or its pointwise value exceeds $\eta > 0$.

Solution. The first bad set is $\{M(f-g) > \eta\}$ and has measure at most $3\varepsilon/\eta$. The second has measure at most ε/η. Their union has measure at most $4\varepsilon/\eta$. Outside it, for every h,

$$\frac{1}{m(I(t,h))}\int_{I(t,h)} |f(s)-f(t)|\,\mathrm{d}m(s) \le 2\eta + \sup_{d(s,t)<h} |g(s)-g(t)|.$$

This is an effective estimate once a specific continuous approximation and its modulus of continuity are supplied. Knowledge of $\|f\|_1$ alone supplies neither that approximation nor its modulus. Thus the qualitative differentiation theorem does not secretly provide a uniform numerical rate for all integrable functions with a given norm.

Chapter 12

Poisson averages and boundary reconstruction

The measure-theoretic conclusion of the preceding chapter concerns averages over arcs. A harmonic function in the disk instead averages with the Poisson kernel. The next task is to compare these two averaging processes without presuming that boundary data are continuous. This comparison is also the point where approach geometry enters: a radial path fixes an angle, whereas a nontangential approach permits the angle to drift by an amount comparable to the distance to the boundary.

12.1 Derivation and elementary properties of the kernel

For $0 \le r < 1$ define

$$P_r(t) = \frac{1 - r^2}{1 - 2r\cos t + r^2}.$$

The geometric series, absolutely and uniformly convergent for a fixed $r < 1$, gives

$$P_r(t) = \operatorname{Re} \frac{1 + re^{it}}{1 - re^{it}} = \sum_{n \in \mathbb{Z}} r^{|n|} e^{int} = 1 + 2\sum_{n=1}^{\infty} r^n \cos(nt). \tag{12.1}$$

Termwise integration is justified by uniform convergence. Since $\int e^{int}\, \mathrm{d}m(t) = 0$ for nonzero integer n, we obtain $\int P_r \, \mathrm{d}m = 1$. Positivity follows from the quotient formula. For $f \in L^1$, set

$$\mathcal{P}f(re^{ix}) = \int_{\mathbb{T}} P_r(x - t) f(t) \, \mathrm{d}m(t).$$

At a fixed interior point the kernel is bounded, so the integral is absolutely convergent. On a compact subdisk, every derivative of the kernel is uniformly bounded: differentiate either its rational expression, whose denominator is bounded away from zero, or its uniformly convergent series of derivatives. Dominated convergence permits differentiation under the integral. Each term $r^{|n|}e^{inx}$ is harmonic, including the negative frequencies, so $\mathcal{P}f$ is harmonic, componentwise for complex f.

Proposition 12.1 (Positivity, contraction, and uniqueness for continuous data)**.** *Poisson averaging preserves constants and positivity. For $p = 1, 2$,*

$$\|P_r * f\|_p \le \|f\|_p.$$

For bounded data, $|\mathcal{P}f(z)| \le \|f\|_\infty$. If f is continuous on $\mathbb{T}$, then $P_r * f \to f$ uniformly as $r \uparrow 1$. The resulting harmonic function is the unique harmonic function continuous on the closed disk with boundary values f.

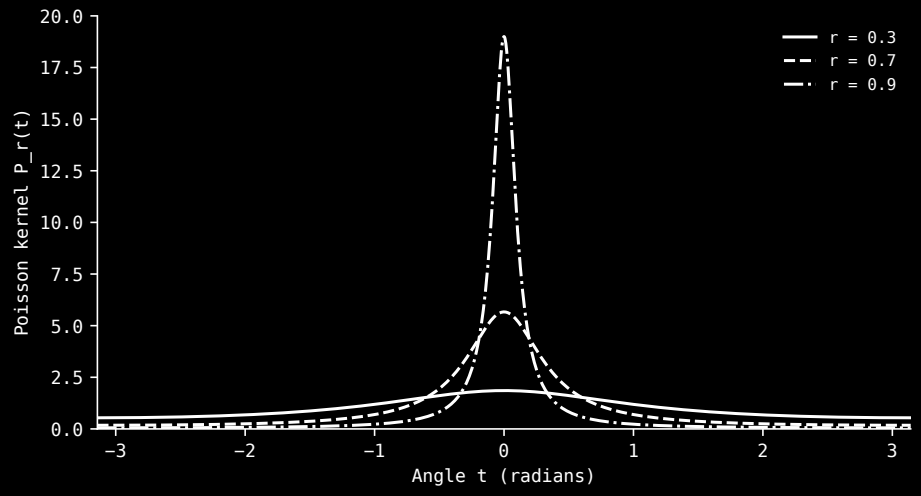


Figure 12.1: The exact Poisson kernel sampled at $r = 0.3, 0.7, 0.9$. Each curve has integral one against $\mathrm{d}m = \mathrm{d}t/(2\pi)$; increasing r concentrates that mass near angle zero. The curves illustrate the analytic formula, rather than certify convergence or a numerical error bound.

Proof. A positive integral of total mass one preserves constants and positivity. The pointwise triangle inequality proves the L^∞ bound. Integrate $|P_r * f| \le P_r * |f|$ and use interchange of the nonnegative integrals and translation invariance to get the L^1 contraction. Weighted Cauchy–Schwarz, with weight $P_r(x-t)$ of integral one, gives $|P_r * f(x)|^2 \le P_r * |f|^2(x)$, and integration proves the L^2 case.

For uniform convergence, fix $\delta > 0$. On $d(t,0) \ge \delta$, $P_r(t) \to 0$ uniformly, as its numerator tends to zero and its denominator is bounded below for r close to one. Split

$$|P_r * f(x) - f(x)| \le \int P_r(t)|f(x-t) - f(x)| \, \mathrm{d}m(t)$$

into $d(t,0) < \delta$ and its complement. The first part is bounded by the modulus of continuity of f at δ, because the kernel mass is one. The second is at most $2\|f\|_\infty$ times a mass tending uniformly to zero. First make δ small and then make $1 - r$ small. Writing $\omega_f(\delta) = \sup_{d(s,t)\le\delta} |f(s) - f(t)|$, the same splitting gives an explicit bound. Since $1 - 2r\cos t + r^2 \ge 1 - \cos\delta$ when $r \ge 1/2$ and $d(t,0) \ge \delta$,

$$\|P_r * f - f\|_\infty \le \omega_f(\delta) + \frac{2(1-r^2)}{1-\cos\delta}\|f\|_\infty, \qquad \tfrac{1}{2} \le r < 1, \quad 0 < \delta \le \pi.$$

The estimate uses the supplied modulus of this particular continuous datum. For uniqueness, the difference of two candidates is harmonic, continuous on the compact closed disk, and zero on its boundary. Apply the maximum principle to its real and imaginary parts and to their negatives. □

The continuity condition in the last uniqueness statement is substantial. Later we construct a positive, unbounded harmonic function with radial limit zero at almost every point. It does not contradict the proposition because it is not continuous on the closed disk, and it also does not contradict the bounded analytic uniqueness theorem, whose hypotheses differ.

12.2 Kernel bounds and nontangential approach

Put $\delta = 1 - r$. For $r \ge 1/2$ and $|t| \le \pi$, the inequalities $2t^2/\pi^2 \le 1 - \cos t \le t^2/2$ give

$$\delta^2 + \frac{2}{\pi^2}t^2 \le 1 - 2r\cos t + r^2 \le \delta^2 + t^2.$$

Together with $\delta \le 1 - r^2 \le 2\delta$, these imply

$$\frac{\delta}{\delta^2 + t^2} \le P_r(t) \le \frac{\pi^2 \delta}{\delta^2 + t^2}. \tag{12.2}$$

The lower bound is not needed for convergence, but it records the scale: a boundary layer of angular width comparable to δ carries a nonvanishing fraction of the kernel mass.

For $A \ge 0$ and $t_0 \in \mathbb{T}$, call

$$\Gamma_A(t_0) = \{re^{ix} : 1/2 < r < 1,\ d(x, t_0) \le A(1 - r)\}$$

a nontangential region. The radial segment is $A = 0$. These regions are equivalent near the boundary to usual Stolz regions $|z - e^{it_0}| \le C(1 - |z|)$, with constants depending on each other. Indeed $|re^{ix} - e^{it_0}| \le (1 - r) + |e^{ix} - e^{it_0}|$ proves one direction. Conversely $|e^{ix} - e^{it_0}| \le |re^{ix} - e^{it_0}| + (1 - r)$ and $d(x, t_0) \le (\pi/2)|e^{ix} - e^{it_0}|$ prove the other. Thus, with $z = re^{ix}$ and $\delta = 1 - r$, the aperture conversion is

$$\begin{aligned} d(x, t_0) \le A\delta &\implies |z - e^{it_0}| \le (A + 1)\delta, \\ |z - e^{it_0}| \le C\delta &\implies d(x, t_0) \le \tfrac{\pi}{2}(C + 1)\delta. \end{aligned}$$

If $d(x, t_0) \le A\delta$, the triangle inequality implies

$$\delta^2 + d(t, t_0)^2 \le (2 + 2A^2)(\delta^2 + d(t, x)^2).$$

Thus, with $C_A = \pi^2(2 + 2A^2)$, the upper bound becomes

$$P_r(x - t) \le C_A \frac{\delta}{\delta^2 + d(t, t_0)^2}. \tag{12.3}$$

No assertion of uniformity as $A \to \infty$ is made.

Lemma 12.2 (Poisson maximal control)**.** *For each finite $A \ge 0$ there is a finite constant B_A such that*

$$\sup_{z \in \Gamma_A(t_0)} |\mathcal{P}f(z)| \le B_A M f(t_0), \qquad f \in L^1.$$

Proof. Fix $z = re^{ix} \in \Gamma_A(t_0)$ and $\delta = 1 - r$. Split the circle into $d(t, t_0) < \delta$ and rings $2^{j-1}\delta \le d(t, t_0) < 2^j\delta$, stopping once the outer radius reaches π. On the first set, the kernel bound is C_A/δ, and the integral of $|f|$ is at most $m(I(t_0, \delta))Mf(t_0) = \delta Mf(t_0)/\pi$. On a ring the kernel is at most $C_A 2^{2-2j}/\delta$, while the integral of $|f|$ is bounded by $\min(2^j\delta/\pi, 1)Mf(t_0)$. Even on the last ring this is at most $2^j\delta Mf(t_0)/\pi$. The ring contribution is therefore at most $(4C_A/\pi)2^{-j}Mf(t_0)$. Summing the geometric series proves the claim, for example with $B_A = 5C_A/\pi$. □

For $N_A f(t) = \sup_{z \in \Gamma_A(t)} |\mathcal{P}f(z)|$, the maximal estimate and Theorem 11.5 combine without an additional regularity assumption on $f \in L^1$:

$$m\{N_A f > \lambda\} \le m\{Mf > \lambda/B_A\} \le \frac{3B_A}{\lambda}\|f\|_1, \qquad \lambda > 0, \quad B_A = 10\pi(1 + A^2).$$

Measurability follows by taking rational $r \in (1/2, 1)$ and rational $q \in [-1, 1]$, with angular offset $x - t = A(1 - r)q$. Interior continuity makes this countable supremum equal to $N_A f(t)$, including when $A = 0$.

Theorem 12.3 (Poisson convergence at Lebesgue points)**.** *Let $f \in L^1(\mathbb{T})$ and let t_0 be a Lebesgue point of f. For every finite A,*

$$\lim_{\substack{z \to e^{it_0} \\ z \in \Gamma_A(t_0)}} \mathcal{P}f(z) = f(t_0).$$

Consequently the nontangential limit exists and equals $f(t_0)$ at almost every boundary point.

Proof. Subtract the constant $f(t_0)$ and write $g(t) = |f(t) - f(t_0)|$. Given $\varepsilon > 0$, choose $\eta > 0$ such that

$$\int_{I(t_0,h)} g \, \mathrm{d}m \le \varepsilon m(I(t_0, h)) \quad (0 < h \le \eta).$$

In the dyadic-ring proof of Lemma 12.2, every ring whose outer radius is at most η contributes at most its corresponding constant times ε. Their entire sum is at most $B_A\varepsilon$. Choose the final inner ring so that its outer radius lies between $\eta/2$ and η; when δ is sufficiently small such a ring exists. All remaining points have $d(t, t_0) \ge \eta/2$. By (12.3), their total contribution is at most

$$\frac{4C_A\delta}{\eta^2}\|g\|_1,$$

which tends to zero. Thus the upper limit of $|\mathcal{P}f(z) - f(t_0)|$ is at most $B_A\varepsilon$. Let $\varepsilon \downarrow 0$. The almost-everywhere conclusion follows from Theorem 11.7. The same set of Lebesgue points works for every A: no uncountable intersection of full-measure sets is being taken. □

This proof isolates the two different kinds of smallness. Near the target point, the boundary data have small local average oscillation. Away from that point, the kernel itself becomes small. Neither condition says that f must be bounded or continuous near the point. In particular a dense set of boundary discontinuities is compatible with the conclusion.

12.3 Fourier reconstruction and an elementary completeness proof

Define the Fourier coefficients of $f \in L^1$ by

$$\widehat{f}(n) = \int_{\mathbb{T}} f(t)e^{-int} \, \mathrm{d}m(t), \qquad n \in \mathbb{Z}.$$

The exponentials have orthonormality $\int e^{int}\overline{e^{ikt}} \, \mathrm{d}m = 1$ if $n = k$ and zero otherwise. For an L^2 function, subtracting a finite Fourier sum and expanding its squared norm gives Bessel's inequality

$$\sum_{|n| \le N} |\widehat{f}(n)|^2 \le \|f\|_2^2.$$

This inequality alone does not prove that the Fourier coefficients determine f. We next prove the required density, rather than assume it.

For $N \ge 0$ set

$$F_N(t) = \frac{1}{N+1}\left|\sum_{k=0}^{N} e^{ikt}\right|^2 = \sum_{|n| \le N} \left(1 - \frac{|n|}{N+1}\right) e^{int}.$$

The equality follows by counting pairs (j, k) with $j - k = n$. Thus $F_N \ge 0$, $\int F_N \, \mathrm{d}m = 1$, and, away from $t = 0$,

$$F_N(t) = \frac{1}{N+1}\frac{\sin^2((N+1)t/2)}{\sin^2(t/2)} \le \frac{1}{(N+1)\sin^2(t/2)}.$$

For continuous f, the near/far splitting used for the Poisson kernel therefore proves $F_N * f \to f$ uniformly. Every $F_N * f$ is a trigonometric polynomial. Continuous approximation from Lemma 11.1 now shows that trigonometric polynomials are dense in both L^1 and L^2.

Theorem 12.4 (Fourier completeness and Parseval identity)**.** *For $f \in L^2$, the symmetric Fourier sums converge to f in L^2, and*

$$\|f\|_2^2 = \sum_{n\in\mathbb{Z}} |\widehat{f}(n)|^2.$$

Conversely every square-summable sequence $(b_n)_{n\in\mathbb{Z}}$ is the Fourier coefficient sequence of one and only one L^2 function.

Proof. Let $S_N f = \sum_{|n|\le N} \widehat{f}(n)e^{int}$. Orthogonality shows that $S_N f$ is the nearest element to f in the finite-dimensional space of degree-N trigonometric polynomials: for any such q,

$$\|f - q\|_2^2 = \|f - S_N f\|_2^2 + \|S_N f - q\|_2^2.$$

Density implies that $\|f - S_N f\|_2 \to 0$. Expanding the norm of $S_N f$ and taking the limit gives Parseval. Conversely the partial sums with coefficients b_n are Cauchy in L^2 by orthogonality, hence converge by Lemma 11.3. The coefficient functionals are continuous by Cauchy–Schwarz, so the limit has the prescribed coefficients. A function with all coefficients zero is orthogonal to every trigonometric polynomial; density, or the first part of the theorem, makes its norm zero. This proves uniqueness up to equality almost everywhere. □

The same orthogonality and Cauchy–Schwarz calculations identify the approximation error and the continuity used for coefficients:

$$\|f - S_N f\|_2^2 = \sum_{|n|>N} |\widehat{f}(n)|^2,$$
$$|\widehat{f}(n) - \widehat{g}(n)| = \left|\int (f-g)e^{-int}\,\mathrm{d}m\right| \le \|f-g\|_2 \qquad (f, g \in L^2).$$

Uniform convergence of the kernel series in (12.1) permits integration against $f \in L^1$:

$$\mathcal{P}f(re^{ix}) = \sum_{n\in\mathbb{Z}} r^{|n|}\widehat{f}(n)e^{inx}. \tag{12.4}$$

The series is absolutely convergent since $|\widehat{f}(n)| \le \|f\|_1$. In particular, the boundary datum of a holomorphic Poisson integral has no negative frequencies. This one-sided spectral condition distinguishes analytic traces from arbitrary bounded measurable data.

12.4 Solved investigations: kernels and traces

Investigation 12.5 (A single Fourier mode)**.** Compute the Poisson extension of e^{int} for every integer n. Decide which of these extensions are holomorphic.

Solution. Orthogonality in (12.1) gives $\mathcal{P}(e^{int})(re^{ix}) = r^{|n|}e^{inx}$. If $n \ge 0$ this is z^n and is holomorphic. If $n = -k < 0$ it is $\overline{z}^k$, which is antiholomorphic and is not holomorphic for $k \ge 1$; for example its Wirtinger derivative with respect to $\overline{z}$ is $k\overline{z}^{k-1}$, not identically zero. Both kinds are harmonic. This elementary calculation is the mechanism behind the trace characterization in the next chapter: positivity of a kernel yields harmonicity, whereas a one-sided Fourier spectrum yields holomorphy.

Investigation 12.6 (A boundary jump)**.** Let $f(t) = 1$ for $0 < t < \pi$ and $f(t) = 0$ for $-\pi < t < 0$. Find the radial Poisson limit at the two jump points and at every other point. Can the value assigned to f at a jump change the Poisson integral?

Solution. At every point in the interiors of the two semicircles the function is locally constant, hence a Lebesgue point. The limits there are one and zero. At $t = 0$, evenness of P_r gives

$$\int_0^{\pi} P_r(t)\,\frac{\mathrm{d}t}{2\pi} = \frac{1}{2},$$

so the radial value is exactly $1/2$ for every r. Symmetry at π gives the same answer there. Altering either endpoint value changes the function only on a null set and does not change any Poisson integral. Therefore a boundary representative can have a prescribed value at a jump which disagrees with the radial limit. The theorem is deliberately stated at Lebesgue points, where the average oscillation condition determines the appropriate value.

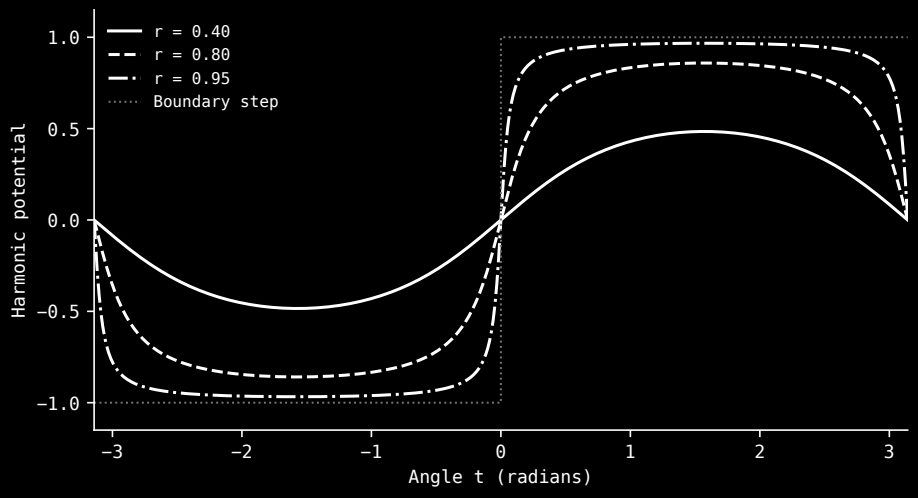


Figure 12.2: Poisson smoothing of the jump data $\operatorname{sign}(\sin t)$ at $r = 0.4, 0.8, 0.95$. The plotted function is twice the solution of Investigation 12.6 minus one; equivalently it is $(2/\pi)\arg((1+z)/(1-z))$. The right-half-plane argument takes values in $(-\pi/2, \pi/2)$. These are samples of an exact harmonic formula.

Investigation 12.7 (Uniform rates require regularity)**.** Suppose $|f(s) - f(t)| \le L d(s,t)^{\alpha}$ for $0 < \alpha < 1$. Show that $|P_r * f(t) - f(t)| \le C_{\alpha} L (1-r)^{\alpha}$ for $r \ge 1/2$. What changes when $\alpha = 1$?

Solution. Put $\delta = 1 - r$. The upper kernel bound gives

$$|P_r * f(t) - f(t)| \le \pi L \delta \int_0^{\pi} \frac{s^{\alpha}}{\delta^2 + s^2}\,\mathrm{d}s = \pi L \delta^{\alpha} \int_0^{\pi/\delta} \frac{u^{\alpha}}{1+u^2}\,\mathrm{d}u.$$

For $0 < \alpha < 1$ the last integral is at most $1/(\alpha+1) + 1/(1-\alpha)$, by splitting at one. This is an explicit admissible C_{α}/π. For $\alpha = 1$, the integral is $\frac{1}{2}\log(1 + \pi^2/\delta^2)$, so the elementary estimate becomes $O(L\delta \log(1/\delta))$. The endpoint logarithm is not a numerical artifact: this argument uses only a Lipschitz modulus and no cancellation in the boundary data. Extra differentiability or a more specific function may permit a better rate, but it is not supplied by the same bound.

Investigation 12.8 (No universal boundary speed)**.** Show that no function $\varepsilon(r) \to 0$ can bound $\|P_r * f - f\|_2$ for every f with $\|f\|_2 \le 1$.

Solution. For $f_N(t) = e^{iNt}$, the norm of f_N is one and $\|P_r * f_N - f_N\|_2 = 1 - r^N$. For every fixed $r < 1$, this tends to one as $N \to \infty$. Hence the supremum of the error over the unit ball is

at least one for every $r < 1$. The claimed uniform rate is impossible. For a fixed f, convergence still holds: approximate f by a finite trigonometric polynomial, use contraction for the tail, and take $r \to 1$ on the finitely many retained modes. The order of the quantifiers is the whole issue. A bounded norm controls the total energy, but it does not say where that energy sits in frequency.

Chapter 13

Hardy traces and Fatou's boundary theorem

Source correspondence. Lyubich, §8.4, Fatou Theorem.

The source asserts that a bounded holomorphic function in the disk has radial limits for almost every angle and refers the proof to a separate text. We prove a stronger nontangential conclusion, while keeping the original radial conclusion visible as its immediate special case. The proof has two stages: construct a measurable boundary trace, and prove convergence to that trace along all approaches inside a fixed Stolz region. The first stage is algebraic and Hilbert-space based; the second is the real-variable argument already completed in Chapter 12.

13.1 The square-integrable analytic class

Definition 13.1. For a holomorphic function F on $\mathbb{D}$, put

$$\|F\|_{H^2}^2 = \sup_{0<r<1} \int_{\mathbb{T}} |F(re^{it})|^2 \, \mathrm{d}m(t).$$

The space H^2 consists of functions with this finite quantity. The space H^∞ consists of bounded holomorphic functions, with $\|F\|_{H^\infty} = \sup_{z\in\mathbb{D}} |F(z)|$.

A power series $F(z) = \sum_{n\geq 0} a_n z^n$ converges uniformly on each closed subdisk. Orthogonality of the exponentials, first for finite sums and then by uniform convergence on $|z| = r$, gives

$$\int |F(re^{it})|^2 \, \mathrm{d}m(t) = \sum_{n\geq 0} |a_n|^2 r^{2n}. \tag{13.1}$$

Every term on the right increases with r. Thus the supremum in the H^2 definition is also the limit as $r \uparrow 1$, and

$$\|F\|_{H^2}^2 = \sum_{n\geq 0} |a_n|^2.$$

One can obtain the last equality without invoking a theorem about exchanging an infinite sum and a supremum. For every finite N, taking $r \to 1$ bounds $\sum_{n=0}^{N} |a_n|^2$ by the supremum. Conversely every weighted sum is at most $\sum_{n\geq 0} |a_n|^2$. Increasing N proves equality.

Theorem 13.2 (The H^2 trace theorem)**.** *Let F be holomorphic in $\mathbb{D}$. The following are equivalent:*

1. $F \in H^2$;

2. its Taylor coefficients satisfy $\sum_{n\geq 0} |a_n|^2 < \infty$;

3. there is $f \in L^2(\mathbb{T})$ with $\widehat{f}(n) = 0$ for $n < 0$ and $F = \mathcal{P}f$.
The boundary function f is unique up to null sets, has coefficients $\widehat{f}(n) = a_n$ for $n \geq 0$, and satisfies

$$\|f\|_2 = \|F\|_{H^2}, \tag{13.2}$$

$$\|F(r\,\cdot) - f\|_2^2 = \sum_{n\geq 0} |a_n|^2 (1 - r^n)^2 \longrightarrow 0. \tag{13.3}$$

At every Lebesgue point of f, F has nontangential limit f.

Proof. The coefficient identity proves the equivalence of the first two conditions. Under the second, Fourier completeness constructs the unique $f \in L^2$ with coefficients a_n for nonnegative n and zero otherwise. It belongs to L^1 because the measure of the circle is one. Formula (12.4) gives

$$\mathcal{P}f(re^{it}) = \sum_{n\geq 0} a_n r^n e^{int} = F(re^{it}).$$

Conversely, the Poisson series of any L^2 function without negative frequencies is holomorphic: the series and its derivative converge uniformly on compact subdisks by Cauchy–Schwarz and the convergence of $\sum n^2 r^{2n-2}$ for $r < 1$. Its squared Taylor coefficient sum is $\|f\|_2^2$ by Parseval, so it lies in H^2. For the derivative step, differentiating the geometric series gives $\sum_{n\geq 1} n^2 \rho^{2n-2} = (1 + \rho^2)/(1 - \rho^2)^3$. Consequently, for $0 \leq \rho < 1$ and $M > N \geq 0$,

$$\sup_{|z|\leq\rho} \left| \sum_{n=N+1}^{M} n a_n z^{n-1} \right| \leq \left(\sum_{n>N} |a_n|^2 \right)^{1/2} \left(\frac{1 + \rho^2}{(1 - \rho^2)^3} \right)^{1/2} \longrightarrow 0 \quad (N \to \infty).$$

The tail tends to zero uniformly in M, proving the asserted compact convergence of derivatives with a fixed interior radius. Parseval also gives both displayed norm identities. To prove the limit in (13.3), choose N with the coefficient tail smaller than a prescribed ε; the tail is bounded by that ε for every r, and the finite initial sum tends to zero. In the notation of that split, for each integer $N \geq 1$ one has

$$\|F(r\,\cdot) - f\|_2^2 \leq (1 - r^N)^2 \sum_{n=0}^{N} |a_n|^2 + \sum_{n>N} |a_n|^2,$$

$$\limsup_{r\uparrow 1} \|F(r\,\cdot) - f\|_2^2 \leq \sum_{n>N} |a_n|^2 \longrightarrow 0 \quad (N \to \infty).$$

The order of the two limits keeps the finite-frequency argument separate from control of the coefficient tail. Finally Theorem 12.3 applies to f, giving the nontangential conclusion. Uniqueness follows from the Fourier coefficients, not from an unproved assertion that radial limits determine arbitrary holomorphic functions. □

There is an immediate, useful interior estimate:

$$|F(z)| \leq \left(\sum |a_n|^2 \right)^{1/2} \left(\sum |z|^{2n} \right)^{1/2} = \frac{\|F\|_{H^2}}{\sqrt{1 - |z|^2}}. \tag{13.4}$$

This is a bounded point-evaluation functional on each compact subdisk. Its blowup near the circle is expected: an L^2 trace may be unbounded. The estimate does not say that F blows up at almost every point. The trace theorem gives the opposite qualitative conclusion: a finite nontangential limit exists almost everywhere.

13.2 Bounded holomorphic functions

Theorem 13.3 (Fatou, with nontangential conclusion)**.** *Let $F : \mathbb{D} \to \mathbb{C}$ be holomorphic and suppose $|F(z)| \le M < \infty$ for every $z \in \mathbb{D}$. There is a measurable $f : \mathbb{T} \to \mathbb{C}$, unique almost everywhere, such that $|f| \le M$ almost everywhere and, for almost every t,*

$$F(z) \longrightarrow f(t) \quad \text{as } z \to e^{it} \text{ within every fixed } \Gamma_A(t),\ A < \infty.$$

In particular $\lim_{r\uparrow 1} F(re^{it}) = f(t)$ almost everywhere. Moreover $F = \mathcal{P}f$, and for every finite $1 \le p < \infty$,

$$\int |F(re^{it}) - f(t)|^p \, \mathrm{d}m(t) \longrightarrow 0.$$

Proof. Boundedness implies $\|F\|_{H^2} \le M$. The trace theorem provides $f \in L^2$ and its almost-everywhere nontangential limits. At every point where the radial limit exists, it is a limit of numbers of modulus at most M, hence $|f(t)| \le M$. This argument could alternatively use an almost-everywhere convergent subsequence of the L^2 limits, but the Poisson convergence theorem already gives the full radial limit. For finite p, the difference tends to zero almost everywhere and is bounded in modulus by $2M$ outside a fixed null set. Dominated convergence therefore proves the last assertion. Uniqueness follows either from the unique H^2 trace or by comparing the radial limits on the intersection of two full-measure sets. □

The historical theorem belongs to Fatou's work on boundary behavior of Taylor series [2]. The result here is not an assertion of convergence along every curve approaching almost every boundary point. The aperture A must remain finite. Nor does it assert that the trace is continuous, that the exceptional set is countable, or that the function extends holomorphically through almost every boundary point. These stronger statements would require different hypotheses and are not used below.

Proposition 13.4 (Characterization of bounded analytic traces)**.** *An L^∞ function f is the almost-everywhere boundary trace of a bounded holomorphic function if and only if $\widehat{f}(n) = 0$ for every $n < 0$. In that case the function is $\mathcal{P}f$ and*

$$\|F\|_{H^\infty} = \|f\|_{L^\infty}.$$

Proof. Necessity follows from Theorem 13.2, since $H^\infty \subset H^2$. For sufficiency, the Poisson series has only nonnegative frequencies and is holomorphic by the same compact-convergence argument. Positivity and mass one of the kernel give $|F(z)| \le \|f\|_\infty$. Its nontangential trace is f at Lebesgue points. Conversely the radial limit of a function bounded by $\|F\|_{H^\infty}$ has that same bound, so $\|f\|_\infty \le \|F\|_{H^\infty}$. The two inequalities give equality, and the Poisson representation supplies uniqueness. □

13.3 A second construction of the boundary datum

The Fourier-coefficient proof exploits holomorphy early. There is a different route to the representation for bounded harmonic functions, which is useful when the starting object is a real potential and no analytic power series has been supplied. We include it with its common dependency clearly stated: both routes ultimately use Poisson convergence at Lebesgue points. The construction below changes the compactness and representation step; it is not an independent replacement for the real-variable differentiation argument.

Lemma 13.5 (Weak subsequences in L^2)**.** *If $\|f_j\|_2 \le M$, there are a subsequence f_{j_k} and $f \in L^2$ with $\|f\|_2 \le M$ such that*

$$\int f_{j_k} \overline{g} \, \mathrm{d}m \longrightarrow \int f \overline{g} \, \mathrm{d}m \qquad (g \in L^2).$$

Proof. Each Fourier coefficient lies in the closed disk of radius M. List the integers and successively choose convergent subsequences for the listed coefficients. The diagonal subsequence makes every coefficient converge, say to b_n. For every finite set S, Bessel's inequality gives $\sum_{n\in S} |b_n|^2 \le M^2$ after taking limits. Thus $\sum_{n\in\mathbb{Z}} |b_n|^2 \le M^2$, and Fourier completeness gives the function f. Convergence of pairings holds for trigonometric polynomials by coefficient convergence. For general $g \in L^2$, choose such a polynomial q with $\|g - q\|_2 < \varepsilon$. Cauchy–Schwarz bounds both omitted pairings by $M\varepsilon$. Taking $k \to \infty$ first and then $\varepsilon \downarrow 0$ proves the claim. This supplies the exact sequential compactness used here without assuming a general functional-analysis compactness theorem. For the polynomial q just chosen, the two approximation errors enter as

$$\left|\int (f_{j_k} - f)\overline{g}\ \mathrm{d}m\right| \le \left|\int (f_{j_k} - f)\overline{q}\ \mathrm{d}m\right| + 2M\|g - q\|_2,$$
$$\limsup_{k\to\infty} \left|\int (f_{j_k} - f)\overline{g}\ \mathrm{d}m\right| \le 2M\varepsilon.$$

Here g and q are fixed before the subsequence index tends to infinity. □

Theorem 13.6 (Bounded harmonic representation)**.** *Every bounded real or complex harmonic function u on $\mathbb{D}$ is the Poisson integral of a unique $f \in L^\infty(\mathbb{T})$. If $|u| \le M$, then $|f| \le M$ almost everywhere. It has nontangential limit f at almost every point.*

Proof. Choose $R_j \uparrow 1$ and set $f_j(t) = u(R_j e^{it})$. These functions are bounded by M and hence by M in L^2. Take the weak subsequence and limit f from Lemma 13.5. For fixed $z = re^{ix}$ and $R_j > r$, uniqueness for the continuous Dirichlet problem in the radius R_j disk gives

$$u(z) = \int P_{r/R_j}(x - t) f_j(t)\ \mathrm{d}m(t).$$

The kernels converge uniformly, and thus in L^2, to $P_r(x-t)$. The uniform L^2 bound on f_j controls the error from this moving test function. Weak convergence handles the fixed limiting kernel. Hence $u(z) = \mathcal{P}f(z)$. More explicitly, on the selected subsequence write $K_k(t) = P_{r/R_{j_k}}(x - t)$ and $K(t) = P_r(x - t)$. For the fixed point $z = re^{ix}$ and all sufficiently large k,

$$\left|u(z) - \int Kf\ \mathrm{d}m\right| \le \left|\int (K_k - K) f_{j_k}\ \mathrm{d}m\right| + \left|\int K(f_{j_k} - f)\ \mathrm{d}m\right|$$
$$\le M\|K_k - K\|_2 + \left|\int K(f_{j_k} - f)\ \mathrm{d}m\right| \longrightarrow 0.$$

The first term uses strong kernel convergence; the second uses weak convergence against the fixed real kernel $K \in L^2$.

To prove the essential bound directly, suppose a measurable set $E = \{|f| > M + \varepsilon\}$ had positive measure. Use $g = 1_E f/|f| \in L^2$ as the weak test function. Then

$$\int_E |f|\ \mathrm{d}m = \lim_k \int_E f_{j_k} \frac{\overline{f}}{|f|}\ \mathrm{d}m \le Mm(E)$$

after taking real parts, contradicting $\int_E |f| \ge (M + \varepsilon)m(E)$. Thus $|f| \le M$ almost everywhere. Poisson convergence gives the boundary limits. If two data produce the same harmonic function, formula (12.4) gives the same Fourier coefficients; Fourier uniqueness then makes the data equal almost everywhere. □

Applying this theorem to the real and imaginary parts of a bounded holomorphic function gives another route to Fatou's theorem. The weak construction does not require the one-sided Taylor spectrum to establish existence. Once the representation is known, holomorphy implies that the negative Fourier coefficients vanish, recovering the spectral description. The two routes therefore serve different inputs: one starts from analytic coefficients, the other from bounded harmonic boundary circles.

13.4 Solved investigations: analytic boundary phenomena

Investigation 13.7 (Sharp evaluation in H^2)**.** Show that the constant in (13.4) is sharp for each fixed $w \in \mathbb{D}$, and identify a function attaining it.

Solution. Take

$$F_w(z) = \frac{\sqrt{1-|w|^2}}{1-\overline{w}z} = \sqrt{1-|w|^2}\sum_{n\geq 0}\overline{w}^{\,n}z^n.$$

Its squared coefficient sum is $(1-|w|^2)\sum|w|^{2n} = 1$. At $z = w$ its value is $(1-|w|^2)^{-1/2}$, attaining the estimate. Equality is the equality case of Cauchy–Schwarz: the coefficient sequence is proportional to $(\overline{w}^{\,n})$. This example shows that the apparent boundary blowup in the bound cannot be removed uniformly over the H^2 unit ball, even though every individual member has finite limits almost everywhere.

Investigation 13.8 (An H^2 function that is not bounded)**.** For $0 < \alpha < 1/2$, use the branch of $F(z) = (1-z)^{-\alpha}$ determined by $F(0) = 1$. Show that $F \in H^2$ but $F \notin H^\infty$.

Solution. The right half-plane contains $1 - \mathbb{D}$, so the logarithm with argument between $-\pi/2$ and $\pi/2$ defines the branch. For $r \geq 1/2$,

$$|1-re^{it}|^2 = (1-r)^2 + 2r(1-\cos t) \geq \frac{2t^2}{\pi^2} \quad (|t| \leq \pi).$$

Hence $|F(re^{it})|^2 \leq C_\alpha |t|^{-2\alpha}$ away from the single point $t = 0$. The right side is integrable precisely in the range used here. For $r < 1/2$, the elementary bound $|1 - re^{it}| \geq 1/2$ gives a uniform estimate. These two estimates prove the H^2 bound. Along the real radius, $F(r) = (1-r)^{-\alpha} \to \infty$, so the function is unbounded. The failure at one boundary point is consistent with the H^2 trace theorem. The example also shows why boundedness is a sufficient, rather than necessary, hypothesis for almost-everywhere finite limits.

Investigation 13.9 (A singular inner factor and approach geometry)**.** For $a > 0$, define

$$S_a(z) = \exp\left(-a\frac{1+z}{1-z}\right).$$

Find its boundary modulus away from 1, its radial limit at 1, and a sequence approaching 1 on which the modulus does not tend to zero.

Solution. The real part of $(1+z)/(1-z)$ equals $(1-|z|^2)/|1-z|^2 > 0$, so $|S_a(z)| \leq 1$ in the disk. At $e^{it} \neq 1$, the quotient has a finite purely imaginary limit, so the boundary value has modulus one. On the real radius, $S_a(r) = \exp[-a(1+r)/(1-r)] \to 0$. This is also the nontangential limit at 1: in a fixed Stolz region, $|1-z| \leq C(1-|z|)$, and the positive real part is at least $1/[C^2(1-|z|)]$, which tends to infinity. For a tangential sequence set $z_t = (1-t^4)e^{it}$, $t \downarrow 0$. Then $1-|z_t|^2 \sim 2t^4$ and $|1-z_t|^2 \sim t^2$, so $|S_a(z_t)| \to 1$. The function therefore has no unrestricted limit at 1, despite its radial and nontangential limit zero there. Boundedness alone does not make all approach geometries equivalent.

Investigation 13.10 (Boundary data forbidden by holomorphy)**.** Can the indicator of a proper arc of positive length be the boundary trace of a bounded holomorphic function? Give two arguments, one spectral and one using the uniqueness theorem that will follow.

Solution. Rotate the arc to $(0, \ell)$ with $0 < \ell < 2\pi$. Its coefficient at $n = -1$ is

$$\widehat{1_{(0,\ell)}}(-1) = \frac{e^{i\ell}-1}{2\pi i} \neq 0.$$

It violates Proposition 13.4. For the second argument, if a bounded holomorphic function had this trace, it would have trace zero on the complementary arc, a set of positive measure. Theorem 14.3 below would make it identically zero, contradicting trace one on the original arc. The first proof is elementary and does not depend on the later theorem; the second illustrates the stronger rigidity that will be proved there. Arbitrary bounded measurable data do have bounded harmonic Poisson extensions, so the obstruction is specifically analytic.

Investigation 13.11 (A quantitative trace approximation from coefficients)**.** Suppose an H^2 function has known coefficients $a_0, \dots, a_N$ and a certified tail bound $\sum_{n>N} |a_n|^2 \le \tau^2$. Bound its radial L^2 boundary error without making a pointwise claim.

Solution. Formula (13.3) gives

$$\|F(r\,\cdot) - f\|_2^2 \le \sum_{n=0}^{N} |a_n|^2 (1 - r^n)^2 + \tau^2.$$

If the known coefficients themselves have errors $|a_n - \widetilde{a}_n|$ with squared sum at most σ^2, the triangle inequality adds at most σ to a corresponding L^2 estimate for the truncated data. The square-root of the displayed right side controls an exceptional set: for any $\eta > 0$,

$$m\{|F(re^{it}) - f(t)| > \eta\} \le \frac{\sum_{n=0}^{N} |a_n|^2 (1 - r^n)^2 + \tau^2}{\eta^2}.$$

This is a bound at a specified radius and threshold. It does not locate individual exceptional angles, certify a uniform boundary error, or prove that a numerical coefficient tail is small without an independent tail bound. The theorem identifies exactly what additional information a validated numerical calculation would need.

Chapter 14

Logarithmic rigidity and boundary uniqueness

Source correspondence. Lyubich, §8.4, Uniqueness Theorem.

A nonzero holomorphic function can have infinitely many zeros approaching the boundary. The identity theorem alone therefore says nothing about vanishing boundary values on a set of positive length: the accumulation points are outside the open domain. The missing ingredient is logarithmic control. Boundedness prevents the mean logarithmic size from falling to negative infinity while the function remains nonzero inside.

The source discusses the classical attribution to F. and M. Riesz or Privalov. The theorem proved here is the precise bounded holomorphic statement in the source. We do not silently replace radial limits by unrestricted limits, and we do not claim the most general angular Privalov theorem for arbitrary unbounded holomorphic functions. Our first proof uses zeros and Jensen's formula. The second uses a regularized subharmonic logarithm and avoids factoring zeros. Their common prerequisites are elementary complex analysis and the integration results already proved.

14.1 The logarithmic mean and its zero correction

Lemma 14.1 (The mean of a logarithmic distance)**.** *For $a \in \mathbb{C}$ and $r > 0$ with $|a| \neq r$,*

$$\int_{\mathbb{T}} \log|re^{it} - a| \, \mathrm{d}m(t) = \log \max(r, |a|).$$

Proof. If $|a| < r$, write $\log|re^{it} - a| = \log r + \operatorname{Re}\log(1 - (a/r)e^{-it})$. The logarithm is given by the uniformly convergent power series $-\sum_{n\geq 1}(a/r)^n e^{-int}/n$. Every nonconstant frequency has mean zero, giving $\log r$. If $|a| > r$, factor out $-a$ instead and apply the same argument to $(r/a)e^{it}$, giving $\log|a|$. Only these noncritical radii are needed below; zeros on the integration circle will be avoided explicitly rather than hidden in an improper integral convention. □

Theorem 14.2 (Jensen's formula at admissible radii)**.** *Let F be holomorphic on $\mathbb{D}$, with $F(0) \neq 0$. For $0 < r < 1$ such that F has no zero on $|z| = r$, list the zeros $a_1, \ldots, a_N$ in $|z| < r$ with their multiplicities. Then*

$$\int \log|F(re^{it})| \, \mathrm{d}m(t) = \log|F(0)| + \sum_{j=1}^{N} \log \frac{r}{|a_j|}. \tag{14.1}$$

In particular the logarithmic mean is at least $\log|F(0)|$.

Proof. Zeros of a nonzero holomorphic function are isolated. Compactness of the closed radius-r disk, and the absence of boundary zeros, imply there are only finitely many inside. Divide by their linear factors:

$$H(z) = \frac{F(z)}{\prod_{j=1}^{N}(z - a_j)}.$$

The apparent singularities are removable by the multiplicity definition. There is a slightly larger disk around the closed radius-r disk on which H is holomorphic and zero-free. On that simply connected disk, H'/H has a primitive L; differentiating He^{-L} shows it is a nonzero constant. After adding a logarithm of that constant to L, we obtain $H = e^L$. Hence $\log|H| = \operatorname{Re} L$ is harmonic and has circle mean $\log|H(0)|$. The mean value property follows directly from the power series of L, or from the harmonic mean value theorem. Apply Lemma 14.1 to each factor, obtaining

$$\int \log|F(re^{it})| \, \mathrm{d}m = \log|H(0)| + N \log r.$$

Since $|H(0)| = |F(0)|/\prod_j |a_j|$, this is the formula. Each term $\log(r/|a_j|)$ is positive. No zero at zero occurs because $F(0) \neq 0$. □

Theorem 14.3 (Positive-length boundary uniqueness)**.** *Let $F : \mathbb{D} \to \mathbb{C}$ be bounded and holomorphic. Suppose there is a measurable set $E \subset \mathbb{T}$ of positive measure such that*

$$\lim_{r\uparrow 1} F(re^{it}) = c \qquad (t \in E).$$

Then $F \equiv c$. It is enough that the asserted equality hold almost everywhere on a positive-measure set.

First proof: logarithmic means. Subtract c. If the result is identically zero there is nothing to prove. Otherwise remove its zero at the origin: write $F(z) - c = z^k G(z)$ with $G(0) \neq 0$. The quotient is holomorphic by the Taylor expansion and is bounded. Indeed outside $|z| < 1/2$ its modulus is bounded by $2^k\|F - c\|_\infty$, and inside that disk the maximum principle gives the same bound from the circle. Multiplying G by a nonzero constant, assume $|G| \leq 1$. It still has radial limit zero on E.

The zeros of G form a countable set: each compact subdisk contains finitely many, and the disk is a countable union of compact subdisks. Thus choose radii $r_j \uparrow 1$ avoiding all zero moduli. Jensen's formula gives

$$\int -\log|G(r_j e^{it})| \, \mathrm{d}m(t) \leq -\log|G(0)| < \infty.$$

The integrands are nonnegative. At every point of E where the radial limit is zero, they tend to $+\infty$. Fatou's integral lemma therefore makes the integral of their lower limit at most the finite right side. But a nonnegative function infinite on a positive-measure set has infinite integral. This contradiction proves the result. The same argument works if a null subset of E is discarded. The same contradiction can be written using only finite truncation levels: for every $T > 0$, Fatou's integral lemma gives

$$\begin{aligned} Tm(E) &\leq \int \liminf_j \min\{T, -\log|G(r_j e^{it})|\} \, \mathrm{d}m(t) \\ &\leq \liminf_j \int \min\{T, -\log|G(r_j e^{it})|\} \, \mathrm{d}m(t) \leq -\log|G(0)|. \end{aligned}$$

Letting T increase is impossible when $m(E) > 0$ and $G(0) \neq 0$. □

The proof needs radial limits only on E. It does not use the existence of limits elsewhere. Thus uniqueness and the Fatou existence theorem are logically separate statements, even though they combine naturally in the source appendix. The argument also identifies why a single boundary zero causes no contradiction: a function can become arbitrarily small in a shrinking angular region while the logarithmic mean stays bounded below.

14.2 A second proof through regularized subharmonicity

A real C^2 function v on a planar domain is subharmonic in the smooth sense if $\Delta v \geq 0$. We need only this smooth case. If v is continuous on a closed disk and subharmonic inside, and h is harmonic with the same boundary values, then $v \leq h$. To verify this maximum principle, consider $v - h + \varepsilon(|z|^2 - R^2)$ on a radius-R disk. Its Laplacian is at least $4\varepsilon > 0$. A positive interior maximum would have nonpositive second derivatives in coordinate directions and hence nonpositive Laplacian, a contradiction. On the boundary the function is zero. Let $\varepsilon \downarrow 0$. This proves the comparison needed below without invoking distributional subharmonic theory.

For holomorphic G and $\varepsilon > 0$, differentiation using the Cauchy–Riemann equations gives

$$\Delta \log(|G|^2 + \varepsilon) = \frac{4\varepsilon |G'|^2}{(|G|^2 + \varepsilon)^2} \geq 0. \tag{14.2}$$

For example, write $u = |G|^2$. Then $\Delta u = 4|G'|^2$ and $|\nabla u|^2 = 4|G|^2|G'|^2$. Substitution into $\Delta \log(u + \varepsilon) = \Delta u/(u + \varepsilon) - |\nabla u|^2/(u + \varepsilon)^2$ gives the formula, including at zeros because $\varepsilon > 0$ keeps every denominator positive.

Second proof of Theorem 14.3. Again subtract c and rescale so that the resulting G satisfies $|G| \leq 1$. If it is not identically zero, choose an interior point z_0 with $G(z_0) \neq 0$. There is no need to remove zeros at the origin. For fixed $\varepsilon > 0$ put

$$v_\varepsilon(z) = \log \frac{|G(z)|^2 + \varepsilon}{1 + \varepsilon} \leq 0.$$

On a radius-r disk with $r > |z_0|$, the subharmonic comparison with the Poisson extension of its continuous boundary values gives

$$v_\varepsilon(z_0) \leq \int P_{|z_0|/r}(\arg z_0 - t) v_\varepsilon(re^{it}) \, \mathrm{d}m(t).$$

If $z_0 = 0$ interpret the kernel as one. For fixed ε, all values lie in the bounded interval $[\log(\varepsilon/(1 + \varepsilon)), 0]$. For an explicit dominator in the forthcoming radius limit, put $a = |z_0|$ and restrict to $r \geq (1 + a)/2$. The kernel quotient then gives

$$0 < P_{a/r}(\arg z_0 - t) \leq \frac{1 + a/r}{1 - a/r} \leq \frac{1 + 3a}{1 - a},$$
$$|P_{a/r}(\arg z_0 - t) v_\varepsilon(re^{it})| \leq \frac{1 + 3a}{1 - a} \log \frac{1 + \varepsilon}{\varepsilon} < \infty.$$

This bound is constant in t and r for fixed z_0 and $\varepsilon > 0$; at $a = 0$ the kernel is again interpreted as one. The Fatou theorem supplies radial limits $g(t)$ almost everywhere, and uniform convergence of the kernels as $r \uparrow 1$, together with dominated convergence, gives

$$v_\varepsilon(z_0) \leq \int P_{|z_0|}(\arg z_0 - t) \log \frac{|g(t)|^2 + \varepsilon}{1 + \varepsilon} \, \mathrm{d}m(t).$$

On E, the logarithm is $\log(\varepsilon/(1 + \varepsilon))$ almost everywhere; elsewhere it is at most zero. Denote

$$\omega_{z_0}(E) = \int_E P_{|z_0|}(\arg z_0 - t) \, \mathrm{d}m(t) > 0.$$

Positivity follows from positivity of the continuous kernel and $m(E) > 0$. The denominator bound $|e^{it} - z_0| \le 1 + |z_0|$ makes this positivity quantitative:

$$\omega_{z_0}(E) = \int_E \frac{1 - |z_0|^2}{|e^{it} - z_0|^2}\, \mathrm{d}m(t) \ge \frac{1 - |z_0|}{1 + |z_0|}\, m(E) > 0.$$

We obtain

$$v_\varepsilon(z_0) \le \omega_{z_0}(E) \log \frac{\varepsilon}{1 + \varepsilon}.$$

As $\varepsilon \downarrow 0$, the left side tends to the finite number $\log |G(z_0)|^2$, while the right side tends to $-\infty$. This is impossible. Unlike the first proof, this route uses almost-everywhere existence supplied by Fatou, but it avoids zero factorization and Jensen's formula. Both dependency changes are explicit. □

14.3 Quantitative smallness and equality examples

The same regularization proves a useful estimate with a nonzero error threshold. It is a conditional stability statement: the interior value is controlled by an actual almost-everywhere boundary bound on a known set, not by finitely many sampled boundary values.

Theorem 14.4 (Two boundary levels)**.** *Let $F \in H^\infty$, let f be its trace, and let E be measurable. Suppose $0 < \eta \le M$, $|f| \le \eta$ almost everywhere on E, and $|f| \le M$ almost everywhere on its complement. Then*

$$|F(z)| \le \eta^{\omega_z(E)} M^{1 - \omega_z(E)}, \qquad z \in \mathbb{D},$$

where $\omega_z(E) = \int_E P_{|z|}(\arg z - t)\, \mathrm{d}m(t)$. At the center this reads $|F(0)| \le \eta^{m(E)} M^{1 - m(E)}$.

Proof. The bounded trace characterization first implies $|F| \le M$ throughout the disk. Apply the subharmonic comparison to $\frac{1}{2}\log(|F|^2 + \varepsilon)$ and pass the outer radius to one exactly as in the second uniqueness proof. This gives

$$\tfrac{1}{2}\log(|F(z)|^2 + \varepsilon) \le \tfrac{1}{2}\omega_z(E)\log(\eta^2 + \varepsilon) + \tfrac{1}{2}(1 - \omega_z(E))\log(M^2 + \varepsilon).$$

Let $\varepsilon \downarrow 0$. If $F(z) = 0$, the desired inequality is immediate; otherwise the left side tends to $\log |F(z)|$. Exponentiation proves the statement. The case $\eta = M$ is simply the maximum bound. The case $m(E) = 0$ gives no improvement, as it should. □

For a measurable E, define the holomorphic function

$$H_E(z) = \int_E \frac{e^{it} + z}{e^{it} - z}\, \mathrm{d}m(t).$$

On compact subdisks, the kernel and its derivatives are uniformly bounded, so differentiation under the integral is justified. Its real part is $\omega_z(E)$. If $\lambda = \log(M/\eta)$, then

$$F_E(z) = M \exp[-\lambda H_E(z)] \tag{14.3}$$

is holomorphic, zero-free, and bounded by M. Its modulus is exactly $M \exp[-\lambda \omega_z(E)]$, which is the right side of the two-level estimate. The differentiation theorem and Poisson convergence imply $\omega_z(E) \to 1_E(t)$ nontangentially at almost every point. Fatou supplies the complex limit of F_E, and therefore its boundary modulus is η on E and M off E, almost everywhere. This proves sharpness of the modulus estimate. It does not claim that the boundary phase is piecewise constant; in fact the holomorphic coupling forces a nontrivial phase.

14.4 Zeros and the necessity of the measure threshold

Corollary 14.5 (The Blaschke necessary condition)**.** *If a bounded holomorphic function is not identically zero and its nonzero zeros, listed with multiplicity, are a_j, then*

$$\sum_j (1 - |a_j|) < \infty.$$

Proof. Remove a possible finite-order zero at the origin and rescale to get a bounded G with $G(0) \neq 0$ and $|G| \leq 1$, as above. Jensen gives

$$\sum_{|a_j|<r} \log \frac{r}{|a_j|} \leq -\log |G(0)|$$

for radii avoiding zeros. Given any finite collection of zeros, take $r \uparrow 1$ to bound its sum of $\log(1/|a_j|)$ by the same constant. Increase the finite collection to all zeros. The inequality $1 - x \leq -\log x$ for $0 < x \leq 1$, obtained by integrating $1/t \geq 1$ from x to one, proves the stated summability. This is only the necessary condition; construction of an infinite Blaschke product is not needed for the theorem and is not being asserted without a convergence argument. The argument also records a finite counting bound with the same normalization. If $N_G(r)$ counts the nonzero zeros of G in $|z| \leq r$ with multiplicity, then, for $0 < r < 1$,

$$(1 - r)N_G(r) \leq \sum_{|a_j|\leq r} (1 - |a_j|) \leq \sum_j \log \frac{1}{|a_j|} \leq -\log |G(0)|,$$
$$N_G(r) \leq \frac{-\log |G(0)|}{1 - r}.$$

The bound depends on the nonzero center value of the normalized function, as the Jensen argument requires. □

Investigation 14.6 (A boundary zero of infinite order)**.** Use S_a from Investigation 13.9 to show that a bounded nonzero holomorphic function may approach zero faster than every power of $1 - r$ along a radius. Explain why this does not contradict uniqueness.

Solution. For any integer $N \geq 0$,

$$\frac{S_a(r)}{(1 - r)^N} = \exp\left[-a\frac{1 + r}{1 - r} - N \log(1 - r)\right] \longrightarrow 0,$$

because $1/(1 - r)$ dominates $|\log(1 - r)|$. Nevertheless $S_a(0) = e^{-a} \neq 0$. Its radial zero occurs at the single angle $t = 0$, which has measure zero. Jensen's logarithmic budget is preserved because the very negative logarithm is concentrated in a narrowing region. Thus neither arbitrarily rapid decay at one point nor numerical underflow along one ray supplies a positive-measure uniqueness hypothesis.

Investigation 14.7 (A sharp center estimate)**.** Suppose $\|F\|_\infty \leq 1$ and its trace has modulus at most 10^{-6} on a set of normalized angular measure $1/3$. Bound $|F(0)|$ and decide whether the exponent can be improved from these data alone.

Solution. Theorem 14.4 gives $|F(0)| \leq (10^{-6})^{1/3} = 10^{-2}$. The function in (14.3), with $M = 1$, $\eta = 10^{-6}$ and the given set E, has $H_E(0) = m(E) = 1/3$ and $|F_E(0)| = 10^{-2}$. It satisfies exactly the required almost-everywhere boundary modulus bounds, so the exponent cannot be uniformly increased. If the location of E is known and an interior point other than the center is used, the relevant exponent is its Poisson mass $\omega_z(E)$, not simply its angular length. This distinction anticipates the change of basepoint in harmonic measure.

Investigation 14.8 (A harmonic counterexample to analytic uniqueness)**.** Construct a nonzero bounded harmonic function whose boundary trace is zero on a set of positive measure. Then construct an unbounded positive harmonic function whose radial trace is zero almost everywhere.

Solution. For the first, take the Poisson extension of the indicator of a proper arc. It is bounded between zero and one, nonzero because its center value is the arc's positive normalized length, and its trace vanishes on the complementary arc. This shows that the analytic uniqueness theorem is not a theorem for arbitrary bounded real harmonic functions with partially vanishing boundary data. For the second, set

$$u(z) = \operatorname{Re} \frac{1+z}{1-z} = \frac{1-|z|^2}{|1-z|^2}.$$

It is positive and harmonic in the disk. For every $e^{it} \neq 1$, the radial limit is zero. At 1, $u(r) = (1+r)/(1-r) \to \infty$. Since $u(0) = 1$, it is not zero. The missing boundary mass is concentrated at one point; bounded harmonic representation does not apply. This also explains why pointwise almost-everywhere convergence cannot by itself justify interchanging a boundary limit with an integral.

Investigation 14.9 (Interior zeros approaching too slowly)**.** Can a nonzero bounded holomorphic function vanish at all points $a_n = 1 - 1/n$, $n \geq 2$? What does the necessary condition say for $b_n = 1 - 1/n^2$?

Solution. For the first sequence, $\sum_{n\geq 2}(1 - |a_n|) = \sum_{n\geq 2} 1/n = \infty$. Corollary 14.5 rules it out. The divergence of the harmonic series follows, for instance, by grouping terms between 2^k and $2^{k+1} - 1$, each group having sum at least $1/2$. For b_n, the sum is $\sum 1/n^2 < \infty$, as comparison with $\int_1^\infty x^{-2}\,\mathrm{d}x$ shows. Thus the necessary condition does not rule it out. That conclusion is deliberately weaker than existence: a necessary condition being satisfied is not a construction. Infinite product existence would require a separate proof of local uniform convergence and the intended zero set.

Investigation 14.10 (A positive measure of exact agreement)**.** Let F, G be bounded holomorphic functions with boundary traces f, g. Suppose $f = g$ on a measurable set of positive measure. Show $F = G$. Why does equality of $|f|$ and $|g|$ on the whole circle not suffice?

Solution. The difference $F - G$ is bounded and holomorphic, and has radial trace zero on the given set outside the union of the two null exceptional sets. The uniqueness theorem gives $F - G \equiv 0$. For the modulus-only assertion, take $F(z) = 1$ and $G(z) = z$. Both boundary moduli equal one everywhere, but their values and interior behavior differ. More strongly, $G(z) = S_a(z)$ has boundary modulus one almost everywhere while its modulus at zero is $e^{-a} < 1$. Thus phase information is essential. A plot of boundary magnitudes cannot certify equality of analytic functions.

Chapter 15

Almost-everywhere landing and harmonic measure

Source correspondence. Lyubich, §8.4, Exercise 8.19 and Remark 8.20.

The angular variable belongs to the ideal circle. The point where a ray lands belongs to the geometric boundary. These are different spaces, and a landing map may identify many angles or fail to exist on an exceptional set. We now transfer the almost-everywhere theorem carefully between them. The transfer produces harmonic measure and a precise interpretation of the source's statement about almost all boundary points being accessible. Nothing in this interpretation identifies harmonic measure with Euclidean arclength, and nothing asserts that all rays land without an additional geometric hypothesis.

15.1 The exterior normalization and its bounded analytic reduction

Let $K \subset \mathbb{C}$ be a compact connected set with more than one point, whose complement in the sphere is simply connected. Such a full continuum is the hull considered here. Let

$$\Omega = \widehat{\mathbb{C}} \setminus K,$$

and let $F : \{w \in \widehat{\mathbb{C}} : |w| > 1\} \to \Omega$ be a conformal bijection with $F(\infty) = \infty$ and expansion

$$F(w) = cw + c_0 + O(1/w), \qquad c > 0. \tag{15.1}$$

The number c is fixed by the hull and the chosen unit-circle normalization; it is not generally one. The external ray at angle t is $r \mapsto F(re^{it})$, $r > 1$. The ray lands if this expression has a finite limit as $r \downarrow 1$. The conformal existence and the meaning of the normalization are the uniformization inputs of this section; the boundary assertion is proved below.

Lemma 15.1 (Boundedness near the source circle)**.** *For every finite $R > 1$, F is bounded on $1 < |w| \le R$. Consequently*

$$G(z) = zF(1/z), \qquad 0 < |z| < 1,$$

extends to a bounded holomorphic function on $\mathbb{D}$ with $G(0) = c$.

Proof. If F were unbounded on that annulus, there would be w_n with $1 < |w_n| \le R$ and $F(w_n) \to \infty$ in the sphere. The inverse conformal map F^{-1} is continuous at the interior point ∞ of Ω and takes it to ∞. Hence $w_n = F^{-1}(F(w_n)) \to \infty$, contradicting $|w_n| \le R$. This uses interior continuity at infinity, not any boundary extension.

The Laurent expansion gives $G(z) = c + c_0 z + O(z^2)$ near zero, so the singularity there is removable. For $1/2 \le |z| < 1$, apply the annular bound with $R = 2$ and multiply by $|z| \le 1$. On $|z| \le 1/2$, continuity on a compact disk supplies a bound. Thus $G \in H^\infty$ and $G(0) = c > 0$. An explicit bound is available from the one annulus already controlled. Put $M_2 = \sup_{1<|w|\le 2} |F(w)| < \infty$. The maximum principle for the removable extension of G gives

$$\sup_{1/2\le|z|<1} |G(z)| \le M_2,$$
$$\sup_{|z|\le 1/2} |G(z)| \le \sup_{|z|=1/2} |G(z)| \le \tfrac{1}{2} M_2, \qquad \|G\|_{H^\infty} \le M_2.$$

No distance from a point in the interior of the hull enters this bound. □

Theorem 15.2 (Almost every external ray lands)**.** *For the hull and normalization above, $F(re^{it})$ has a finite limit $L(t) \in \partial K$ as $r \downarrow 1$ for almost every t.*

Proof. Apply Fatou's theorem to the bounded analytic G from Lemma 15.1. If $z = \rho e^{-it}$, then

$$F(\rho^{-1} e^{it}) = \rho^{-1} e^{it} G(\rho e^{-it}).$$

The right side has a finite limit for almost every t, since reflection $t \mapsto -t$ preserves circle measure. Call it $L(t)$. It belongs to the closure of Ω, being a limit of points of Ω. It cannot lie in the interior of K, whose neighborhood is disjoint from Ω. It cannot lie in Ω: continuity of F^{-1} at that interior point would give $F^{-1}(L(t)) = e^{it}$, whereas the inverse takes values in $|w| > 1$. Therefore $L(t) \in \partial K$. This proves the source exercise without assuming local connectivity or a continuous extension at every angle. □

Choosing a point of K and taking the reciprocal of $F(w)$ minus that point would not be a valid shortcut in this generality. If the hull has empty interior, the reciprocal may become arbitrarily large near its boundary. The bounded function $zF(1/z)$ avoids that error by using the controlled pole at infinity instead of an assumed positive distance from an interior point of K.

15.2 An independent geometric route through area

For conformal maps, almost-everywhere landing also follows from finite spherical area. This route is materially different from Fatou's general bounded-function proof: it uses injectivity to control area and does not construct a Hardy trace. We give the proof because it separates the analytic theorem, which applies to bounded functions of arbitrary multiplicity, from the geometric theorem, which applies to univalent maps with possibly unbounded images.

Use the spherical length element

$$\mathrm{d}s_{\mathrm{sph}} = \frac{2|\,\mathrm{d}w|}{1 + |w|^2}$$

and the corresponding area element $\mathrm{d}A_{\mathrm{sph}} = 4\,\mathrm{d}x\,\mathrm{d}y/(1+|w|^2)^2$. The total area of the sphere is 4π: polar integration gives $8\pi \int_0^\infty r(1+r^2)^{-2}\,\mathrm{d}r = 4\pi$. For a meromorphic conformal map $\phi : \mathbb{D} \to \widehat{\mathbb{C}}$, its spherical stretch factor is

$$\lambda_\phi(z) = \frac{2|\phi'(z)|}{1 + |\phi(z)|^2}.$$

At a pole this expression is interpreted in the reciprocal coordinate. It is invariant under replacing ϕ by $1/\phi$, because $2|(1/\phi)'|/(1+|1/\phi|^2) = 2|\phi'|/(1+|\phi|^2)$. Thus the apparent coordinate singularity does not affect length or area.

Theorem 15.3 (Finite radial spherical length almost everywhere)**.** *Let $\phi : \mathbb{D} \to \Omega \subset \widehat{\mathbb{C}}$ be a conformal bijection onto a proper domain. For almost every t, the curve $r \mapsto \phi(re^{it})$, $1/2 \le r < 1$, has finite spherical length and therefore has a spherical endpoint in $\partial\Omega$. More quantitatively, writing*

$$\ell(t) = \int_{1/2}^{1} \lambda_\phi(re^{it})\, \mathrm{d}r,$$

one has

$$\int_0^{2\pi} \ell(t)^2\, \mathrm{d}t \le (\log 2)\, \mathrm{Area}_{\mathrm{sph}}(\phi\{1/2 < |z| < 1\}) \le 4\pi \log 2.$$

Proof. The change-of-variables formula for a one-to-one C^1 map gives

$$\int_0^{2\pi} \int_{1/2}^{1} \lambda_\phi(re^{it})^2 r\, \mathrm{d}r\, \mathrm{d}t = \mathrm{Area}_{\mathrm{sph}}(\phi\{1/2 < |z| < 1\}).$$

To justify coordinates if a pole lies in the annulus, omit a small disk around it, apply the formula in the finite chart, and increase the omitted sets to their complement; the reciprocal chart shows that the omitted pole has zero area. Exhaustion by compact subannuli and monotone convergence handle the open outer boundary. Injectivity prevents multiplicity factors in this equality. The right side is at most the area 4π of the sphere.

Tonelli's theorem therefore makes $E(t) = \int_{1/2}^{1} \lambda_\phi(re^{it})^2 r\, \mathrm{d}r$ finite for almost every t. For such an angle, weighted Cauchy–Schwarz gives

$$\ell(t)^2 \le E(t) \int_{1/2}^{1} \frac{\mathrm{d}r}{r} = E(t) \log 2.$$

Integrate this inequality to obtain the quantitative claim. Finite length makes the curve Cauchy as $r \uparrow 1$: the distance between any two late points is bounded by the intervening length, which is at most a tail of a convergent nonnegative integral. The sphere is complete, being a compact metric space, so the endpoint exists. It cannot lie inside Ω, because continuity of ϕ^{-1} there would force the preimage sequence to converge to an interior point while its modulus tends to one. It belongs to the closure of Ω, so it lies in the boundary. At every angle with $E(t) < \infty$, the Cauchy estimate can also be read directly from its energy tail. For $1/2 \le r < s < 1$,

$$\begin{aligned} d_{\mathrm{sph}}(\phi(re^{it}), \phi(se^{it}))^2 &\le \log(s/r) \int_r^s \lambda_\phi(ue^{it})^2 u\, \mathrm{d}u \\ &\le \log(1/r) \int_r^1 \lambda_\phi(ue^{it})^2 u\, \mathrm{d}u \longrightarrow 0 \quad (r \uparrow 1). \end{aligned}$$

The final bound is uniform over $s \in (r, 1)$ at this fixed angle, which is the Cauchy criterion needed for the endpoint. □

There is also a mean-square endpoint estimate at every fixed starting radius. Let $0 < r_0 < 1$ and let $L(t)$ denote the spherical endpoint on the full-measure landing set. Repeating the same weighted Cauchy–Schwarz argument on $[r_0, 1)$ gives

$$\int_{\mathbb{T}} d_{\mathrm{sph}}(\phi(r_0 e^{it}), L(t))^2\, \mathrm{d}m(t) \le \frac{\log(1/r_0)}{2\pi}\, \mathrm{Area}_{\mathrm{sph}}(\phi\{r_0 < |z| < 1\}) \le 2\log(1/r_0).$$

The distance is bounded by the remaining radial length, which explains the first inequality; arbitrary values on the exceptional null set do not change the integral. This estimate is uniform over conformal bijections in the spherical metric, despite the absence of a uniform pointwise landing rate. It is an average statement over source angles. For a threshold $\eta > 0$, the angles where the displayed endpoint distance exceeds η have measure at most $2\log(1/r_0)/\eta^2$. Such a bound does not identify the bad angles or validate a numerically estimated endpoint, but it does

quantify exactly one consequence of the geometric area proof. If the image annulus has a smaller known area, its actual area improves the estimate.

For a bounded planar image, the same proof uses Euclidean length and area, giving

$$\int_0^{2\pi} \ell_{\mathrm{Euc}}(t)^2 \, \mathrm{d}t \le (\log 2)\,\mathrm{Area}(\Omega).$$

A bounded set has finite Euclidean area, and injectivity again supplies the required equality with $\int |\phi'|^2$. For an unbounded image, Euclidean area may be infinite even though the spherical statement is uniform. Substituting Euclidean area without checking finiteness would remove the essential hypothesis of this particular proof.

Apply Theorem 15.3 to $\phi(z) = F(1/z)$, with the removable spherical interpretation at zero. It is a conformal bijection onto Ω, so almost every ray has a spherical endpoint. Since infinity is an interior point of Ω, that endpoint is finite. This gives a second proof of Theorem 15.2, independent of the bounded analytic reduction. The two proofs have different additional outputs: the Hardy route gives a measurable analytic trace and nontangential control, while the area route gives finite radial length and an explicit integral bound.

15.3 Defining the landing measure

First consider a bounded simply connected domain $U \subset \mathbb{C}$ and a conformal bijection $\phi : \mathbb{D} \to U$. Boundedness permits direct use of Fatou's theorem. At almost every angle there is a finite limit

$$L(t) = \lim_{r \uparrow 1} \phi(re^{it}) \in \partial U.$$

The boundary membership follows by the same inverse-continuity argument used for exterior rays. The set where the limit exists is measurable: use any fixed sequence $r_j \uparrow 1$, the Cauchy criterion for its values, and then intersect with the full-measure set on which the complete radial limit exists. Equivalently the complete limit can be expressed using suprema over rational radii and continuity in r. On this measurable set, the limit is a measurable function as a pointwise limit of continuous functions. Assign any fixed boundary point to the remaining null set. This gives a measurable map $L : \mathbb{T} \to \partial U$; the assignment on the exceptional set will not change any of the following integrals.

Definition 15.4 (Harmonic measure through the landing map)**.** For $a = \phi(w) \in U$ and Borel $A \subset \partial U$, define

$$\omega_U^a(A) = \int_{\mathbb{T}} 1_A(L(t)) \frac{1 - |w|^2}{|e^{it} - w|^2} \, \mathrm{d}m(t).$$

At $a = \phi(0)$ this is the pushforward of normalized angular measure under L. For the exterior domain and the normalization (15.1), define harmonic measure at infinity by

$$\omega_\Omega^\infty(A) = m\{t : L(t) \in A\}, \qquad A \subset \partial K \text{ Borel}.$$

These are probability measures. Nonnegativity and total mass one follow from the Poisson kernel. Countable additivity follows by applying monotone convergence to the partial sums of indicators of disjoint Borel sets. There is no implicit measure on inaccessible points chosen by geometric intuition: the measure has been explicitly transported from the circle. The next proposition checks that it does not depend on the arbitrary choice of a disk uniformization.

Proposition 15.5 (Independence of the disk coordinate)**.** *The measure ω_U^a is unchanged if ϕ is replaced by another conformal bijection of the disk onto U and w is replaced by the preimage of the same a. For fixed $a, b \in U$, the measures ω_U^a and ω_U^b have the same null sets.*

Proof. Two disk uniformizations differ by a disk automorphism τ. Such an automorphism has the form $e^{i\beta}(b+z)/(1+\bar{b}z)$ with $|b|<1$. It extends smoothly to the closed disk, maps the circle bijectively to itself, and has a nonvanishing boundary derivative. Thus it preserves null sets in both directions, since it and its inverse are Lipschitz on the compact circle. It also takes radial approaches into fixed nontangential regions at the corresponding boundary point: near the circle its derivative and inverse derivative are bounded, while $1-|\tau(z)|^2$ is comparable to $1-|z|^2$ by the elementary identity below. Consequently the Fatou boundary functions for $\phi\circ\tau$ and ϕ satisfy $L_{\phi\circ\tau}(\zeta)=L_\phi(\tau(\zeta))$ outside a null set. This is why the nontangential version, rather than radial convergence alone without an approach theorem, was useful.

It remains to check the measure density. Rotations preserve normalized length, so omit $e^{i\beta}$. For $\tau(z)=(b+z)/(1+\bar{b}z)$, direct subtraction gives

$$1-|\tau(w)|^2=\frac{(1-|b|^2)(1-|w|^2)}{|1+\bar{b}w|^2},$$
$$|\tau(\zeta)-\tau(w)|^2=\frac{(1-|b|^2)^2|\zeta-w|^2}{|1+\bar{b}\zeta|^2|1+\bar{b}w|^2},$$
$$|\tau'(\zeta)|=\frac{1-|b|^2}{|1+\bar{b}\zeta|^2}\quad(|\zeta|=1).$$

Therefore

$$P_{\tau(w)}(\tau(\zeta))|\tau'(\zeta)|=P_w(\zeta),\qquad P_w(\zeta)=\frac{1-|w|^2}{|\zeta-w|^2}.$$

Changing the circle variable in the defining integral proves invariance. For the null-set claim, each P_w is bounded above and below by positive constants on the circle:

$$\frac{1-|w|}{1+|w|}\le P_w(\zeta)\le\frac{1+|w|}{1-|w|}.$$

Thus all such weighted circle measures have the same null sets, and so do their pushforwards under the same L. For explicit basepoint comparison, set $\alpha_w=(1-|w|)/(1+|w|)>0$. Integrating the two kernel bounds over $L^{-1}(A)$ first gives $\alpha_w m(L^{-1}(A))\le\omega_U^{\phi(w)}(A)\le\alpha_w^{-1}m(L^{-1}(A))$. Therefore, for $w,v\in\mathbb{D}$ and every Borel $A\subset\partial U$,

$$\alpha_w\alpha_v\,\omega_U^{\phi(v)}(A)\le\omega_U^{\phi(w)}(A)\le\frac{\omega_U^{\phi(v)}(A)}{\alpha_w\alpha_v}.$$

These constants are finite for fixed basepoints; no uniform bound as a basepoint approaches the boundary is asserted. □

15.4 Accessible mass and the absence of atoms

An angle at which the ray lands supplies an explicit access curve to its endpoint. Thus there is a measurable set of angles of measure one whose endpoints are accessible. To make the corresponding target-measure claim without assuming that images of measurable sets are measurable, we now construct a Borel set of accessible endpoints carrying all the mass.

Lemma 15.6 (A measurable set carrying accessible mass)**.** *In the bounded-domain and exterior-hull settings above, there is a Borel subset of accessible boundary points with harmonic measure one.*

Proof. Write $\Phi(r,t)$ for the radial parametrization in the disk coordinate; for the exterior setting use $F(r^{-1}e^{it})$. It is continuous for $r<1$, and has a spherical limit for almost every t. For positive

integers k and $n \geq 2$, let

$$C_{k,n} = \bigcap_{\substack{r,s\in\mathbb{Q} \\ 1-1/n\leq r,s<1}} \{t : d_{\mathrm{sph}}(\Phi(r,t),\Phi(s,t)) \leq 1/k\}.$$

Each set is closed because it is an intersection of closed inverse images under continuous functions. As n increases these sets increase, and their union has measure one because every convergent radial curve is Cauchy. For each $j,k \geq 1$, choose $n(j,k)$ so that $m(\mathbb{T} \setminus C_{k,n(j,k)}) < 2^{-j-k}$; continuity of measure from below allows this choice. The compact set

$$K_j = \bigcap_{k=1}^{\infty} C_{k,n(j,k)}$$

has measure at least $1 - 2^{-j}$. On K_j the radial family is uniformly Cauchy near $r = 1$. The rational restriction can be removed by continuity in r and s. Completeness of the sphere gives a limit, and uniform convergence of the continuous maps along any fixed sequence $r \uparrow 1$ makes $L|_{K_j}$ continuous. Every point of $L(K_j)$ is an actual ray endpoint and is therefore accessible. The image $L(K_j)$ is compact. Consequently $A = \bigcup_{j\geq 1} L(K_j)$ is Borel and consists of accessible points. Its preimage contains every K_j, so has angular measure one. The bounded Poisson weights do not charge its null complement. Thus $\omega(A) = 1$ for every indicated basepoint. The successive measure bounds making this conclusion possible are

$$m(\mathbb{T} \setminus K_j) \leq \sum_{k\geq 1} m(\mathbb{T} \setminus C_{k,n(j,k)}) \leq \sum_{k\geq 1} 2^{-j-k} = 2^{-j},$$
$$m(\mathbb{T} \setminus L^{-1}(A)) \leq \inf_{j\geq 1} m(\mathbb{T} \setminus K_j) = 0.$$

For the bounded-domain weight $P_w \leq \alpha_w^{-1}$ the target complement thus has mass at most $\alpha_w^{-1} m(\mathbb{T} \setminus L^{-1}(A)) = 0$; for the exterior normalization the weight is one. □

This proves the source's accessibility statement in an ordinary Borel measure setting. It does not assert that geometric arclength has the same null sets, or that the full accessibility set itself has any particular topological regularity. The explicitly constructed Borel subset is enough.

Theorem 15.7 (No point has positive harmonic measure)**.** *For the bounded simply connected domain and the exterior hull considered above, every singleton boundary point has harmonic measure zero.*

Proof. For bounded U, fix $b \in \partial U$. If $m\{t : L(t) = b\} > 0$, the bounded holomorphic function $\phi - b$ has radial trace zero on a positive-measure set. Theorem 14.3 would make $\phi \equiv b$, contradicting injectivity. Thus that angle set has measure zero. Weighting by any Poisson density preserves its zero measure, proving the assertion for every interior basepoint.

For the exterior hull, suppose $F(re^{it}) \to b$ on a positive-measure set of angles. In the disk coordinate $z = \rho e^{-it}$, the bounded analytic function $G(z) = zF(1/z)$ has trace be^{-it} on the reflected set. Hence the bounded holomorphic function $G(z) - bz$ has trace zero on a positive-measure set. Uniqueness would give $G(z) = bz$, contradicting $G(0) = c > 0$. Therefore the exterior landing measure has no atoms either. □

A boundary point may have many accesses and many landing angles, but this theorem rules out a positive-length set of angles landing at one point. It does not bound the cardinality of a null set of angles. A null set can be uncountable, so atomlessness is a measure statement rather than a finite-multiplicity theorem. In a locally connected setting the continuous landing map makes these distinctions visible as fibers of a continuous circle-to-boundary map; the theorem still controls only the measure of each individual fiber.

15.5 Boundary data and the Dirichlet interpretation

For bounded Borel $g : \partial U \to \mathbb{R}$, define

$$u(\phi(w)) = \int g(L(t))P_w(e^{it})\ \mathrm{d}m(t) = \int_{\partial U} g\ \mathrm{d}\omega_U^{\phi(w)}.$$

The composition $g \circ L$ is measurable and bounded. Its Poisson integral is harmonic, and composition with a conformal inverse preserves harmonicity: the planar Laplacian transforms by the positive factor $|(\phi^{-1})'|^2$, as a chain-rule calculation using the Cauchy–Riemann equations shows. Thus u is a bounded harmonic function on U. Its pulled-back nontangential trace equals $g \circ L$ at almost every ideal angle. This is a complete assertion for arbitrary bounded Borel data; it is not automatically a claim of continuity at every geometric boundary point.

Proposition 15.8 (Continuous geometric data when the map extends)**.** *Suppose in addition that ϕ extends continuously from the closed disk onto $\overline{U}$. If g is continuous on ∂U, then the function u just defined extends continuously to $\overline{U}$ with boundary values g, and it is the unique such harmonic extension.*

Proof. The circle function $g \circ \phi$ is continuous. It agrees almost everywhere with $g \circ L$, so their Poisson integrals agree. Proposition 12.1 gives a function continuous on the closed disk with those circle values. To establish continuity in the geometric closure, take $z_n \in U$ with $z_n \to b \in \partial U$ and write $w_n = \phi^{-1}(z_n)$. Every subsequence of w_n has a further subsequence converging in the compact closed disk. Its limit cannot be interior, because then continuity and injectivity would give an interior limit for z_n. Let the limit be $\zeta \in \mathbb{T}$. Continuity of ϕ gives $\phi(\zeta) = b$, and continuity of the disk Poisson solution gives $u(z_n) \to g(b)$ along this further subsequence. If the full sequence failed to tend to $g(b)$, a subsequence separated from $g(b)$ by a fixed positive amount would contradict this conclusion. Thus the geometric boundary limit exists and equals $g(b)$. Uniqueness follows from the maximum principle on the bounded domain: a continuous difference on the compact closure has zero boundary values, so both it and its negative have nonpositive maxima. One may also pull back to the disk and use the same principle there. □

The local-connectivity theorem elsewhere in this volume supplies a common sufficient condition for the continuous extension in this proposition. The present proof only uses the extension itself and does not reprove or weaken that geometric theorem. For rough domains without such an extension, the almost-everywhere trace interpretation remains valid and is the appropriate conclusion of the construction.

15.6 Solved investigations: landing and transported measure

Investigation 15.9 (A corrected exterior scaling)**.** Let $K = \{|z| \le R\}$ with $R > 0$. Determine the normalized exterior map, the function G, the landing measure at infinity, and the coefficient c in (15.1).

Solution. The map is $F(w) = Rw$, so $c = R$ and $G(z) = zR/z = R$ after removing the singularity at zero. Every ray lands at Re^{it}, and the landing measure is uniform angular measure on the radius-R circle. Its density with respect to Euclidean arclength $\mathrm{d}s = R\,\mathrm{d}t$ is $1/(2\pi R)$. Thus the measure is normalized to total mass one, not to Euclidean length $2\pi R$. An assertion $F(w) \sim w$ for every hull would fail already for these circles unless $R = 1$. The general leading coefficient is geometric data, not a harmless choice that can always be removed while retaining the fixed hull and unit source circle.

Investigation 15.10 (A finite-length tail estimate)**.** Using Theorem 15.3, bound the normalized angular measure of rays whose spherical length from radius $1/2$ to one exceeds $L > 0$.

Solution. The theorem and the elementary size estimate applied to ℓ^2 give

$$m\{t : \ell(t) > L\} \le \frac{1}{2\pi L^2} \int_0^{2\pi} \ell(t)^2 \, \mathrm{d}t \le \frac{2 \log 2}{L^2}.$$

One may replace the right side by its minimum with one. If the spherical area of the image annulus is known more sharply, use $(\log 2)\,\mathrm{Area}_{\mathrm{sph}}\,/(2\pi L^2)$ instead. The estimate controls a distribution of total lengths, not the endpoint location at a prescribed angle. It also gives no uniform landing rate for every ray: a small set may contain arbitrarily long or nonlanding rays without violating the bound.

Investigation 15.11 (Basepoint sensitivity in the disk)**.** For $U = \mathbb{D}$ and $a = \rho \in (0, 1)$, compare harmonic measure of a short arc around 1 with the same-length arc around -1.

Solution. The densities at the central points are

$$P_\rho(0) = \frac{1+\rho}{1-\rho}, \qquad P_\rho(\pi) = \frac{1-\rho}{1+\rho}.$$

For arcs of angular half-width $h \downarrow 0$, continuity of the density gives their masses asymptotic to $(h/\pi)P_\rho(0)$ and $(h/\pi)P_\rho(\pi)$. Their ratio tends to $((1+\rho)/(1-\rho))^2$. Both measures assign zero to exactly the same sets, but their numerical weights can differ greatly as the basepoint approaches the boundary. "Almost every boundary point" is therefore basepoint invariant within the domain, while quantitative probability estimates are not basepoint independent.

Investigation 15.12 (A nonlanding set and image measure)**.** Suppose the landing map is undefined on a null set N of angles. Explain why assigning arbitrary endpoints on N does not change harmonic measure. Does a null set of geometric boundary arclength necessarily have zero harmonic measure under the definitions alone?

Solution. Two completed landing maps differ only on N. For every Borel target set A, the two indicators of its preimage differ only on N. Integrating against the bounded Poisson density gives identical values. The same is true for the uniform measure at infinity. Thus the arbitrary completion is harmless for the measure, though it must not be mistaken for a genuine landing assertion on N. No arclength conclusion follows from this construction alone. The measure of A is controlled by the angular measure of $L^{-1}(A)$, and the definition supplies no Lipschitz bound or absolute-continuity relation between L and geometric arclength. Additional boundary regularity would be needed to establish such a relation. This is a limitation of the available hypotheses, not an assertion that the two measures always differ for every domain.

Investigation 15.13 (No positive-length collapse)**.** Assume a continuous boundary extension of a conformal map from the disk onto a bounded planar domain maps an entire nondegenerate circle arc to one geometric boundary point. Show that this is impossible. State what remains possible without contradicting the argument.

Solution. An arc of positive angular length has positive normalized measure. For a bounded target domain, subtracting the proposed boundary value from the bounded conformal map gives a bounded holomorphic function with radial trace zero on that arc. Positive-length uniqueness forces the map to be constant, contradicting conformality. Equivalently, Theorem 15.7 says that the point would have positive harmonic measure, which is impossible. The proof does not forbid two or more separate angles from sharing an endpoint, nor does it forbid an uncountable null fiber. It rules out positive angular measure of a fiber, not all failures of injectivity of the boundary extension.

15.7 The source appendix's exact conclusion

The chain of proved statements is now explicit. A bounded holomorphic function has an L^∞ trace and finite nontangential limits outside a null set. A positive-length set of equal boundary values forces that function to be constant. An exterior conformal map can be reduced to a bounded analytic function by removing its controlled pole, so its rays land almost everywhere. Independently, injectivity and finite spherical area give finite radial spherical length almost everywhere. The landing map transports angular measure to an atomless measure on the geometric boundary, carried by a Borel set of accessible endpoints.

These statements explain the source's connection with holomorphic dynamics, but they do not prove an ergodic theorem for any polynomial. Such a theorem would additionally need a specified dynamical system, invariance or quasi-invariance of the relevant measure, and an appropriate dynamical argument. Nor do the almost-everywhere landing statements settle local connectivity: a null exceptional set can still obstruct a continuous extension on the whole circle. These are mathematical distinctions within the classical theory, not unfinished numerical checks that could be removed by drawing more rays.

Chapter 16

Boundary traces, Dirichlet energy and normal flux

Boundary correspondence identifies where data belong. A boundary-value problem also needs a function space in which those data have controlled size. Continuous data, square-integrable data and finite-energy data are different classes. Even on the round disk, a continuous boundary function can require infinite Dirichlet energy. This chapter makes the distinction explicit and provides the energy identities used in the physical applications.

The circle is parametrized by e^{it}, $0 \le t < 2\pi$, with normalized measure $dm = dt/(2\pi)$. Fourier coefficients are $c_n = \int h(e^{it})e^{-int}\,dm(t)$, $n \in \mathbb{Z}$. Thus Parseval's identity is $\|h\|_2^2 = \sum_{n\in\mathbb{Z}} |c_n|^2$. The underlying Fourier completeness and Poisson representation are developed in Theorem 12.4 and the preceding analysis chapters. The energy integral on the disk uses ordinary unnormalized planar area. Keeping those two conventions separate explains the factor 2π below.

16.1 An exact spectral energy formula

Let $h \in L^2(\partial\mathbb{D}, m)$ and put

$$u(re^{it}) = \sum_{n\in\mathbb{Z}} c_n r^{|n|} e^{int}, \qquad 0 \le r < 1.$$

This is the Poisson extension. Cauchy–Schwarz gives absolute convergence on every smaller disk because $\sum r^{2|n|} < \infty$. Differentiated series also converge locally uniformly: factors polynomial in $|n|$ are dominated by a geometric sequence on a smaller disk. The extension is therefore smooth and harmonic in the interior.

The convergence bound can be written with its exact geometric factor:

$$\sum_{n\in\mathbb{Z}} |c_n| r^{|n|} \le \Big(\sum_n |c_n|^2\Big)^{1/2} \Big(1 + 2\sum_{n\ge 1} r^{2n}\Big)^{1/2} = \|h\|_2 \sqrt{\frac{1+r^2}{1-r^2}}.$$

For each fixed smaller radius the factor is finite; it is not uniform as $r \uparrow 1$.

For a complex-valued function define

$$E(u; V) = \int_V (|u_x|^2 + |u_y|^2)\,dA.$$

For a real-valued function this is the usual Dirichlet integral, without a factor $1/2$. The physical energy of a model may multiply this integral by conductivity, permittivity, or another specified coefficient.

Theorem 16.1 (Fourier characterization of finite energy)**.** *For $0 < R < 1$,*

$$E(u; B(0,R)) = 2\pi \sum_{n\in\mathbb{Z}} |n|\,|c_n|^2 R^{2|n|}.$$

Consequently

$$E(u;\mathbb{D}) = 2\pi \sum_{n\in\mathbb{Z}} |n|\,|c_n|^2,$$

where both sides may be $+\infty$. In particular, finite energy is equivalent to convergence of the weighted series.

Proof. First consider a finite Fourier sum. In polar coordinates its radial and angular derivatives are

$$u_r = \sum_{n\neq 0} |n| c_n r^{|n|-1} e^{int}, \qquad u_t = \sum_{n\neq 0} inc_n r^{|n|} e^{int}.$$

Orthogonality on the circle makes every mixed-frequency integral vanish. Since $|\nabla u|^2 = |u_r|^2 + r^{-2}|u_t|^2$, the contribution of frequency $n \neq 0$ is

$$2\pi \int_0^R 2n^2 |c_n|^2 r^{2|n|-2} r\,dr = 2\pi |n|\,|c_n|^2 R^{2|n|}.$$

The constant term has zero derivative. This proves the identity for finite sums. For the infinite series and a fixed $R < 1$, choose $R < R' < 1$. The differentiated series converges uniformly on the closed R disk, using Cauchy–Schwarz with the summable weights $n^2(R/R')^{2|n|}$ and $\sum |c_n|^2 (R')^{2|n|}$. Integration therefore passes to the limit of the finite sums. Finally, let $R \uparrow 1$. The energy integrals increase to the energy on $\mathbb{D}$, and the nonnegative series increases term by term. Monotone convergence proves the last identity even when the result is infinite. □

Define the circle Sobolev space H^s, for real s, by the Fourier norm

$$\|h\|_{H^s}^2 = \sum_{n\in\mathbb{Z}} (1+n^2)^s |c_n|^2.$$

For negative s, this defines a completion of trigonometric polynomials, which can equivalently be interpreted as distributions through their Fourier coefficients. The present arguments only need the coefficient-space definition. Since $\sqrt{1+n^2}$ is comparable to $1+|n|$, the finite-energy traces in L^2 are exactly $H^{1/2}$. The comparison is explicit:

$$\sqrt{1+n^2} \le 1 + |n| \le \sqrt{2}\sqrt{1+n^2}.$$

Thus $\|h\|_2^2 + E(u)/(2\pi)$ is an equivalent squared norm on $H^{1/2}$, with these numerical constants.

In norm notation, the comparison reads

$$\|h\|_{H^{1/2}}^2 \le \|h\|_2^2 + \frac{E(P[h])}{2\pi} \le \sqrt{2}\,\|h\|_{H^{1/2}}^2.$$

The zero Fourier coefficient contributes to the norm but not to the energy.

16.2 The variational meaning of the extension

We give a precise minimization statement without assuming an unproved trace theorem. Let $H^1(\mathbb{D})$ be the space of square-integrable functions whose distributional first derivatives are square-integrable. Its norm is $\|v\|_{H^1}^2 = \|v\|_{L^2(\mathbb{D})}^2 + E(v)$. Let $H_0^1(\mathbb{D})$ denote the closure of smooth compactly supported functions in this norm. Declaring that v has the same boundary data as u

means, in this variational statement, that $v - u \in H^1_0(\mathbb{D})$. We do not use that phrase to assert pointwise continuity of v on the closed disk.

For completeness, the H^1 space just defined is complete. If v_j is Cauchy in its norm, completeness of planar L^2 gives limits v and g_x, g_y for the functions and their two weak derivatives. For every smooth compactly supported test function φ, pass to the limit in $\int v_j \partial_x \varphi = -\int (\partial_x v_j)\varphi$ using Cauchy–Schwarz. The result is the weak derivative identity for v, g_x; the y identity follows in the same way. Thus $v \in H^1$ and $v_j \to v$ in H^1. This is the only completeness step needed in the following minimization argument.

Theorem 16.2 (Dirichlet minimization in the stated affine class)**.** *If $h \in H^{1/2}$ and u is its Poisson extension, then $u \in H^1(\mathbb{D})$. For every $w \in H^1_0(\mathbb{D})$,*

$$E(u + w) = E(u) + E(w).$$

Hence u is the unique energy minimizer in $u + H^1_0(\mathbb{D})$.

Proof. For Fourier partial sums, orthogonality gives

$$\|u\|^2_{L^2(\mathbb{D})} = \pi \sum_{n \in \mathbb{Z}} \frac{|c_n|^2}{|n| + 1}.$$

The same equality for the infinite sum follows by convergence of the nonnegative series. The energy formula shows that the partial sums are Cauchy in H^1. Their local uniform limit is u, so their H^1 limit has the same function and weak derivatives; hence $u \in H^1$.

For smooth compactly supported w, integration by parts and $\Delta u = 0$ give $\int_{\mathbb{D}} \nabla u \cdot \overline{\nabla w}\, dA = 0$. If $w_j \to w$ in H^1, Cauchy–Schwarz passes this identity to the limit.

Specifically,

$$\left| \int_{\mathbb{D}} \nabla u \cdot \overline{\nabla (w_j - w)}\, dA \right| \le E(u)^{1/2} E(w_j - w)^{1/2} \longrightarrow 0,$$

and hence

$$E(u + w) - E(u) = E(w) + 2 \operatorname{Re} \int_{\mathbb{D}} \nabla u \cdot \overline{\nabla w}\, dA = E(w) \ge \tfrac{1}{4} \|w\|^2_{L^2(\mathbb{D})}.$$

The last inequality is the zero-boundary estimate established immediately below and makes the uniqueness conclusion quantitative.

Expanding $|\nabla(u + w)|^2$ and taking the real part of the cross term proves the displayed equality. If equality of energies holds, $E(w) = 0$. To exclude a nonzero constant in H^1_0, extend a compactly supported smooth w_j by zero to the square $[-1, 1]^2$. On every horizontal line,

$$|w_j(x, y)|^2 \le 2 \int_{-1}^{1} |\partial_x w_j(s, y)|^2\, ds.$$

Integration over x, y gives $\|w_j\|^2_{L^2(\mathbb{D})} \le 4 \|\partial_x w_j\|^2_{L^2(\mathbb{D})}$. Passing to the limit gives the same inequality for w. If $E(w) = 0$, then $w = 0$ in L^2, proving uniqueness. □

This formulation is stronger than an informal least-energy picture because the comparison class and the meaning of boundary data are specified. It is also deliberately narrower than a general trace theorem for an arbitrary rough domain. Transferring the statement to a physical boundary requires a chosen conformal parametrization and the corresponding energy class; it does not turn arbitrary arclength data into the same Fourier space.

16.3 Normal derivatives and the Dirichlet-to-Neumann operator

For a finite Fourier sum, the outward radial derivative at the unit circle is

$$\Lambda h = \sum_{n\in\mathbb{Z}} |n| c_n e^{int}.$$

The multiplier $|n|$ defines the disk Dirichlet-to-Neumann operator. Its kernel consists of constants, reflecting the fact that a constant potential produces no field. It is positive and self-adjoint on finite sums under the normalized circle inner product.

Proposition 16.3 (Flux as a weak boundary functional)**.** *The operator Λ extends continuously from $H^{1/2}$ to $H^{-1/2}$, with norm at most one for the displayed inhomogeneous norms. For $h, k \in H^{1/2}$,*

$$\langle \Lambda h, k\rangle = \sum_n |n| c_n \overline{d_n}, \qquad E(P[h]) = 2\pi \langle \Lambda h, h\rangle.$$

If $h \in H^1$, the radial derivatives of its harmonic extension converge in L^2 to Λh as $r \uparrow 1$.

Proof. The coefficient norm satisfies

$$\|\Lambda h\|^2_{H^{-1/2}} = \sum_n \frac{n^2|c_n|^2}{\sqrt{1+n^2}} \le \sum_n \sqrt{1+n^2}|c_n|^2.$$

The pairing converges absolutely by Cauchy–Schwarz with weights $|n|$, and the energy identity is Theorem 16.1. For $h \in H^1$, $\sum n^2|c_n|^2 < \infty$. The coefficients of u_r are $|n|c_n r^{|n|-1}$ for $n \neq 0$. For $r \ge 1/2$ the factors $r^{|n|-1}$ are bounded by one and tend to one. Dominated convergence in the summable coefficient squares gives the L^2 limit. The zero-frequency coefficient remains zero.

For $h \in H^1$, the asserted norm convergence is precisely

$$\|u_r(r\,\cdot) - \Lambda h\|_2^2 = \sum_{n\neq 0} n^2|c_n|^2 |r^{|n|-1} - 1|^2 \longrightarrow 0, \qquad 0 \le |r^{|n|-1} - 1|^2 \le 1.$$

The summable majorant is $n^2|c_n|^2$, not an assumed pointwise bound for the normal derivative. □

For a general $H^{1/2}$ trace the normal derivative need not be an ordinary square-integrable function. The weak pairing remains meaningful and is the appropriate notion of total work against another boundary potential. Writing a pointwise flux formula without the stronger regularity hypothesis would discard exactly the distinction the Sobolev scale records.

16.4 Conformal transfer of energy

Theorem 16.4 (Planar conformal invariance of the Dirichlet integral)**.** *Let $f : U \to V$ be conformal and bijective between plane domains and let v be continuously differentiable on V. Then*

$$E(v \circ f; U) = E(v; V),$$

allowing either side to be infinite. On a smooth boundary arc where f extends differentiably with nonzero derivative, arclength scales by $|f'|$ and normal derivative scales by $|f'|^{-1}$.

Proof. At an interior point, Df is $|f'|$ times an orthogonal matrix. The chain rule gives $|\nabla(v\circ f)|^2 = |f'|^2(|\nabla v|^2 \circ f)$, with the same formula componentwise for complex v. The Jacobian of f is $|f'|^2$. Change variables on compact exhaustions and then pass to the limit by monotone

convergence. On the indicated boundary arc, the tangent vector is dilated by $|f'|$; the oriented normal is rotated by the same rotation. Applying the chain rule in the normal direction gives the reciprocal factor when one solves for the target normal derivative.

Assume also that v has continuous first derivatives up to the image boundary arc. With $u = v \circ f$, the local boundary transformation is

$$ds_V = |f'|\, ds_U, \qquad (\partial_{\nu_V} v) \circ f = |f'|^{-1} \partial_{\nu_U} u, \qquad ((\partial_{\nu_V} v) \circ f)\, |f'|\, ds_U = \partial_{\nu_U} u\, ds_U.$$

The cancellation is valid on the smooth nondegenerate arc specified in the theorem; it explains invariance of integrated flux there.

□

The interior energy identity needs no smooth physical boundary. The boundary flux formula does need the stated local regularity. In particular, the identity does not justify dividing by a boundary derivative at a cusp where that derivative is zero, infinite, or nonexistent. Wedge and slit models provide explicit limiting interpretations in the applications rather than an unrestricted use of the smooth formula.

Investigation 16.5 (A single real Fourier mode)**.** For boundary data $h(e^{it}) = A\cos(nt)$, $n \geq 1$, compute the harmonic extension, its energy, its outward normal derivative and its energy inside the circle of radius R.

Solution. The nonzero coefficients are $c_n = c_{-n} = A/2$, giving $u(re^{it}) = Ar^n \cos(nt)$. Thus $E(u) = \pi n A^2$, $\partial_\nu u = nA\cos(nt)$ and $E(u; B(0,R)) = \pi n A^2 R^{2n}$. The field concentrates near the boundary as n increases: the fraction of energy inside R is R^{2n}. That exact identity explains why high-frequency boundary information is hard to recover from measurements on a fixed interior circle.

Investigation 16.6 (Continuous data with infinite energy)**.** Consider

$$h(e^{it}) = \sum_{k=1}^{\infty} \frac{2^{-k/2}}{\sqrt{k}} \cos(2^k t).$$

Prove that h is continuous, but its Poisson extension has infinite energy.

Solution. The absolute sum of the coefficient amplitudes is bounded by $\sum_{k\geq 1} 2^{-k/2} < \infty$. The series therefore converges uniformly to a continuous function. Its frequencies are distinct, and Theorem 16.1 gives energy $\pi \sum_{k\geq 1} 2^k (2^{-k}/k) = \pi \sum_{k\geq 1} 1/k = \infty$. The extension still converges continuously to its boundary data, by the continuous-data Poisson theorem. Hence continuous boundary solvability and finite energy are separate requirements, even on the smoothest possible domain. A finite truncation at $k = K$ has energy $\pi \sum_{k=1}^{K} 1/k$, an exact analytic value rather than a simulated one.

Investigation 16.7 (A jump and its cost)**.** Let $h(e^{it})$ be 1 for $0 < t < \pi$ and -1 for $\pi < t < 2\pi$. Show that $h \in L^2$ but its harmonic extension has infinite energy.

Solution. The function has modulus one almost everywhere. Its sine coefficients are $4/(\pi n)$ for positive odd n, and zero for even n. This follows by integrating the sine separately over the two semicircles. A real sine mode of amplitude a_n contributes $\pi n a_n^2$ to the energy. Consequently the total is $(16/\pi) \sum_{n \text{ odd}} 1/n = \infty$. The Poisson extension is a bounded harmonic solution with the prescribed almost-everywhere trace. Finite electrode jumps are therefore compatible with bounded potential but can produce a divergent idealized field energy unless the physical model resolves the jump or excludes its endpoints.

Investigation 16.8 (Scaling a conducting disk)**.** Let u solve a disk problem and put $v(z) = u(z/R)$ on $|z| < R$. Compare the two Dirichlet energies and the corresponding normal derivatives.

Solution. The gradient of v is R^{-1} times the gradient of u in scaled coordinates, while area is multiplied by R^2. The two factors cancel, so the energies agree. On the boundary, normal derivative is multiplied by R^{-1} while arclength is multiplied by R, so the integrated flux against a correspondingly scaled test potential is unchanged. This is a two-dimensional statement. In dimension d, the same scaling of the Dirichlet integral produces R^{d-2}; no analogous scale independence is being claimed for arbitrary spatial dimension.

Chapter 17

Recovering boundary information from interior data

The Poisson operator smooths boundary oscillation. This makes the forward Dirichlet problem stable but makes its inverse unstable. The distinction persists even when the geometry is exactly known, every arithmetic operation is exact, and the entire interior measurement circle is observed. It is therefore an information limitation rather than a defect of a particular numerical implementation.

Fix $0 < r < 1$. Write $P_r h$ for the function on the measurement circle with Fourier coefficients $r^{|n|}c_n$. Both boundary and measured functions are represented on the angular interval with normalized L^2 norm. The observation model is

$$y = P_r h + e, \qquad \|e\|_2 \le \delta.$$

The error is deterministic and can be adversarial. It is not assumed to be independent random noise. No stochastic confidence level is attached to the bounds in this chapter.

17.1 Forward stability and inverse discontinuity

Proposition 17.1 (Contraction and exact uniqueness)**.** $\|P_r h - P_r k\|_2 \le \|h - k\|_2$. *Exact data $P_r h$ uniquely determine $h \in L^2$, but the inverse on its range is not a bounded operator from L^2 to L^2.*

Proof. Parseval gives

$$\|P_r(h-k)\|_2^2 = \sum_n r^{2|n|}|c_n - d_n|^2 \le \sum_n |c_n - d_n|^2.$$

Every multiplier is nonzero, so $P_r h = P_r k$ forces equality of all Fourier coefficients and hence $h = k$ in L^2. For the unit-norm mode $h_n(e^{it}) = e^{int}$, the image norm is $r^n \to 0$ while $\|h_n\|_2 = 1$. A bounded inverse would give $1 \le Cr^n$ for all n, which is impossible.

The spectral obstruction may also be expressed as

$$P_r(e^{int}) = e^{-\tau|n|}e^{int}, \qquad \frac{\|e^{int}\|_2}{\|P_r(e^{int})\|_2} = e^{\tau|n|} \longrightarrow \infty, \qquad \tau = -\log r > 0.$$

Every multiplier is positive, while their infimum is zero; this is the precise coexistence of injectivity and inverse instability.

□

Uniqueness is therefore not a stability estimate. The formal coefficient inversion $c_n = r^{-|n|}y_n$ amplifies measurement errors exponentially. The rate is governed by the depth $\tau = -\log r$ of the measurement circle: the amplification at frequency n is $e^{\tau|n|}$. A procedure that keeps all noisy coefficients cannot have a uniform boundary error bound under only an L^2 bound on the noise.

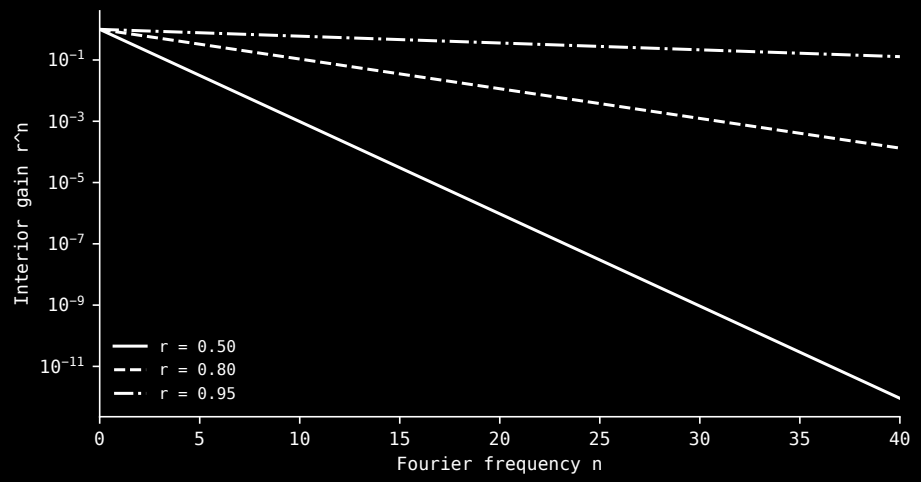


Figure 17.1: The Poisson multiplier r^n at three observation radii. Higher angular frequencies are attenuated more strongly. These curves plot the exact analytic multiplier, not experimental recovery data.

17.2 A regularized reconstruction with an explicit prior

Assume $\|h\|_{H^s} \le M$ with $s > 0$, and let y_n be the Fourier coefficients of the observed function. Define the spectral cutoff

$$\widehat{h}_N(e^{it}) = \sum_{|n|\le N} r^{-|n|} y_n e^{int}.$$

This definition assumes access to the Fourier coefficients of the entire measurement function. Computing them from finitely many point samples incurs an additional quadrature error, treated in the later computational chapter. The present model isolates information loss through interior propagation.

Theorem 17.2 (Bias and noise under a Sobolev prior)**.** *For every integer $N \ge 0$,*

$$\|\widehat{h}_N - h\|_2 \le r^{-N}\delta + M(1 + (N+1)^2)^{-s/2}.$$

If $0 < \delta < M$ and $N = \lfloor \log(M/\delta)/(2|\log r|) \rfloor$, the first term is at most $\sqrt{M\delta}$ and the second term tends to zero at a logarithmic rate as $\delta/M \downarrow 0$.

Proof. The retained coefficients have errors $r^{-|n|}e_n$. Parseval and $|n| \le N$ give a squared error at most $r^{-2N}\sum_{|n|\le N}|e_n|^2 \le r^{-2N}\delta^2$. The discarded true coefficients satisfy

$$\sum_{|n|>N} |c_n|^2 \le (1 + (N+1)^2)^{-s} \sum_{|n|>N} (1+n^2)^s |c_n|^2 \le M^2(1 + (N+1)^2)^{-s}.$$

These error parts have disjoint Fourier supports, so in fact the square of the total is bounded by the sum of their squared bounds. Taking a square root and then using $\sqrt{a^2+b^2} \le a + b$ proves the stated estimate. For the proposed cutoff, $N|\log r| \le \frac{1}{2}\log(M/\delta)$. Exponentiation yields

$r^{-N}\delta \le \sqrt{M\delta}$. Since $N+1$ grows linearly with $\log(M/\delta)$, the bias estimate has the claimed logarithmic behavior. No limit in r is taken.

The orthogonality used above gives the sharper squared identity and bound

$$\begin{aligned}\|\widehat{h}_N - h\|_2^2 &= \sum_{|n|\le N} r^{-2|n|}|e_n|^2 + \sum_{|n|>N} |c_n|^2 \\ &\le r^{-2N}\delta^2 + M^2(1+(N+1)^2)^{-s}.\end{aligned}$$

If $L = \log(M/\delta) > 0$ and $\tau = |\log r|$, the chosen N also gives

$$\|\widehat{h}_N - h\|_2 \le \sqrt{M\delta} + M\left(\frac{2\tau}{L}\right)^s, \qquad N+1 > \frac{L}{2\tau}.$$

This makes the dependence on the fixed observation radius explicit.

□

The theorem contains an actual stopping rule: choose a finite cutoff from M, s, r, δ. The rule is meaningful only when those quantities have the stated interpretation. In particular, choosing a visually smooth cutoff does not verify an assumed Sobolev bound. The prior is a mathematical constraint on admissible boundary data, not a property inferred from one successful reconstruction.

Theorem 17.3 (A matching logarithmic obstruction)**.** *Let an arbitrary reconstruction rule T assign an L^2 boundary function to each observation y. For $0 < \delta < M$, put*

$$n = \left\lceil \frac{\log(M/\delta)}{|\log r|} \right\rceil.$$

There are real boundary data with $\|h\|_{H^s} \le M$ and admissible noise for which

$$\|T(y) - h\|_2 \ge M(1+n^2)^{-s/2}.$$

The conclusion does not assume that T is linear, continuous or computable.

Proof. Set $A = \sqrt{2}M(1+n^2)^{-s/2}$ and $h_\pm(e^{it}) = \pm A\cos(nt)$. Their H^s norms equal M and their L^2 norms equal $a = M(1+n^2)^{-s/2}$. Their propagated norms are $r^n a \le r^n M \le \delta$. Thus the same observation $y = 0$ is admissible for either signal, by taking $e_\pm = -P_r h_\pm$. The signals are separated by $\|h_+ - h_-\|_2 = 2a$. The triangle inequality implies that $T(0)$ is at distance at least a from one of them. This proves the bound.

The minimax step is the elementary two-point inequality

$$2a = \|h_+ - h_-\|_2 \le \|T(0) - h_+\|_2 + \|T(0) - h_-\|_2 \le 2\max_{\sigma\in\{+,-\}} \|T(0) - h_\sigma\|_2.$$

Its quantifier is "for every T, at least one sign," so no choice of a nonlinear reconstruction rule can remove the obstruction.

□

For fixed r and s, the upper and lower estimates have the same $\log(M/\delta)^{-s}$ order as $\delta/M \to 0$. The result concerns deterministic worst-case boundary recovery under this normed model. It does not claim optimal numerical work, optimal sampling, or a rate for a different physical noise model. When $\delta \ge M$, the zero reconstruction has error at most M, and opposite constant signals $\pm M$ show that M is also a lower bound. When $\delta = 0$, exact uniqueness holds but does not make the inverse uniformly stable under nonzero perturbations.

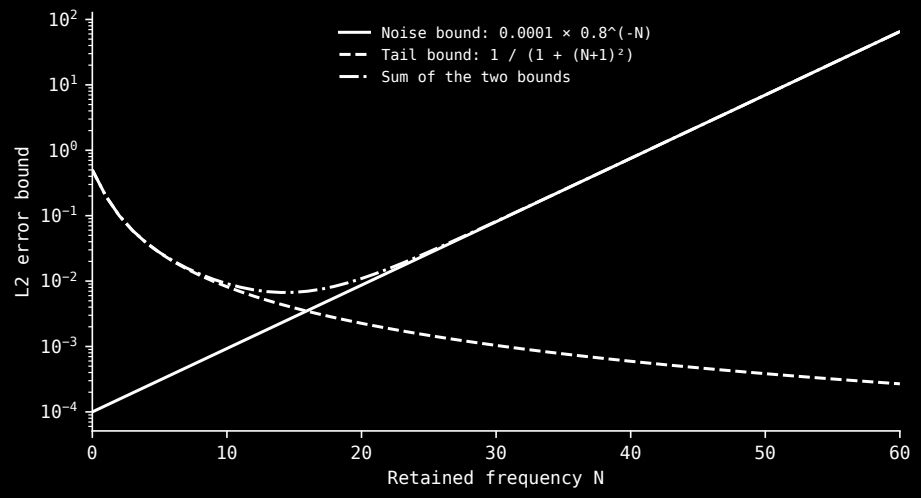


Figure 17.2: The two terms of the Sobolev recovery bound for $r = 0.8$, $\delta = 10^{-4}$, $M = 1$ and $s = 2$. Increasing the cutoff reduces the prior tail and amplifies noise. The sum is a proved upper-bound formula; it is not an observed error curve.

17.3 Analytic priors change the rate

Suppose now that h is the boundary trace of a holomorphic function H on a neighborhood of the closed disk $|z| \le \rho$, with $\rho > 1$ and $|H(z)| \le M$ on that closed disk. Its coefficients vanish for $n < 0$, and Cauchy's estimate gives $|c_n| \le M\rho^{-n}$ for $n \ge 0$. This is stronger information than any fixed Sobolev bound.

Theorem 17.4 (Hölder recovery under an analytic-radius prior)**.** *For $0 < \delta < M$, define*

$$\beta = \frac{\log \rho}{\log(\rho/r)}, \qquad N = \left\lfloor \frac{\log(M/\delta)}{\log(\rho/r)} \right\rfloor.$$

The nonnegative-frequency cutoff satisfies

$$\|\widehat{h}_N - h\|_2 \le \left(1 + \frac{1}{\sqrt{1-\rho^{-2}}}\right) M^{1-\beta}\delta^{\beta}.$$

For every reconstruction rule there is an admissible pair of data and noise with error at least $\rho^{-1}M^{1-\beta}\delta^{\beta}$.

Proof. The noise bound remains $r^{-N}\delta$. The geometric coefficient estimate gives tail norm at most $M\rho^{-(N+1)}/\sqrt{1-\rho^{-2}}$. Put $X = \log(M/\delta)/\log(\rho/r)$. Since $N \le X < N+1$,

$$r^{-N}\delta \le r^{-X}\delta = M^{1-\beta}\delta^{\beta}, \qquad M\rho^{-(N+1)} \le M\rho^{-X} = M^{1-\beta}\delta^{\beta}.$$

Adding the two estimates proves the upper bound.

For the lower bound take $n = \lceil X \rceil$ and the two entire functions $H_{\pm}(z) = \pm M\rho^{-n}z^n$. Both satisfy the analytic prior, including on the circle of radius ρ. Their measurement norms are $M(r/\rho)^n \le \delta$, so $y = 0$ is consistent with both. Their boundary norm is $M\rho^{-n} \ge M\rho^{-(X+1)}$. The same two-point triangle argument as before gives the claimed lower bound. These examples show that the exponent is forced by the prior and observation radius, rather than by the particular cutoff method. □

As r approaches one, β approaches one: observations close to the boundary lose less information. As ρ decreases to one with fixed r, the analytic continuation margin vanishes and β approaches

zero. One cannot keep the same Hölder rate while discarding the radius assumption. The endpoint $r = 0$ is excluded because observation only at the center reveals just the constant coefficient.

Investigation 17.5 (Two indistinguishable boundary fields)**.** Take $r = 1/2$, $s = 1$, $M = 1$ and $\delta = 2^{-10}$. Construct two opposite admissible real traces giving the same observation and compute the resulting lower bound for any reconstruction.

Solution. Here $n = 10$. Take $h_{\pm}(e^{it}) = \pm\sqrt{2/101}\cos(10t)$. Each has H^1 norm one and L^2 norm $1/\sqrt{101}$. Its measured norm is $2^{-10}/\sqrt{101} \le \delta$. Noise equal to the negative measurement gives $y = 0$ for both. Any reconstruction has error at least $1/\sqrt{101}$ for one of the traces. All numbers follow exactly from the model; no floating-point experiment is needed to establish the example.

Investigation 17.6 (Why no fixed cutoff works at every noise level)**.** Under the Sobolev prior, explain why taking N fixed as $\delta \to 0$ can leave a nonzero error, while taking $N \to \infty$ too rapidly can amplify noise without bound.

Solution. A fixed cutoff discards every coefficient above N even in exact data. The admissible single mode at $N + 1$, scaled to have H^s norm M, has positive L^2 norm and is reconstructed as zero. Conversely, noise concentrated at frequency N with coefficient δ is amplified to $r^{-N}\delta$. If $N|\log r| - \log(1/\delta) \to +\infty$, this quantity diverges. A consistent choice must control both bias and amplification; the explicit rule in Theorem 17.2 does so.

Investigation 17.7 (The analytic exponent)**.** For $r = 1/2$ and $\rho = 2$, determine the exponent in Theorem 17.4. Compare the observation problems at $r = 1/4$ and at $r = 3/4$, keeping $\rho = 2$.

Solution. At $r = 1/2$, $\beta = \log 2/\log 4 = 1/2$. At $r = 1/4$ it is $\log 2/\log 8 = 1/3$. At $r = 3/4$ it is $\log 2/\log(8/3)$, which is larger than $1/2$ and smaller than one. Moving the observation circle inward decreases the exponent and worsens recovery. The prior is held fixed throughout this comparison; changing the unknown function class would be a different problem.

Chapter 18

Finite observations and honest boundary guarantees

Boundary computation often begins with a finite collection of values. Finite data are useful when joined to a prior, an approximation theorem and a stability estimate. Alone, they cannot certify a whole boundary function. The following construction gives an exact obstruction without relying on rounding, statistical uncertainty or unresolved mathematical conjectures.

18.1 An indistinguishable holomorphic alternative

Theorem 18.1 (Finite interior sampling obstruction)**.** *Let a deterministic procedure choose finitely many points of $\mathbb{D}$, possibly adaptively from earlier sampled values, and then output an approximation to the boundary trace of an unknown holomorphic function bounded by one on $\mathbb{D}$. There is a set of exact replies for which two admissible functions give those same replies and their boundary traces are distance two apart in the supremum norm. Therefore the worst-case boundary supremum error of that procedure is at least one.*

Proof. Run the procedure on the identically zero replies. It chooses a finite list $a_1, \dots, a_m \in \mathbb{D}$ and terminates. Define the finite Blaschke product

$$B(z) = \prod_{j=1}^{m} \frac{z - a_j}{1 - \bar{a}_j z};$$

for $m = 0$ set $B = 1$. Each denominator is nonzero on the closed disk; the disk-automorphism identity in Proposition 1.2 shows $|B| \leq 1$ inside and $|B| = 1$ on the circle. Both B and $-B$ vanish at all queried points. By induction through the deterministic adaptive choices, both produce precisely the same query list and zero replies. The procedure therefore returns the same output for both. Their boundary traces differ by $2B$, of supremum norm two. The triangle inequality forces error at least one for one of them. □

The theorem concerns a whole bounded analytic class, not an arbitrary claim that finite computations are useless. Additional information such as a known degree, a larger analytic disk with a uniform bound, or a finite-dimensional parametric model changes the admissible alternatives. The forward quadrature chapter states such information explicitly before giving error bounds. Randomized procedures require a specified probability model and a different minimax argument; no probabilistic conclusion is inferred here.

Corollary 18.2 (A pointwise form of the obstruction)**.** *For a fixed queried list $a_1, \dots, a_m$ and a point $z_* \in \mathbb{D}$ distinct from all of them, two functions bounded by one give the same zero samples*

but differ at z_* by

$$2\prod_{j=1}^{m}\left|\frac{z_*-a_j}{1-\bar{a}_j z_*}\right|>0.$$

Proof. Evaluate the two functions $\pm B$ from the proof. The product is nonzero because z_* is not a sampled point and no denominator vanishes. Its value can be very small deep inside a well-sampled region. This does not contradict the boundary obstruction, where each factor has modulus one and no such decay occurs.

Writing $\rho_{\mathbb{D}}(z,a)=|(z-a)/(1-\bar{a}z)|$ for the pseudohyperbolic distance, the same construction gives

$$\inf_{v\in\mathbb{C}}\max_{\sigma\in\{+1,-1\}}|v-\sigma B(z_*)|=|B(z_*)|=\prod_{j=1}^{m}\rho_{\mathbb{D}}(z_*,a_j)>0.$$

The equality is attained at $v=0$ and the lower bound follows from the triangle inequality. It concerns these two compatible alternatives.

□

18.2 Boundary samples and finite Fourier models

If the unknown trace is known in advance to be a trigonometric polynomial of degree at most N, then $2N+1$ equally spaced samples determine it. Indeed, if $t_j=2\pi j/(2N+1)$, discrete orthogonality gives

$$c_n=\frac{1}{2N+1}\sum_{j=0}^{2N}h(e^{it_j})e^{-int_j},\qquad -N\le n\le N.$$

To verify the formula, insert the finite Fourier expansion and use the finite geometric sum. The sum is one when the frequency difference is a multiple of $2N+1$ and zero otherwise; within the stated degree range, only equality of frequencies can produce that multiple.

For $L=2N+1$ and $-N\le k,n\le N$, the calculation is

$$\frac{1}{L}\sum_{j=0}^{L-1}e^{2\pi i(k-n)j/L}=\begin{cases}1, & k=n,\\ 0, & k\neq n,\end{cases}\qquad |k-n|\le 2N<L.$$

The strict inequality excludes nonzero multiples of L in this frequency range; it is exactly where the degree hypothesis enters.

This is an exact theorem under an exact degree bound. If that bound is absent, the same samples cannot distinguish frequencies differing by a multiple of the sample count. The functions 1 and $e^{i(2N+1)t}$ agree at every grid point but are different elsewhere. Smoothness and analyticity can bound high-frequency tails, but they must do so quantitatively; the word “smooth” alone is not an error certificate with specified tolerance.

Proposition 18.3 (A conditional grid guarantee)**.** *Suppose a continuous periodic function has Fourier coefficients satisfying $\sum_{n\in\mathbb{Z}}|c_n|<\infty$. Let $L=2N+1$, and form the coefficients $\widetilde{c}_n=L^{-1}\sum_{j=0}^{L-1}h(e^{2\pi ij/L})e^{-2\pi inj/L}$ for $|n|\le N$. Then*

$$\widetilde{c}_n=\sum_{k\in\mathbb{Z}}c_{n+kL},\qquad \left\|h-\sum_{|n|\le N}\widetilde{c}_n e^{int}\right\|_{\infty}\le 2\sum_{|n|>N}|c_n|.$$

Proof. Absolute summability permits interchanging the Fourier series and the finite sample sum. Discrete orthogonality leaves exactly the coefficients in the indicated residue class. The difference between h and its true degree-N truncation is bounded by the tail sum. The coefficient error within the retained frequencies is bounded by $\sum_{|n|\le N}\sum_{k\neq 0}|c_{n+kL}|$. Every omitted integer has a unique representative in $[-N, N]$ modulo L, so this second sum is exactly the same tail sum. The triangle inequality gives the factor two. □

The result exhibits the missing ingredient in a visual grid check: a bound for the unsampled tail. It also distinguishes approximation error from arithmetic error. If each sample has additive error at most ε, each reconstructed coefficient changes by at most ε, so the resulting trigonometric polynomial changes in supremum norm by at most $(2N+1)\varepsilon$. This elementary estimate is conservative but explicit. Sharper noise models can improve it; changing the model must be recorded.

With noisy samples $h(e^{2\pi ij/L}) + \eta_j$, $|\eta_j| \le \varepsilon$, the combined bound follows by summing the coefficient perturbations:

$$|\Delta\widetilde{c}_n| \le L^{-1}\sum_{j=0}^{L-1}|\eta_j| \le \varepsilon,$$

$$\left\| h - \sum_{|n|\le N}(\widetilde{c}_n + \Delta\widetilde{c}_n)e^{int} \right\|_\infty \le 2\sum_{|n|>N}|c_n| + L\varepsilon.$$

The first term is the Fourier tail and its aliasing; the second comes from the declared sample-error bound.

18.3 What a complete boundary claim must specify

A useful boundary calculation states the domain, the marked conformal coordinate, the meaning of trace, the norm of the desired output, and the available information. A physical arc length is not a circle angle; a value at an accessible point is not an unrestricted limit at that point; and a small interior residual is not a bound on an unknown boundary trace without a stability inequality. The theorems in this chapter make these distinctions as mathematical statements with explicit examples, rather than as generic warnings about numerical methods.

For a computed conformal boundary, the geometric error and the function approximation error must also be separated. If a known boundary trace is Lipschitz with constant L in physical distance, perturbing the evaluated physical point by at most η changes the value by at most $L\eta$. This follows directly from the definition of a Lipschitz function. Without such a modulus, a positional error bound has no specified implication for the value error. At a slit tip or a corner, the appropriate modulus may be Hölder rather than Lipschitz; the explicit models in the application chapters compute that exponent from the conformal map.

Investigation 18.4 (Adaptive samples at the origin)**.** Suppose a procedure samples the value at zero m times, with no derivative information. Give two bounded analytic alternatives with identical replies and explain why repeated identical samples do not increase exact information.

Solution. The functions z and $-z$ already give identical zero values at every query and boundary distance two. The product construction would also give $\pm z^m$, but that is not needed: multiplicity in the list is not derivative information. In a noisy statistical model repeated observations could reduce independent random noise, but that would require a different observation model. Under exact value queries, repetition adds no new constraint to the set of compatible analytic functions.

Investigation 18.5 (Three samples and aliasing)**.** Use the sample points $1, e^{2\pi i/3}, e^{4\pi i/3}$. Find two holomorphic polynomials with the same samples, and explain why the degree-one interpolation theorem is not contradicted.

Solution. The polynomials 1 and z^3 agree at all three sample points. The uniqueness theorem for a declared finite Fourier degree applies only to traces whose frequencies lie in $\{-1, 0, 1\}$; z^3 violates that hypothesis. Alternatively, among holomorphic polynomials of degree at most two, three distinct exact samples determine the polynomial by the ordinary root-count argument. Again z^3 lies outside the admissible class. An algorithm cannot obtain a degree restriction merely from the fact that the observed values happen to fit a low-degree polynomial.

Investigation 18.6 (An exponential Fourier tail)**.** Assume $|c_n| \le A\rho^{-|n|}$ for all $n \neq 0$, with $\rho > 1$. Give an explicit supremum error bound for the grid interpolant of Proposition 18.3, including sample errors of magnitude at most ε.

Solution. The omitted absolute tail is at most $2A\rho^{-(N+1)}/(1-\rho^{-1})$. The grid error is therefore at most

$$\frac{4A\rho^{-(N+1)}}{1-\rho^{-1}} + (2N+1)\varepsilon.$$

The first term decreases with N, while the second grows under this worst-case sample-error bound. Selecting N requires balancing both terms. An error-free plot of the interpolant addresses neither the validity of the coefficient prior nor the size of the measurement errors.

Investigation 18.7 (Exact information versus finite cost)**.** Why does uniqueness from the full function $P_r h$ not imply that a finite number of arithmetic operations reconstructs every L^2 boundary trace?

Solution. The full observation contains infinitely many Fourier coefficients. Uniqueness says that the nonzero multiplier $r^{|n|}$ can be inverted coefficient by coefficient; it gives an injective mathematical map. A finite computation can output a finite approximation only after an output norm, tolerance and prior have been specified. The Sobolev and analytic-prior theorems provide such finite approximation rules by bounding the tail. Without a prior there is no uniform finite cutoff, as the single-frequency counterexamples show. Thus exact identifiability, stability and finite information complexity are three separate assertions.

Chapter 19

Potential, flux, and the geometry of a sharp boundary

Conformal boundary geometry has direct consequences for two-dimensional potential problems. A narrow physical region can carry a substantial interval of ideal angles, and a single physical point can represent two boundary sides. Both facts affect the interpretation of a boundary condition. The explicit slit and wedge calculations in this chapter separate the geometry from the constitutive assumptions of a physical model.

19.1 The model and the quantities it predicts

Let $\Omega \subset \mathbb{R}^2$ be a plane region occupied by a homogeneous, isotropic material. For steady scalar conduction with constant conductivity $\kappa > 0$, assume the flux law $j = -\kappa \nabla u$ and conservation $\operatorname{div} j = 0$ in the absence of sources. These assumptions give $\Delta u = 0$. If u is temperature, j has the corresponding heat-flux units; if u is electrical potential, j is a current density. The same Laplace equation arises in electrostatics with $E = -\nabla u$ and constant permittivity $\epsilon > 0$ in a charge-free region. In that interpretation the energy per unit length in the invariant axial direction is

$$\mathcal{E}' = \frac{\epsilon}{2} \int_\Omega |\nabla u|^2 \, \mathrm{d}A.$$

The prime on $\mathcal{E}'$ indicates energy per unit axial length, not a derivative. A two-dimensional cross-section describes an ideal system invariant along that axis; end effects of a finite object are outside this model.

For these equations, the conformal energy identity in Theorem 16.4 transports the Dirichlet integral without a scale factor. A pointwise field does have a scale factor. If $z = F(w)$ and $v(w) = u(F(w))$, the chain rule and the fact that the derivative of a conformal map is a rotation times multiplication by $|F'|$ give

$$|\nabla u(F(w))| = \frac{|\nabla v(w)|}{|F'(w)|}. \tag{19.1}$$

Writing R_ϑ for the rotation determined by $F'(w)$ makes the vector transformation, including its direction, explicit:

$$DF(w) = |F'(w)| R_\vartheta, \qquad \nabla_w v = DF(w)^{\mathsf{T}} \nabla_z u(F(w)),$$
$$j(F(w)) = -\frac{\kappa}{|F'(w)|} R_\vartheta \nabla_w v.$$

Thus conformal invariance of total energy does not mean invariance of local field magnitude. A derivative tending to zero can concentrate a field near a boundary point even when the total energy remains finite.

We treat the displayed constitutive laws as explicit premises. The calculations establish consequences of that model. They do not assert that a physical material remains linear at arbitrarily high fields or that an ideal sharp tip persists at atomic scales.

19.2 An equipotential annulus with an exact flux

Let K be a locally connected full continuum, with the exterior coordinate $w = B(z)$ of Chapter 9. Fix $T > 0$ and consider the region between K and its analytic equipotential E_{e^T}:

$$\Omega_T = F(\{1 < |w| < e^T\}).$$

Prescribe potential zero on the inner conductor and V on the outer equipotential. A candidate solution is

$$u(z) = \frac{V}{T} \log |B(z)|. \tag{19.2}$$

For a locally connected K, the inverse map extends continuously, so these values are attained on the prime-end boundary and agree on all accesses to each physical point. In the examples of a circle and a slit they are also visibly the continuous physical boundary values. More generally, the extended inverse map on the compact closed annulus is a continuous surjection onto the physical closure. The annular potential is constant on every fibre of this map: it is zero on all inner-boundary fibres and V on the outer boundary, while the map is injective inside. It therefore descends continuously to the physical closure. To verify the last assertion without a quotient-space theorem, take any convergent physical sequence, lift it to the compact annulus, pass to convergent subsequences there, and note that every possible limit gives the same fibre value. Failure of convergence of the full potential sequence would contradict this subsequence property.

Proposition 19.1 (Energy and current in an equipotential annulus)**.** *For the problem just described,*

$$\int_{\Omega_T} |\nabla u|^2 \, \mathrm{d}A = \frac{2\pi V^2}{T}, \qquad \mathcal{E}' = \frac{\pi \epsilon V^2}{T}.$$

The magnitude of the conductive flux per unit axial length from the outer conductor toward the inner one is $I' = 2\pi\kappa|V|/T$. The electrical capacitance per unit axial length, in the electrostatic interpretation, is $C' = 2\pi\epsilon/T$.

Proof. In the w-annulus the potential is $v(w) = (V/T) \log |w|$, with $|\nabla v| = |V|/(T|w|)$. Direct polar integration gives

$$\int_1^{e^T} \int_0^{2\pi} \frac{V^2}{T^2 r^2} r \, \mathrm{d}\theta \, \mathrm{d}r = \frac{2\pi V^2}{T}.$$

Conformal invariance transports this integral to Ω_T and the energy formula follows. On a circle $|w| = r$, the integral of the radial derivative is $\int_0^{2\pi} (V/(Tr)) r \, \mathrm{d}\theta = 2\pi V/T$. Under a conformal map, a normal derivative is divided by $|F'|$ while arclength is multiplied by $|F'|$. Their product is unchanged. The same flux integral therefore holds on every interior equipotential in Ω_T. Multiplication by κ gives the signed conductive flux and taking its magnitude gives the stated I'. In electrostatics the charge magnitude is $Q' = 2\pi\epsilon|V|/T$, so $Q'/|V|$ gives C' for $V \neq 0$; the same coefficient defines the linear response at $V = 0$. On corresponding smooth curves, with corresponding unit normals, the cancellation can be recorded before integration:

$$\partial_{n_z} u \, \mathrm{d}s_z = \frac{\partial_{n_w} v}{|F'(w)|} |F'(w)| \, \mathrm{d}s_w = \partial_{n_w} v \, \mathrm{d}s_w.$$

□

The flux computation can be made on $E_{\epsilon t}$ for $0 < t < T$, where the boundary is analytic. It does not presume a classical unit normal or an arclength density on an arbitrary rough inner hull. The limiting total charge is well defined by these enclosing equipotentials. A pointwise charge density on the physical boundary requires additional regularity or an explicit model such as the slit below.

Uniqueness is also transparent in the annulus. The difference of two continuous harmonic solutions with the prescribed boundary values is zero on both boundary circles after conformal pullback. The maximum principle makes the difference zero throughout. The same conclusion holds for finite-energy weak solutions with the stated traces by testing their difference against itself. These are two distinct function-space formulations; one should state which boundary values are available before applying either argument.

19.3 The charge on the two sides of a slit

For $K_a = [-a, a]$, differentiation of its inverse formula gives

$$\frac{B_a'(z)}{B_a(z)} = \frac{1}{\sqrt{z^2 - a^2}}, \qquad |\nabla g_{K_a}(z)| = \frac{1}{|\sqrt{z^2 - a^2}|}.$$

To check the first identity directly, put $s = \sqrt{z^2 - a^2}$ with $s' = z/s$. Then $B_a' = (1 + z/s)/a = (z + s)/(as) = B_a/s$. For $x \in (-a, a)$, the square root has limiting values $\pm i\sqrt{a^2 - x^2}$ on the two sides. The magnitude of the normal derivative of g_{K_a} on either side is consequently

$$\frac{1}{\sqrt{a^2 - x^2}}. \tag{19.3}$$

For potential (19.2), multiply this by $|V|/T$. The electrostatic charge magnitude per unit physical boundary length and per unit axial length on either side is $\epsilon|V|/(T\sqrt{a^2 - x^2})$. Its sign depends on which conductor is held at the higher potential. With the slit at zero and the outer conductor at $V > 0$, the slit charge is negative.

Integrating one side gives

$$\int_{-a}^{a} \frac{\mathrm{d}x}{\sqrt{a^2 - x^2}} = \pi.$$

Both sides together give 2π, agreeing with Proposition 19.1. Counting the physical interval only once without recording that it has two exposed sides would lose a factor of two. Dividing the total side-resolved flux by 2π gives the angle measure computed in (10.2). This provides a direct analytic check of the landing-angle calculation.

Near the right tip, write $x = a - s$ with $s > 0$. Then

$$\frac{1}{\sqrt{a^2 - x^2}} = \frac{1}{\sqrt{2as - s^2}} = \frac{1}{\sqrt{2a}} s^{-1/2}(1 + O(s/a)).$$

The charge on an interval of length δ next to the tip is therefore of order $\sqrt{\delta}$, even though the pointwise density is unbounded. The pointwise singularity and the integrated quantity answer different questions. An approximation of the total charge can be accurate while its largest sampled density continues to increase under mesh refinement. There is also a finite, nonasymptotic bound. For $0 < \delta < a$, integrate the inequalities $(2a - \delta)s \le 2as - s^2 \le 2as$ on $0 < s < \delta$:

$$\sqrt{\frac{2\delta}{a}} \le \int_0^{\delta} \frac{\mathrm{d}s}{\sqrt{2as - s^2}} \le 2\sqrt{\frac{\delta}{2a - \delta}}.$$

Multiplication by $\epsilon|V|/T$ gives the corresponding one-side charge bounds in the stated electrostatic model.

19.4 A wedge and the exponent selected by its opening

Let

$$W_{\alpha,L} = \{re^{i\theta} : 0 < r < L,\ 0 < \theta < \alpha\}, \qquad 0 < \alpha \le 2\pi,$$

where the two sides are retained as distinct boundary sides if $\alpha = 2\pi$. Define $p = \pi/\alpha > 0$. The branch $z^p = \exp(p(\log r + i\theta))$ maps the wedge conformally to an upper half-disk after the appropriate scale factor. The angular branch is part of the definition; using a principal power with an unrelated cut could identify or exclude the wrong side.

Proposition 19.2 (A wedge mode and its field)**.** *For a real amplitude V, the function*

$$u(r,\theta) = V(r/L)^p \sin(p\theta)$$

is the unique harmonic function continuous on the closed wedge, with value zero on its two radial sides and vertex, and value $V\sin(p\theta)$ on its outer arc. Its gradient magnitude is

$$|\nabla u| = \frac{|V|p}{L^p} r^{p-1}.$$

For $V \neq 0$, the field tends to zero at the vertex if $\alpha < \pi$, has constant magnitude if $\alpha = \pi$, and diverges if $\alpha > \pi$.

Proof. The function is the imaginary part of Vz^p/L^p in the chosen branch, so it is harmonic. Alternatively, substituting in the polar Laplacian

$$\Delta u = u_{rr} + r^{-1}u_r + r^{-2}u_{\theta\theta}$$

gives the factor $p(p-1) + p - p^2 = 0$. The boundary values follow from $\sin 0 = \sin \pi = 0$ and $p > 0$. Continuity at the vertex follows from $|u| \le |V|(r/L)^p$ uniformly in θ. The algebra selecting the exponent can also be displayed for a separated expression with real λ and $\mu > 0$, at every $r > 0$:

$$r^2\Delta(r^\lambda \sin(\mu\theta)) = (\lambda^2 - \mu^2)r^\lambda \sin(\mu\theta), \qquad \mu\alpha = n\pi \quad (n = 1, 2, \ldots).$$

Zero side values select the angular frequencies $\mu = np$; continuity of a nonzero mode at the vertex selects the positive radial exponent $\lambda = np$. The difference of two such solutions is continuous on the compact closure and harmonic inside, with zero boundary values. The maximum principle, applied to the difference and its negative, proves uniqueness. Finally

$$u_r = \frac{Vp}{L^p} r^{p-1}\sin(p\theta), \qquad r^{-1}u_\theta = \frac{Vp}{L^p} r^{p-1}\cos(p\theta).$$

Squaring and adding gives the claimed magnitude. Its three limiting regimes follow from the sign of $p - 1$. □

The material occupies the wedge. Thus a protruding conducting tip can correspond to an exterior material angle exceeding π, even when the conductor's own interior angle is small. Confusing these two angles reverses the prediction of concentration. A zero-thickness slit tip has material angle 2π, so $p = 1/2$, agreeing with the square-root field obtained from the exact Joukowski map.

Proposition 19.3 (Finite energy of the wedge mode)**.** *For $0 < R \le L$, the energy of this mode within distance R of the vertex is*

$$\mathcal{E}'(R) = \frac{\epsilon\alpha p V^2}{4}(R/L)^{2p} = \frac{\epsilon\pi V^2}{4}(R/L)^{2p}.$$

The flux magnitude into either grounded side over $0 < r < R$ is $\kappa|V|(R/L)^p$. The sum of the signed outward normal derivatives on the two sides and the circular arc is zero.

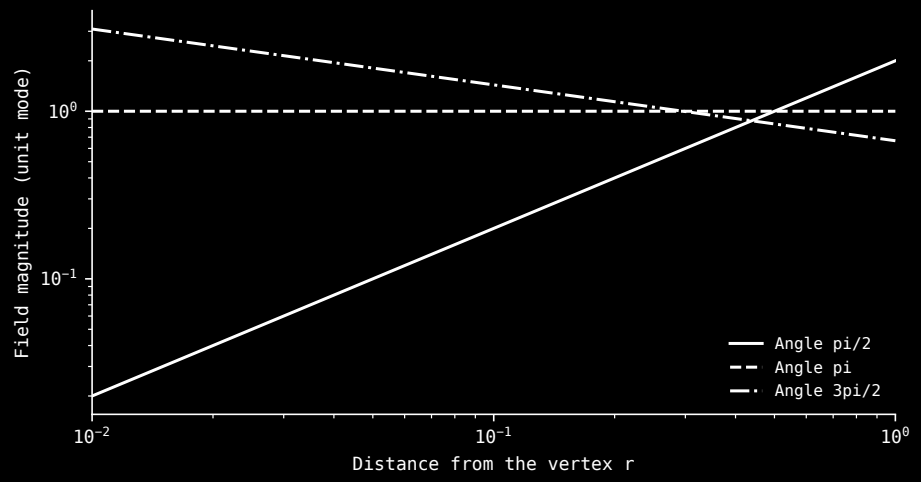


Figure 19.1: Field magnitude $(\pi/\alpha)r^{\pi/\alpha-1}$ of the first wedge mode with $|V| = L = 1$, for material angles $\alpha = \pi/2, \pi, 3\pi/2$. The curves are sampled evaluations of the exact formula, on positive radii. Their limiting behaviours at zero follow from the proved exponent and are not inferred from the smallest sampled radius.

Proof. Using Proposition 19.2,

$$\frac{\epsilon}{2}\int_0^R \int_0^\alpha \frac{V^2 p^2}{L^{2p}} r^{2p-2} r \, \mathrm{d}\theta \, \mathrm{d}r = \frac{\epsilon \alpha p V^2}{4L^{2p}} R^{2p}.$$

The integral converges because $p > 0$; field divergence for $p < 1$ has not caused energy divergence. On the side $\theta = 0$, the outward normal of the material is $-e_\theta$, so $\partial_n u = -r^{-1}u_\theta = -Vpr^{p-1}/L^p$. On $\theta = \alpha$ the outward normal is $+e_\theta$ and $\cos(p\alpha) = -1$, giving the same derivative. Its integral on each side is $-V(R/L)^p$. On the outer arc,

$$\int_0^\alpha u_r(R,\theta) R \, \mathrm{d}\theta = Vp(R/L)^p \int_0^\alpha \sin(p\theta) \, \mathrm{d}\theta = 2V(R/L)^p.$$

The signed sum is zero, as conservation requires. Multiplication by κ and taking the relevant magnitude gives the stated conductive flux. For a truncated wedge with an inner circle, its flux tends to zero as that circle shrinks, since it is proportional to its radius raised to p. □

This calculation gives both a singular pointwise observable and a finite integrated observable from one exact solution. The field exponent $p-1$ alone does not determine whether a numerically computed energy converges. The area factor $r \, \mathrm{d}r$ must be included. It also shows why a uniform bound on sampled field values is an unsuitable acceptance criterion for a model whose correct solution is unbounded at the tip.

19.5 An incompatible boundary condition and divergent energy

Keep the same wedge, but impose potential zero on the side $\theta = 0$ and potential V on the side $\theta = \alpha$. The exact harmonic function

$$v(r,\theta) = V\theta/\alpha$$

has those side values and is independent of r. Unless $V = 0$, it does not extend continuously to the vertex: different angles give different limiting values. Its field magnitude is $|V|/(\alpha r)$. On a wedge truncated at radii δ and R, its energy is

$$\mathcal{E}'(\delta, R) = \frac{\epsilon V^2}{2\alpha} \log(R/\delta). \tag{19.4}$$

The calculation is direct: $|\nabla v|^2 = V^2/(\alpha^2 r^2)$, so the angular integration gives α and the radial integration gives $\log(R/\delta)$. The energy diverges as $\delta \downarrow 0$.

There is no contradiction with Proposition 19.3. The first boundary condition has matching values at the vertex and selects a positive radial power. The second has a jump between sides meeting at the vertex and selects an angular function with no radial decay. Finite energy is a property of the geometry together with the boundary data, not of the opening angle alone. Rounding the vertex at a specified physical scale replaces δ by a positive cutoff, but the resulting number belongs to that rounded model.

19.6 Which corner mode is actually present?

The opening angle determines the admissible exponents, but the boundary data determine which coefficients are nonzero. This distinction matters when a physical interpretation predicts a singular field solely from a picture of a reentrant corner. The following finite-mode statement makes the dependence on the data explicit without requiring convergence results for an infinite Fourier series.

Proposition 19.4 (Finite wedge data and cancellation of the first mode)**.** *Let $b_1, \dots, b_q$ be real numbers and prescribe outer-arc data $h(\theta) = \sum_{n=1}^{q} b_n \sin(np\theta)$, with zero data on the two radial sides. The unique continuous harmonic solution is*

$$u(r,\theta) = \sum_{n=1}^{q} b_n (r/L)^{np} \sin(np\theta).$$

If m is the smallest index with $b_m \neq 0$, then, uniformly in angle,

$$|\nabla u(r,\theta)| = \frac{|b_m| mp}{L} (r/L)^{mp-1}(1 + O((r/L)^p)) \qquad (r \downarrow 0).$$

Its energy inside radius $R \leq L$ is exactly

$$\mathcal{E}'(R) = \frac{\epsilon\pi}{4} \sum_{n=1}^{q} n b_n^2 (R/L)^{2np}.$$

Proof. Each term is the imaginary part of a branch of $b_n(z/L)^{np}$, so the finite sum is harmonic and has the stated boundary values. It tends uniformly to zero at the vertex. The maximum principle gives uniqueness as before. The gradient magnitude of its nth term is $|b_n| npL^{-1}(r/L)^{np-1}$. The triangle inequality bounds the norm of the gradient of the terms after m, divided by the leading gradient magnitude, by

$$\sum_{n=m+1}^{q} \frac{n|b_n|}{m|b_m|} (r/L)^{(n-m)p} = O((r/L)^p).$$

The reverse triangle inequality supplies the corresponding lower bound for the full gradient norm. This proves the uniform asymptotic, even at angles where the leading potential itself vanishes: its radial and angular derivative components do not vanish simultaneously. For instance, with $C_m(r) = |b_m| mpL^{-1}(r/L)^{mp-1}$, the upper and reverse triangle estimates combine into one relative-error bound:

$$\left| \frac{|\nabla u(r,\theta)|}{C_m(r)} - 1 \right| \leq \sum_{n=m+1}^{q} \frac{n|b_n|}{m|b_m|} (r/L)^{(n-m)p}.$$

The right-hand side is independent of θ, which makes the uniformity of the conclusion explicit.

For the energy, the angular inner product of the gradients of modes n and k contains

$$\sin(np\theta)\sin(kp\theta) + \cos(np\theta)\cos(kp\theta) = \cos((n-k)p\theta).$$

Its integral from 0 to α is zero for $n \neq k$, since $p\alpha = \pi$, and equals α for $n = k$. The radial integral of mode n is the one in Proposition 19.3 with exponent np and amplitude b_n, giving $\epsilon\alpha npb_n^2(R/L)^{2np}/4$. Since $\alpha p = \pi$, summing proves the formula. □

For example, at the reentrant angle $\alpha = 3\pi/2$ the fundamental exponent is $p = 2/3$. If $b_1 = 0$ and $b_2 \neq 0$, the field instead behaves as $r^{1/3}$ and vanishes at the corner. The geometry permits a singular mode, but these particular data do not excite it. This is a mathematical cancellation statement about the imposed boundary data. It is not a claim that a measured boundary profile has exactly zero first coefficient. Uncertainty in that coefficient can restore a small singular term which eventually dominates sufficiently close to the ideal vertex.

If both b_1 and b_2 are nonzero, a useful crossover scale is obtained by equating their gradient magnitudes: $|b_1|p(r/L)^{p-1} = 2|b_2|p(r/L)^{2p-1}$. When $|b_1| < 2|b_2|$, the solution is $r/L = (|b_1|/(2|b_2|))^{1/p}$, which lies in the modeled radial range. Above that scale the second mode can dominate the measured field; below it the first mode dominates. The existence of an experimentally accessible range with a different apparent exponent therefore does not by itself refute the leading asymptotic of the ideal corner model.

Investigation 19.5 (A circle between concentric electrodes)**.** For concentric circles of radii a and $b > a$, derive the potential, capacitance per unit length, and energy from the exterior normalization.

Solution. Here $B(z) = z/a$ and $T = \log(b/a)$. Thus $u(z) = V\log(|z|/a)/\log(b/a)$, $C' = 2\pi\epsilon/\log(b/a)$, and $\mathcal{E}' = \pi\epsilon V^2/\log(b/a)$. The ratio b/a is dimensionless. The units of C' are those of permittivity, capacitance per length, while $C'V^2/2$ has energy per length units. This exact control also checks the factor of two between the Dirichlet integral and electrostatic energy.

Investigation 19.6 (An ellipse surrounding a slit)**.** The inner conductor is $[-a, a]$ and the outer conductor is the confocal ellipse with major semiaxis $A > a$. Find T, its minor semiaxis, and the capacitance per unit length.

Solution. Equation (10.1) gives $A = a\cosh T$, hence $T = \operatorname{arcosh}(A/a)$. The minor semiaxis is $a\sinh T = \sqrt{A^2 - a^2}$. Proposition 19.1 yields $C' = 2\pi\epsilon/\operatorname{arcosh}(A/a)$. The result is for this confocal outer conductor, not for an arbitrary circle of radius A. Specifying only the largest outer radius would not determine the conformal annulus parameter.

Investigation 19.7 (Resolve a side-charge fraction)**.** For the slit model with $V \neq 0$, what fraction of the total charge magnitude lies on the upper side between 0 and a? What fraction lies within physical distance δ of the right tip on both sides?

Solution. The upper side contributes half of the total charge; its portion $[0, a]$ contributes half again, so the first fraction is $1/4$. For the second, divide the two-sided integral $2\int_{a-\delta}^{a}(a^2 - x^2)^{-1/2}\,\mathrm{d}x$ by 2π. The result is $\pi^{-1}\arccos(1-\delta/a)$ for $0 < \delta < 2a$. It tends to zero like $\sqrt{2\delta/a}/\pi$. The divergent density therefore does not place a finite fraction of charge at the point itself.

Investigation 19.8 (A reentrant angle and an acute angle)**.** Compare the first wedge modes for material angles $3\pi/2$ and $\pi/2$. Give their field exponents and the exponents governing energy within radius R.

Solution. For $\alpha = 3\pi/2$, $p = 2/3$, so the field is proportional to $r^{-1/3}$ and the local energy to $R^{4/3}$. For $\alpha = \pi/2$, $p = 2$, so the field is proportional to r and the local energy to R^4. Both local energies tend to zero as $R \downarrow 0$. The first field is unbounded and the second vanishes. The energy comparison includes the area element and cannot be obtained by integrating the field magnitude alone.

Investigation 19.9 (A measured peak is not a cutoff-independent quantity)**.** Suppose a model has field $Cr^{-1/2}$ near a slit tip and a numerical scheme samples only radii $r \geq h$. How does its largest sampled field scale with h? Does that predict the limiting local energy?

Solution. The largest sampled value is approximately $Ch^{-1/2}$ and diverges as the sampling scale decreases. Its divergence is the expected behaviour of the ideal field. The energy density is proportional to C^2/r, whose area integral over a sector of radius R is proportional to $\int_0^R (C^2/r) r \, \mathrm{d}r = C^2 R$. Thus the local energy is finite and tends to zero with R. The sampled maximum and the energy have different limiting contracts; neither can be substituted for the other in a convergence statement.

Investigation 19.10 (A boundary jump remains singular at every angle)**.** For the angular solution $v = V\theta/\alpha$, determine whether choosing an acute material angle makes its energy finite at the vertex.

Solution. For every fixed $\alpha > 0$ and nonzero V, formula (19.4) diverges logarithmically as the inner cutoff tends to zero. Making α smaller increases the prefactor $\epsilon V^2/(2\alpha)$; it does not remove the logarithm. The boundary values remain incompatible at the common vertex. The vanishing-field conclusion for an acute wedge applied to a different boundary condition, the first sine mode with matching zero side values.

Chapter 20

Sampling a boundary with a quantitative contract

A mathematical boundary theorem and a finite array of samples have different outputs. Local connectivity gives continuity of a landing map, but by itself supplies no numerical modulus of continuity. A plot may suggest that a narrow feature has disappeared when the feature merely falls between adjacent sample points. To make a numerical conclusion, one must specify an analytic neighbourhood, a norm bound, a geometry bound, or another quantitative prior that controls the unsampled region.

This chapter gives two such contracts. The first approximates values and Taylor coefficients of a holomorphic function from circular samples with explicit analytic and sampling error bounds. The second bounds the distance between a sampled polygon and an equipotential curve. All the bounds are mathematical inequalities. No floating-point implementation, CAS transcript, or formal kernel acceptance is inferred from them. The broader literature on exponential convergence of trapezoidal quadrature is reviewed by Trefethen and Weideman [4]; the disk calculations below derive the particular contracts used here.

20.1 Data, normalization, and aliasing

Fix $0 < r < R$, an integer $N \geq 1$, and the roots of unity $\zeta_j = e^{2\pi ij/N}$, $0 \leq j < N$. Suppose f is holomorphic in $|z| < R$ and satisfies $|f(z)| \leq M$ there, with a specified finite M. Write $f(z) = \sum_{k\geq 0} a_k z^k$. The Cauchy estimate is $|a_k| \leq MR^{-k}$, obtained by taking the radius in the integral formula up to R. Define the circular coefficient estimator

$$\widetilde{a}_m = \frac{r^{-m}}{N} \sum_{j=0}^{N-1} f(r\zeta_j)\zeta_j^{-m}, \qquad 0 \leq m < N. \tag{20.1}$$

The power r^{-m} is necessary: without it the estimator would approximate $a_m r^m$ rather than a_m.

Proposition 20.1 (Exact aliasing identity and coefficient error)**.** *For $0 \leq m < N$,*

$$\widetilde{a}_m = a_m + \sum_{\ell\geq 1} a_{m+\ell N} r^{\ell N}, \qquad |\widetilde{a}_m - a_m| \leq MR^{-m}\frac{(r/R)^N}{1-(r/R)^N}.$$

If each sample is replaced by $\widehat{f}_j$ with $|\widehat{f}_j - f(r\zeta_j)| \leq \delta$, and the finite sum is for the moment performed exactly, the additional error is at most δr^{-m}.

Proof. The Taylor series converges absolutely on $|z| = r$, so it can be interchanged with the finite

sum. The roots-of-unity identity

$$\frac{1}{N}\sum_{j=0}^{N-1}\zeta_j^{k-m}=\begin{cases}1, & N \text{ divides } k-m,\\ 0, & \text{otherwise}\end{cases}$$

follows from the finite geometric sum. Since $k \geq 0$ and $0 \leq m < N$, the surviving indices are exactly $k = m + \ell N$ with $\ell \geq 0$. This proves the identity. The Cauchy estimate bounds its tail by $MR^{-m}\sum_{\ell\geq 1}(r/R)^{\ell N}$, the stated geometric series. For the sample perturbation, each weight has modulus r^{-m}/N, so the triangle inequality gives δr^{-m}. □

Aliasing is an exact algebraic identity, not a random error model. The unresolved Taylor coefficients enter in congruence classes modulo N. Increasing precision at fixed N does not remove them. Increasing N controls them only through the analytic bound that makes the coefficient tail small. Likewise, decreasing r reduces the analytic tail but increases the noise factor r^{-m} when $m > 0$.

The estimator for $f^{(m)}(0)$ is $m!\widetilde{a}_m$, so both error terms must be multiplied by $m!$. The factorial is part of the output semantics. A theorem about Taylor coefficients does not automatically give the same numerical bound for derivatives. If $\widehat{a}_m$ uses the perturbed samples and exact finite arithmetic, the two contributions therefore give the derivative error contract

$$|m!\widehat{a}_m - f^{(m)}(0)| \leq m!\left(MR^{-m}\frac{(r/R)^N}{1-(r/R)^N}+\delta r^{-m}\right), \qquad 0 \leq m < N.$$

20.2 From samples to an interior polynomial

Let

$$p_{N-1}(z)=\sum_{m=0}^{N-1}\widetilde{a}_m z^m.$$

This is the polynomial of degree at most $N-1$ interpolating the samples at $r\zeta_j$. To verify interpolation directly, evaluate at one node and substitute (20.1). The inner finite Fourier sum is N at the matching node and zero at the other nodes. Distinctness of the nodes gives uniqueness, since the difference of two such interpolants would have N zeros and degree at most $N-1$. The interpolation weights themselves are finite polynomials:

$$p_{N-1}(z)=\sum_{j=0}^{N-1} f(r\zeta_j)\,\ell_j(z), \quad \ell_j(z)=\frac{1}{N}\sum_{m=0}^{N-1}\left(\frac{z}{r\zeta_j}\right)^m,$$

$$\ell_j(r\zeta_k)=\begin{cases}1, & j=k,\\ 0, & j\neq k.\end{cases}$$

This form avoids introducing a quotient with a removable singularity at a sampling node.

Theorem 20.2 (Uniform interior interpolation bound)**.** *For $0 \leq \rho < r < R$,*

$$\sup_{|z|\leq\rho}|p_{N-1}(z)-f(z)| \leq \frac{M((r/R)^N+(\rho/R)^N)}{(1-\rho/R)(1-(r/R)^N)}.$$

With sample perturbations bounded by δ, the additional uniform error is at most

$$\delta\sum_{m=0}^{N-1}(\rho/r)^m \leq \frac{\delta}{1-\rho/r}.$$

Proof by grouping Taylor coefficients. Group the Taylor series by indices $k = m + \ell N$, $0 \le m < N$. Absolute convergence for $|z| \le \rho < R$ justifies the grouping. The aliasing identity gives

$$p_{N-1}(z) - f(z) = \sum_{m=0}^{N-1} \sum_{\ell \ge 1} a_{m+\ell N} z^m (r^{\ell N} - z^{\ell N}).$$

Taking absolute values and applying the coefficient bound gives

$$|p_{N-1}(z) - f(z)| \le M \sum_{m=0}^{N-1} (\rho/R)^m \sum_{\ell \ge 1} ((r/R)^{\ell N} + (\rho/R)^{\ell N}).$$

Summing and using $\rho \le r$ yields the displayed bound. More explicitly the second geometric tail is at most $(\rho/R)^N/(1-(r/R)^N)$, and the first is $(r/R)^N/(1-(r/R)^N)$. The finite sum over m is at most $(1-\rho/R)^{-1}$. The sample errors give coefficient perturbations at most δr^{-m} by Proposition 20.1; evaluating their polynomial on the smaller disk gives the final geometric sum. □

A contour remainder proof. Choose s with $r < s < R$. Residues at $w = z$ and at the interpolation nodes give

$$f(z) - p_{N-1}(z) = \frac{1}{2\pi i} \int_{|w|=s} \frac{f(w)(z^N - r^N)}{(w^N - r^N)(w - z)} \, \mathrm{d}w.$$

For completeness, the residue at $w = z$ is $f(z)$. At a node w_j, the residue is $f(w_j)(z^N - r^N)/(N w_j^{N-1}(w_j - z))$. Its negative is the Lagrange basis contribution for that node: the polynomial $(z^N - r^N)/(N w_j^{N-1}(z - w_j))$ equals one at w_j and zero at all other nodes. Their sum is the interpolant, proving the remainder identity, first off the nodes and then everywhere by continuity. On the contour,

$$|w^N - r^N| \ge s^N - r^N, \quad |w - z| \ge s - \rho, \quad |z^N - r^N| \le \rho^N + r^N.$$

Its length is $2\pi s$, so the remainder is bounded by $Ms(\rho^N + r^N)/((s^N - r^N)(s - \rho))$. Letting $s \uparrow R$ gives the same estimate. This proof uses the zero polynomial of the interpolation nodes rather than grouping the unseen Taylor coefficients. □

The two proofs expose different parts of the mechanism. The coefficient proof identifies exactly which frequencies alias. The contour proof identifies the distance to the analytic boundary and gives a direct remainder representation. They have common Cauchy-theory foundations, so they should not be described as independent of all shared mathematical dependencies.

20.3 The apparent Cauchy quadrature and its kernel bias

The Cauchy integral formula on $|w| = r$ suggests the discrete expression

$$Q_N(z) = \frac{1}{N} \sum_{j=0}^{N-1} \frac{f(r\zeta_j)}{1 - z/(r\zeta_j)}, \qquad |z| < r.$$

It is tempting to call this simply the interpolant. They are related, but they are not equal.

Proposition 20.3 (Exact correction of the discrete kernel)**.** *For $|z| < r$,*

$$Q_N(z) = \frac{p_{N-1}(z)}{1 - (z/r)^N}.$$

In particular a constant function $f \equiv c$ gives $Q_N(z) = c/(1-(z/r)^N)$, while the corrected expression $(1-(z/r)^N)Q_N(z)$ reproduces c exactly.

Proof. Expand each kernel into its absolutely convergent geometric series. Replace the samples by the values of their interpolating polynomial; this replacement is exact at the nodes. For the monomial w^m, $0 \le m < N$, the roots-of-unity sum selects kernel powers $k = m + \ell N$, $\ell \ge 0$. Its contribution is $z^m \sum_{\ell \ge 0} (z/r)^{\ell N}$. Linearity gives the formula for the full polynomial. For a constant, the interpolant is the constant itself, giving the particular case. □

As z approaches one of the sampling nodes, the denominator in the uncorrected formula becomes small. The exact identity can be used algebraically, but multiplying a large computed value by a small factor can be numerically fragile. Evaluating the polynomial or a suitably stable interpolation formula avoids introducing this cancellation into the mathematical output. Any particular arithmetic implementation still needs its own rounding analysis.

The constant-function control is unusually effective: it detects a kernel normalization error even when the input has no high-frequency content. A method that reports a large variation for a constant function near its sampling circle has failed an algebraic control before any question about rough boundary geometry arises.

20.4 A finite stopping rule with a noise floor

Suppose the desired interior region is $|z| \le \rho < r$. Allocate a positive error budget η to interpolation. Put $q = r/R \in (0, 1)$. Since $(\rho/R)^N \le q^N$, Theorem 20.2 gives the sufficient condition

$$\frac{2Mq^N}{(1 - \rho/R)(1 - q^N)} \le \eta.$$

Solving for q^N yields the explicit finite rule

$$N \ge \frac{\log(\eta(1 - \rho/R)/(2M + \eta(1 - \rho/R)))}{\log q}, \tag{20.2}$$

rounded upward to an integer at least one. Both logarithms in the ratio are negative when $M > 0$. The direction of the inequality follows from division by the negative number $\log q$. If $M = 0$, the function is zero and interpolation error is already zero.

The total error contract must also include $\delta/(1 - \rho/r)$ from the sample data and a separately established bound for arithmetic in the finite calculation. Increasing N cannot make a fixed sample error bound disappear. In particular, if the sample noise term already exceeds the desired total tolerance, the stopping rule for interpolation does not repair the situation. One must improve the input values, move the target region farther inside the sampling circle, or change the target tolerance. For $s = \rho/r \in [0, 1)$, the finite-sum data-error bound and its limit are

$$B_N := \delta \sum_{m=0}^{N-1} s^m = \delta \frac{1 - s^N}{1 - s} \uparrow \frac{\delta}{1 - s} \qquad (N \to \infty).$$

This is a limit of the stated upper bounds, not a claim that every actual sample perturbation attains that worst-case value.

The parameters M and R are hypotheses over a complex neighbourhood. They cannot be certified merely because finitely many observed values are small. A denominator bound in an explicit rational formula, a proved majorant series, or an independently verified enclosure can supply them. Estimating them from the same samples used by the method would require an additional argument with its own assumptions.

20.5 A geometric bound for a sampled curve

Let $\gamma : [0, 2\pi] \to \mathbb{C}$ be twice continuously differentiable and periodic, and suppose $\sup_\theta |\gamma''(\theta)| \le L_2$. Sample it at angles whose consecutive gaps are at most h, and join successive samples by straight segments in parameter order. Let P denote the resulting polygonal curve. The Hausdorff distance between two compact sets is

$$d_H(A, B) = \max\{\sup_{a\in A} \operatorname{dist}(a, B), \sup_{b\in B} \operatorname{dist}(b, A)\}.$$

Proposition 20.4 (Polygonal approximation with a global derivative bound)**.** *Under these hypotheses,* $d_H(\gamma([0, 2\pi]), P) \le L_2 h^2/8$.

Proof. On a parameter interval $[a, b]$ of length $\ell \le h$, let $L(t)$ be the linear interpolant of the two endpoint values and put $e(t) = \gamma(t) - L(t)$. Then $e(a) = e(b) = 0$ and $e'' = \gamma''$. The Dirichlet Green kernel for the second derivative represents $e(t)$ as an integral of $-\gamma''$ against a nonnegative kernel. This identity can also be obtained by integrating e'' twice and using the two endpoint conditions. The integral of that kernel is $(t - a)(b - t)/2$, as is checked by taking $\gamma'' \equiv 1$. Its complete expression, including the sign in the representation, is

$$K(t, s) = \begin{cases} (s - a)(b - t)/(b - a), & a \le s \le t, \\ (t - a)(b - s)/(b - a), & t \le s \le b, \end{cases}$$

$$e(t) = -\int_a^b K(t, s)\gamma''(s)\, \mathrm{d}s, \qquad \int_a^b K(t, s)\, \mathrm{d}s = \frac{(t - a)(b - t)}{2}.$$

Consequently

$$|e(t)| \le \frac{L_2}{2}(t - a)(b - t) \le \frac{L_2\ell^2}{8}.$$

Each parameter point of the curve is matched to a point of the segment and each point of the segment is $L(t)$ for some parameter in the same interval. This proves both directed distance bounds. Taking the maximum over the finitely many intervals proves the result. □

The theorem is geometric, not topological. A small Hausdorff error alone does not prove that a polygon is simple, that it has the correct winding number around a very close point, or that two near portions of a curve are disjoint. Such conclusions require separation or curvature information appropriate to the claim. For a convex ellipse sampled in cyclic order, simplicity follows separately from convexity.

When $\gamma(\theta) = F(re^{i\theta})$, differentiation gives

$$\gamma''(\theta) = -re^{i\theta}F'(re^{i\theta}) - r^2e^{2i\theta}F''(re^{i\theta}).$$

Thus bounds on F' and F'' in a neighbourhood of the circle supply L_2. For example, if each disk of radius d about a point of the circle lies in a holomorphy region where $|F| \le M_F$, the Cauchy estimates give $L_2 \le rM_F/d + 2r^2M_F/d^2$. All quantities refer to the stated neighbourhood. A visually smooth sampled curve is not a substitute for this derivative bound.

20.6 A full geometry contract for the slit model

For the ellipse $\gamma_t(\theta) = F_a(e^{t+i\theta})$, the explicit formula gives $\gamma_t'' = -\gamma_t$ and hence $L_2 = a\cosh t$. Its distance to the limiting slit is also explicit:

Proposition 20.5 (From an equipotential polygon to the slit)**.** *For $t > 0$,*

$$d_H(E_{e^t}, [-a, a]) = a \sinh t.$$

If $P_{t,N}$ is the polygon through $N \geq 3$ equally spaced points of this ellipse, then

$$d_H(P_{t,N}, [-a, a]) \leq a \sinh t + \frac{a \cosh t}{8}(2\pi/N)^2.$$

Proof. Pair the ellipse point $\gamma_t(\theta)$ with $a \cos\theta$ on the slit. Their difference has real and imaginary parts $a(\cosh t - 1)\cos\theta$ and $a \sinh t \sin\theta$. Since $\cosh t - 1 \leq \sinh t$, its modulus is at most $a \sinh t$. Every point of the slit has such a parameter, so this controls both directed distances. At $\theta = \pi/2$, the ellipse point is $ia \sinh t$, whose distance from the real segment is exactly $a \sinh t$. This proves equality. Proposition 20.4 with $h = 2\pi/N$ and $L_2 = a \cosh t$ then gives the second estimate by the triangle inequality for Hausdorff distance. □

The two terms have different causes. The first is the distance between the analytic equipotential being plotted and the intended boundary. The second is its polygonal sampling error. Increasing N at fixed t reduces only the second term. Taking $t \downarrow 0$ at fixed N does not by itself make the polygon a fine representation of the whole segment in parameter order. Both parameters must be controlled against the required output.

For a desired positive geometric tolerance ε, one explicit choice is

$$t = \operatorname{arsinh}(\varepsilon/(2a)), \qquad N \geq \max\{3,\, \pi\sqrt{a \cosh t/\varepsilon}\}.$$

Then each term in Proposition 20.5 is at most $\varepsilon/2$. This is a proved stopping rule for this specified curve model. It does not certify a floating-point evaluation of its vertices unless their coordinate errors are also bounded. If every vertex is perturbed by at most η, the linear interpolation between corresponding vertices changes by at most η, so η can be added to the Hausdorff bound.

20.7 What a finite grid cannot decide

Without a derivative, analyticity, or comparable quantitative bound, finitely many samples cannot control the unsampled curve. Given distinct parameter samples $t_1, \ldots, t_N$, choose a smooth bump supported in an open interval avoiding all samples. Adding an arbitrary multiple of that bump in one coordinate leaves every sample unchanged while moving the intervening curve by an arbitrary distance. The construction can be made periodic by choosing the support away from the identified endpoint. It is a counterexample to every universal geometric error bound based only on those sample values.

Analyticity by itself does not repair the information gap when no quantitative analytic neighbourhood or norm bound is specified. If complex samples are taken at $z_1, \ldots, z_N$, the polynomial $A \prod_j (z - z_j)$ vanishes at every sample for every amplitude A. At any fixed point outside that finite set its value can have arbitrarily large magnitude. This counterexample concerns the absence of a specified norm bound; it does not contradict Theorem 20.2, whose hypotheses include one. Indeed, fixing any $z_* \notin \{z_1, \ldots, z_N\}$ gives the normalized family

$$P_A(z) = A \prod_{j=1}^{N} \frac{z - z_j}{z_* - z_j}, \qquad P_A(z_j) = 0, \qquad P_A(z_*) = A.$$

The amplitude at the unsampled point is prescribed independently of the zero sample values; its growth is excluded only by additional quantitative hypotheses.

The boundary recovery obstruction in Theorem 18.1 addresses the stronger issue that even a bounded analytic family need not permit uniform recovery all the way to the boundary from finitely many interior samples. The present forward bounds instead specify a strictly smaller target disk $|z| \le \rho < r$ and a larger analytic disk $|z| < R$. The gaps between these radii are explicit parameters of the problem. Removing them changes the problem and requires new information.

Investigation 20.6 (An exact alias)**.** For $f(z) = z^{m+N}$ with $0 \le m < N$, compute $\widetilde{a}_m$ and the interpolating polynomial on the radius-r sampling circle. Compare with the true coefficient a_m.

Solution. The true coefficient a_m is zero. At a node, $(r\zeta_j)^{m+N} = r^N(r\zeta_j)^m$, so the interpolating polynomial is $r^N z^m$ and $\widetilde{a}_m = r^N$. This also follows from the aliasing identity with exactly one nonzero tail term. Every sample is exact; the error is caused by finite sampling, not by floating-point roundoff. Replacing $m + N$ by $m + \ell N$ gives the general congruence-class mechanism.

Investigation 20.7 (A constant reveals the uncorrected kernel)**.** Take $f \equiv 1$, $r = 1$, and a real target $z = \rho \in (0, 1)$. Find the exact error of $Q_N(\rho)$ and the error after its algebraic correction. What happens as $\rho \uparrow 1$ at fixed N?

Solution. Proposition 20.3 gives $Q_N(\rho) = 1/(1 - \rho^N)$, so the error is $\rho^N/(1 - \rho^N)$. The corrected value is exactly one. At fixed N, the uncorrected error diverges as $\rho \uparrow 1$. The input has no nonconstant Taylor coefficients, so this is a kernel discretization effect. The algebraically corrected expression should be evaluated in a manner that does not introduce avoidable numerical cancellation near the nodes.

Investigation 20.8 (A completely specified interior error budget)**.** Assume $|f| \le 1$ in $|z| < 2$, sample at $r = 1$, and seek values on $|z| \le 1/2$. Give a sufficient interpolation bound as a function of N, and determine an integer N that makes it smaller than 10^{-6}.

Solution. Theorem 20.2 gives

$$E_N \le \frac{2^{-N} + 4^{-N}}{(3/4)(1 - 2^{-N})}.$$

For $N = 21$, $2^{-N} = 1/2097152 < 4.77 \cdot 10^{-7}$ and $4^{-N} < 2.28 \cdot 10^{-13}$. The denominator exceeds $(3/4)(1 - 5 \cdot 10^{-7})$, so $E_{21} < 6.37 \cdot 10^{-7} < 10^{-6}$. If each sample has absolute error at most 10^{-8}, its additional bound is $10^{-8}/(1 - 1/2) = 2 \cdot 10^{-8}$. These inequalities are an analytic error budget; arithmetic error in the actual finite evaluation would still have to be added.

Investigation 20.9 (Coefficient accuracy and derivative accuracy)**.** Suppose the total bound for an estimator of a_6 is 10^{-9}. What bound follows for the corresponding estimator of $f^{(6)}(0)$? If the sampling radius is halved while sample errors stay fixed, how does their contribution to the coefficient bound change?

Solution. Since $f^{(6)}(0) = 6!a_6 = 720a_6$, the derivative error is at most $7.2 \cdot 10^{-7}$. The sample-noise contribution to a_6 is δr^{-6}; halving r multiplies it by $2^6 = 64$. The analytic aliasing term may decrease at the same time, but that does not cancel the increase in a worst-case absolute noise bound. Choosing the radius therefore requires balancing two distinct errors.

Investigation 20.10 (Choose a radius under a stated coefficient bound)**.** Let $1 \le m < N$, $M > 0$, $\delta > 0$, and restrict sampling to $0 < r \le R/2$. Derive a radius that minimizes the explicit upper bound obtained from Proposition 20.1 by replacing $(1 - (r/R)^N)^{-1}$ with $(1 - 2^{-N})^{-1}$.

Solution. Put $x = r/R$ and $K_N = (1 - 2^{-N})^{-1}$. The resulting total coefficient bound is

$$R^{-m}(\delta x^{-m} + K_N M x^N), \qquad 0 < x \le 1/2.$$

The derivative of the expression in parentheses has the sign of $-m\delta + NK_N M x^{m+N}$. It changes sign once, at

$$x_* = (m\delta/(NK_N M))^{1/(m+N)}.$$

Thus the minimizing radius for this upper bound is $r = R\min\{x_*, 1/2\}$. The function decreases before x_* and increases afterwards, and it tends to infinity at zero, so this is a global minimizer on the stated interval. The conclusion optimizes an explicitly enlarged upper bound, not the unknown actual error. When $\delta = 0$, the bound decreases toward zero as $r \downarrow 0$; the positive-noise calculation and its interior optimum no longer apply. A derivative estimator multiplies the final bound by $m!$.

Investigation 20.11 (An explicit bound for a polygon around a slit)**.** Set $a = 1$ and require Hausdorff error at most $\varepsilon = 10^{-2}$ between a polygon and the slit. Give a pair (t, N) justified by the proved rule, without using a plotted curve as evidence.

Solution. Take $t = \operatorname{arsinh}(0.005)$, so $\sinh t = 0.005$ and $\cosh t = \sqrt{1 + 0.005^2} < 1.000013$. The rule requires $N \geq \pi\sqrt{\cosh t/0.01}$, which is less than 31.417. Thus $N = 32$ suffices. The equipotential-to-slit error is exactly 0.005 and the polygonal term is at most $1.000013\pi^2/(2\cdot 32^2) < 0.00482$. Their sum is less than 0.01. This certifies the exact vertices of the specified mathematical polygon. Any uncertainty in evaluated vertex coordinates must be added separately.

Investigation 20.12 (Why refinement of only one parameter can fail)**.** For the slit polygon, consider $N \to \infty$ with $t > 0$ fixed. What limiting geometric object is being approximated, and which error term survives? Then consider $t \downarrow 0$ with $N = 3$ fixed.

Solution. At fixed t, the polygons converge to the ellipse E_{e^t}, not to the slit. Their distance from the slit tends to $a\sinh t > 0$. With $N = 3$ fixed, the limiting sampled landing locations are $a, -a/2, -a/2$, so the limiting polygonal set is only $[-a/2, a]$. It misses the left third of the slit and has Hausdorff distance $a/2$ from $[-a, a]$. Thus the need to control both t and N is not just an artefact of the upper bound. A concrete choice of fixed sample angles can genuinely miss a boundary endpoint.

Chapter 21

Source correspondence and proof dependencies

The selected source unit is Section 8, “Carathéodory boundary,” of Lyubich’s supplied manuscript [1]. It occupies printed pages 146–152; Section 9 begins later on page 152. The supplied edition has 702 pages and PDF metadata dated September 2023. The source record binds that edition by its file hash. The present chapter gives reading correspondence, not a claim that source exercises and the monograph’s authored investigations have the same numbering or the same population.

The source contains twenty numbered items and six further named theorems. The numbered population consists of nine exercises, three remarks, three lemmas and five corollaries. Definitions, heading subdivisions and the Green-crosscut discussion are separately identified substantive material. The following table preserves source order. A source number in its left column always refers to Lyubich; the linked theorem numbers in its right column refer to this monograph.

Source item	Treatment in this monograph
8.1	Proper-crosscut separation is Proposition 3.2. Its proof uses the one-point compactification of a proper embedded line and the Jordan curve theorem.
8.2	Example 3.5 disproves the literal fixed-parametrization requirement with one common truncation parameter. The geometric version allowing independent cuts or prior reparametrization remains an explicit obligation. Neither form is used in the subsequent area-based construction of landing representatives.
8.3	Continuously indexed fjords can be sampled cofinally; the regular nesting and cofinality conventions are stated in Chapter 3 and used in Proposition 5.2.
8.4	Theorem 4.6 proves short spherical landing crosscuts from finite area. Proposition 5.2 uses them to represent every prime end, with physical endpoint coincidences explicitly allowed.
8.5	The dyadic selection gives a consecutive ratio less than 4; its uniformity in the boundary center follows from the outer-strip area bound after Theorem 4.6. These are separate subparts.
8.6	Theorem 4.4 proves inverse-map control on small continua by comparing an annular upper modulus bound with a radial lower bound. The connectedness qualification is retained.
8.7	Lemma 6.5 proves uniqueness for a constant continuous value on an open boundary arc, using reflection and Morera’s theorem.
8.8	Corollary 4.5 proves convergence of the inverse image of a physically landing curve.

Source item	Treatment in this monograph
8.9	Proposition 5.3 gives the intrinsic ordinary-null-chain criterion with disjoint closed crosscuts. Regular landing chains and their cofinal equivalence are treated in Proposition 5.2.
8.10	Theorem 7.1 proves extension of a domain-preserving physical closure homeomorphism. Example 7.2 refutes the unrestricted boundary-fixing addendum; Proposition 7.3 gives a sufficient boundary-fixed-isotopy replacement.
8.11	The disk conjugate is written with typed composition $H = g \circ h \circ f$. Its extension follows from Theorem 7.1. The source's literal condition of identity on the interior implies identity everywhere by continuity.
8.12	The final section of Chapter 7 constructs the circle of a specified noncuspidal tame end from an annular collar, and proves independence of the inner seam and collar coordinate.
8.13	Proposition 5.4 identifies impressions with complete cluster sets and proves singleton impression if and only if full pointwise continuous extension.
8.14	Investigation 6.10 treats the unbounded face of a finite transversely immersed curve. Boundary multiplicities equal local exterior sector counts through Theorem 8.8; hidden graph edges have multiplicity zero.
8.15	Proposition 9.2 proves that every external ray lands when the hull is locally connected, and that the landing map is continuous and onto.
8.16	Theorem 8.7 gives uniform approach in each fixed Stolz region, with its aperture held fixed.
8.17	Theorem 8.8 supplies a ray for each access to an accessible point.
8.18	Theorem 8.8 proves the angle–access equivalence and unique ray for an access. Proposition 8.9 supplies the subsequent unnumbered Green-crosscut replacement and cofinal-chain argument.
8.19	Theorem 15.2 proves almost-everywhere landing of external rays; the area argument provides a second route under its stated hypotheses. Harmonic-measure consequences keep angle-null sets distinct from arbitrary images of null sets.
8.20	The source's remark about ergodic applications is contextual. No new ergodic theorem, Julia-set local-connectivity result or dynamical classification is claimed by this volume.

21.1 The six named results

The Carathéodory Boundary Theorem is realized by Theorem 5.1, with its geometric chain interpretation in Propositions 5.2 and 5.3. The compactification is first defined through a conformal coordinate; independence of that coordinate, short physical representatives and the stated intrinsic null-chain criterion are then proved. This order avoids assuming physical boundary continuity in order to define it.

The Carathéodory–Torhorst equivalence is Theorem 6.4, and the Conformal Schönflies theorem is Theorem 6.6. Their proofs distinguish continuous extension from boundary injectivity. The slit and comb examples show respectively why these conclusions differ and why local connectivity is needed for the continuous physical extension of all boundary directions.

The Lindelöf theorem is Theorem 8.5. Its proof includes filling the gaps between good radii, reducing an arbitrary spherical domain to a bounded analytic model, and retaining the same access. The Fatou theorem is Theorem 13.3, developed from the measure, differentiation, Poisson

and trace arguments of the radial-limit chapters. The positive-length uniqueness theorem is Theorem 14.3; Jensen and logarithmic arguments state the bounded analytic hypotheses and distinguish the conclusion from a statement about arbitrary harmonic functions.

21.2 Corrections, conventions and remaining source work

The exterior map of a general full continuum satisfies $B(z) = z/\operatorname{cap}(K) + O(1)$, with positive leading coefficient. The source's normalization $B(z) \sim z$ requires capacity one. Scaling a physical hull is a mathematical operation, not a harmless omission of a coefficient. The circular and slit controls check the corrected convention.

Selecting a good radius independently from each dyadic annulus proves a factor less than 4 between consecutive choices. The later landing proof uses that bound. We do not infer the stronger factor 2 from this selection, or claim that every possible selection with that stronger bound is impossible. In the source homeomorphism statement, physical boundary fixing alone is insufficient for unrestricted homeomorphisms: conjugation on the complement of a segment swaps its two accesses. The manuscript records the convention issue and proves a precise sufficient replacement.

A finite-length image of a crosscut can have coincident physical endpoints. The two landing ends are therefore retained separately. Likewise, shrinking diameter alone is not a complete regular-chain condition: the fixed-endpoint chord example demonstrates the missing cofinality. These conventions are stated before the compactification theorem and are not introduced retrospectively to change an assertion's meaning.

Source Exercise 8.2 has two distinct dispositions. Its literal demand for one symmetric parameter interval of the supplied map is false by the explicit two-spiral example. A corrected geometric version allowing independent cuts or prior reparametrization has not been proved here; finite nets and nearest-boundary segments alone do not establish the required disjoint embedded attachments. The source register keeps that corrected obligation open. The principal compactification, continuity, landing and boundary-value proofs use the independent area and modulus route and do not depend on either approximation formulation. No claim is made that every literal source exercise holds as written.

21.3 Dependencies and evidence level

The declared topological inputs are the Jordan curve theorem, its topological Schoenflies form, the arc-in-path theorem, and the planar connected-complement criterion for simple connectivity. They are distinct from the conformal Schoenflies theorem proved here. The planar Riemann mapping existence theorem is the classical analytic input developed in Volume VII. The new arguments specify the local measure, integration, Poisson, Fourier and logarithmic tools they require. An annular-end result starts from a specified conformal collar; it is not a uniformization theorem for arbitrary wild surfaces.

The authored investigations and their solutions are a separate population from the source's nine exercises. The applications are deductions in stated potential models and mathematical sampling contracts, not measured datasets or validated floating-point implementations.

Evidence consists of written mathematics, source comparison and artifact checks. Lean, Rocq, CAS certification and external peer review remain subsequent work; earlier formal supplements do not certify this text. No research priority is asserted for the classical results, corrections or model calculations presented here.

Bibliography

[1] Mikhail Lyubich, *Conformal Geometry and Dynamics of Quadratic Polynomials*, Volumes I–II, supplied 702-page manuscript, PDF metadata 14 September 2023. Principal source: §8, pp. 146–152, ending before §9 on p. 152. Author's book location: `https://www.math.stonybrook.edu/~mlyubich/book.pdf`. Page references concern the supplied file, identified by its SHA-256 in the source record; no byte identity with a later online edition is asserted.

[2] Pierre Fatou, "Séries trigonométriques et séries de Taylor," *Acta Mathematica* 30 (1906), 335–400. `https://doi.org/10.1007/BF02418579`. Historical attribution for boundary-limit theory. The complete original article was not inspected in preparing this edition; the proofs used here are supplied in the text.

[3] Terence Tao, *245A, Notes 5: Differentiation theorems*, author lecture notes, 16 October 2010. Author's differentiation-theorem notes. Supplementary source for the measure-theoretic proof architecture.

[4] Lloyd N. Trefethen and J. A. C. Weideman, "The exponentially convergent trapezoidal rule," *SIAM Review* 56 (2014), 385–458. `https://doi.org/10.1137/130932132`. Author-hosted article. Context for analytic quadrature; the formulas and bounds used in this volume are derived explicitly.

[5] PHI research collective, *Extremal Length and Variational Geometry*, PHI Technical Monographs, Volume VI. Series background on extremal length and variational methods.

[6] PHI research collective, *Hyperbolic Geometry and Holomorphic Contraction*, PHI Technical Monographs, Volume VII. Series background on Schwarz's lemma, planar Riemann mapping and the hyperbolic metric.